Politecnico di Milano

Department of Structural Engineering

Doctoral School in Structural, Earthquake and Geotechnical Engineering

XXIV Cycle

Dual estimation and reduced order modelling of damaging structures

Supervisor

Prof. Stefano Mariani

PhD candidate

Saeed Eftekhar Azam

March 2012

Saeed Eftekhar Azam

Dual estimation and reduced order modelling of damaging structures
© March 2012
Email: s.eftekharazam@stru.polimi.it

Reduced order modelling and dual estimation of damaging structures

A Thesis
Presented to
The Academic Faculty

By

Saeed Eftekhar Azam

As a Partial Fulfillment
of the Requirements for the Degree of
Doctor of Philosophy

In

Structural, Seismic and Geotechnical Engineering

March 2012.

Doctoral School in Structural, Seismic and Geotechnical Engineering
Department of Structural Engineering
Politecnico di Milano

XXIV cycle

Faculty members

Prof. Roberto Paolucci (Coordinator)
Prof. Fabio Biondini
Prof. Gabriella Bolzon
Prof. Claudia Comi
Prof. Alberto Corigliano
Prof. Maria Laura Costantino
Prof. Claudio di Prisco
Prof. Marco di Prisco
Prof. Roberto Felicetti
Prof. Attilio Frangi
Prof. Pietro Gambarova
Prof. Anna Pandolfi
Prof. Federico Perotti
Prof. Alberto Taliercio
Prof. Pasquale Vena

Table of contents

Chapter 1: Introduction 1

1.1 Background and motivation 1

1.2 Objectives and scope 3

1.3 Organization of the thesis 4

Chapter 2: Recursive Bayesian estimation of partially observed dynamic systems 7

2.1 Introduction 7

2.2 Dual estimation of states and parameters of mechanical systems 8

2.3 Recursive Bayesian inference 11

2.4 Linear dynamic state space equations: optimal closed form estimator 12

2.5 Nonlinear dynamic state space equations: approximate Bayesian estimators 15

2.6 Numerical Results for dual estimation of single degree and multi degrees of freedom dynamic systems 27

2.6.1 Single degree-of-freedom dynamic system 28

2.6.2 Multi degrees-of-freedom dynamic system 57

2.7 Summary and conclusions 65

Chapter 3: Model Order Reduction of dynamic systems via Proper Orthogonal Decomposition 66

3.1 Introduction 66

3.2 Structural dynamics and time integration 67

3.3 Fundamentals of Proper Orthogonal Decomposition for dynamic structural systems 68

3.3.1 Principal Component Analysis 70

3.3.2 Singular Value Decomposition 72

3.4 Physical interpretation of proper orthogonal modes 74

3.5 Galerkin projection 74

3.6 Results: Reduced-order modeling of a tall building excited by earthquakes 76

3.7 Summary and conclusion 102

Chapter 4: POD-Kalman observer for linear time invariant dynamic systems 103

4.1 Introduction 103

4.2 Structural feedback control and the Kalman observer 104

4.2 Statistical assessment of residual errors induced by POD 106

4.3 Formulation of Kalman-POD observer for linear time invariant systems 110

4.4 Numerical assessment of POD-Kalman observer for seismic analysis of linear time invariant systems 113

4.5 Summary and conclusion 123

Chapter 5: Dual estimation and reduced order modeling of damaging structures 125

5.1 introduction 125

5.2 State space formulation of shear building-type structural systems 127

5.3 Reduced order modelling of structural systems 129

5.4 Dual estimation of reduced states and parameters of a damaging structure 132

5.5 Numerical results: damage detection in a ten storey shear building 136

5.6 Summary and conclusion 144

Chapter 6: Conclusions 145

6.1 Summary of contributions 145

6.2 Suggestions for future research 149

References 151

Acknowledgements

I owe my gratitude to Professor Stefano Mariani, for his logical way of thinking, thoughtful guidance, warm encouragements, support and practical suggestions. Following my work from the very beginning, his revisions, remarks and ideas contributed a lot to this thesis.

I would like to thank my friends and colleagues who I had opportunity to meet in Italy, they contributed to the friendly atmosphere both in and outside the department, list of their names would become too long to mention.

This thesis is dedicated to my parents and sisters for their great support during these three years.

Chapter 1: Introduction

1.1 Background and motivation

In the developed and industrialized countries, a big part of civil structures and infrastructures was built on the beginning of twentieth century, and therefore have been subject to deterioration; for instance in the USA over 50% of the bridges were constructed before 1940 (Stallings et al. 2000), and it is reported that over 42% of all these bridges are structurally deficient (Klaiber et al. 1987). In Canada, over 40% of currently functional bridges were constructed before 1970, and a large number of them need prompt rehabilitation, strengthening or replacement (ISIS Canada 2007). The Canadian Construction Association estimated that the cost to rehabilitate global infrastructure is around 900 billion US dollars (ISIS Canada 2007). The large amount of the cost to rehabilitate the global infrastructure underlines the importance of developing reliable and cost effective methods for the investments needed for rehabilitation in the next years. Moreover, in seismically active zones, the deterioration due to degradation in the structures may be amalgamated with the damage due to extreme seismic actions.

Recently, structural health monitoring has gained global attention in the civil engineering community with the objective of identifying the damage occurred in civil structures at the earliest possible stage, and estimating the remaining lifetime of the structures themselves. Structural damage caused by corrosion results in degradation of the mechanical properties of the affected components, and therefore it changes the response of the structure as well. Moreover, the failure of the structural components like shear walls, bracings and connections. explicitly changes the system. Hence, the goal of structural health monitoring can be realized by structural system identification; the system corresponding to healthy state should be identified first; in next planned system identifications, possible changes that occur in the system with respect to the structures' healthy state are indications of structural damage. This task, within the frames of non-

destructive vibration-based damage identification is realized either by direct identification of the system, or indirectly; some dynamic characteristics of the system are identified, and possible variations in their value are used to update the system. Instances of former methods include dual estimation of states and parameters of the structure via Bayesian inference techniques (Chatzi, Smyth & Masri 2010), while latter methods make use of modal properties of the structure for detection of the damage (Moaveni et al. 2010).

Figure 1-1: August 1, 2007 Minneapolis I-35W highway bridge collapse

Timely detection of the structural damage allows to prevent the possible casualties and losses caused by a collapse of the structure. A recent instance of a structural catastrophe is the collapse of Minneapolis I-35W highway bridge, seen in Figure 1-1. The steel truss bridge, constructed in 1967, collapsed on August 1, 2007 during rush hour, leading to dozens of causalities (French et al. 2011). Beyond humanistic concerns, the economic impact of the collapse have been considerable: road-user costs due to the unavailability of the river crossing summed up to 220,000 US dollars per day (Xie, Levinson 2011). These statistics underline the economic importance of infrastructure, and therefore substantiates the need for monitoring their health: the I35W St. Anthony Falls Bridge, constructed to replace the collapsed steel truss bridge, contains over 500 instruments to monitor the structural behavior (French et al. 2011). Long-term

monitoring systems are needed to process the data coming from these instruments to detect the damage at the earliest possible stage.

1.2 Objectives and scope

The objective of the work presented in this thesis is to develop damage identification techniques for vibration based non-destructive damage identification of the structures. The emphasis is on the development of fast and robust recursive damage detection algorithms, in order to facilitate the task of online real-time continuous monitoring of civil structures, like e.g. residential buildings, bridges etc.. To this end, four Bayesian filters, namely the extended Kalman filter (EKF), the sigma-point Kalman filter (SPKF), the particle filter (PF) and a hybrid extended Kalman particle filter (EK-PF) are adopted to identify the structural system. To avoid shadowing effects of the structural system, performance of the filters is benchmarked by dual estimation of state and parameters of a single degrees-of-freedom structure featuring nonlinear behaviours: an exponential softening and a bilinear (linear-softening, linear plastic and linear hardening) constitutive laws are studied. It will be seen that the EK-PF outperforms all the other filters studied here. It has to be underlined that, though Bayesian filters have been extensively studied in the automatic control field, their use in structural engineering is still to be investigated. The existing literature offers applications of EKF and SPKF and PF to simplified, low dimensional models; however, to the best of our knowledge, the use of EK-PF has never been reported when dealing with a structural engineering problem. After the performance of the filters are benchmarked when dealing with a single degree-of-freedom system, multi degrees-of-freedom structures are dealt with. In this regard EKF, for its computational efficiency and EK-PF, for its excellent performance dealing with single degree-of-freedom systems, are adopted. It will be shown that performance of EKF and EK-PF is similar when dealing with a two degrees-of-freedom system; however, moving to three and four degrees-of-freedom structures, EK-PF outperforms the EKF in terms of the bias in the estimation. It is realized that, as the number of the degrees-of-freedom increase, the adopted methods lose their accuracy in system identification and therefore, in damage detection. This problem is raised due to the high dimension of the parameter space, i.e. by so-called curse of dimensionality. To cope with this

issue, here we make recourse to reduced order modelling of the systems. As for the model order reduction technique, a method based on the proper orthogonal decomposition (POD) is adopted. Such method makes use of POD to define a subspace in which main dynamic evolution of the system takes place; the vectors that span the POD subspace are called proper orthogonal modes (POMs). Once such a subspace is obtained, a projection method onto the POD subspace is used to reduce the order of the set of governing equations of the system, and then speed-up the calculations. Besides the speeding up the calculations, another striking property of the so-called POMs is that they are sensitive to changes in the system parameters, this property, is here exploited to identify the damage in the structure.

The main contribution of the work presented in this thesis is the development of a recursive stochastic algorithm, by a synergy of dual estimation concept, POD-based order reduction and subspace update. The proposed methodology takes advantage of Bayesian filters (e.g. EKF and EK-PF) for dual estimation of state and parameters of a reduced order model of a time-varying system. Within each time iteration, a Kalman filter is used to update the subspace spanned by the POMs of the structure. The efficiency and effectiveness of the algorithm is verified via pseudo-experimental tests, carried out on a ten-storey shear building. It will be shown that the procedure successfully identifies the state, the model parameters (i.e. the components of the reduced stiffness matrix of the structure) and relevant POMs of the reduced model. Unbiased estimates furnished by the algorithm permits the health monitoring of the structure.

1.3 Organization of the thesis

The research presented in this thesis is partitioned into three main topics, namely: (a) system identification of dynamic systems; (b) model order reduction of dynamic systems; and (c) reduced order model identification of dynamic systems.

In Chapter 2, the first research topic is extensively investigated. Dual estimation of state and parameters of structural state space models is considered; EKF, SPKF, PF and EK-PF are used for parameter identification and state estimation. First, the performance of the filters is

benchmarked by using a single degree-of-freedom nonlinear system; then, application of the filters to multi degrees-of-freedom systems is considered. In this regard, a multi storey shear building is assessed. Limitations for applicability of this approach to the identification of e.g. the stiffness matrix of multi storey structures is highlighted. It is concluded that, due to bias in the estimates, these approaches are not suitable for system identification of shear building structures with more than three storeys.

Chapter 3 is devoted to model order reduction of multi storey buildings. Proper orthogonal decomposition is used for extracting the minimal subspace that features the dominant characteristics of the structure, via information contained in the response of the structure itself. The subspace found by POD is obtained by mathematical manipulation of samples of the response of the structure (gathered in the so-called snapshot matrix), hence it can be load dependent. In case the external excitation is a-priori known, load dependency of the reduced model would not be a problem; however, in case of seismic excitations such condition is not always true. To address this issue and build the snapshot matrix, samples are picked from the response of a case study structure to the El Centro accelerogram; the obtained reduced model then is used to simulate the response of the structure to the Friuli and the Kobe earthquake records. It is observed that POD-based reduced models are robust to changes in input seismic load. Next, efficiency of the method in speeding up the calculations, with high level of fidelity, is numerically investigated.

Chapter 4 investigates the statistical properties of residual errors induced by POD-based reduced order modelling. Such errors enter into the state space equations of the reduced systems in terms of system evolution and observation noise. A fundamental assumption made by recursive Bayesian filters, as exploited in this study, is the whiteness of the aforementioned noises. In this Chapter, null hypothesis of the whiteness of the noise signals is tested by making use of the Bartlett's whiteness test. It is shown that, no matter what the number of POMs retained in the analysis is, the null hypothesis of the whiteness is always to be rejected. However, the spectral power of the embedded periodic signals decreases rapidly by increasing the number of POMs.

The speed-up gained by incorporating POD-based reduced models into Kalman observer of linear time invariant systems, is also addressed in this Chapter.

Chapter 5 approaches the main objective of this research: the dual estimation of the reduced order model, and update of POMs of the structure to provide damage detection in structural system. It is shown that the first POM of the structure is quite sensitive to the intensity and location of the damage: a reduced model, featuring even a single POM, can therefore be used for developing damage detection algorithms. The proposed procedure shows a good performance when applied to pseudo-experimental tests. It is shown that the algorithm estimates the state, model parameters and relevant POMs of the reduced model of a ten storey shear building, featuring convergence to the true values of parameters and POMs used to create the pseudo test.

Final Chapter of the thesis is devoted to the conclusions and suggestions for future work. It is remarked that this thesis proposes a novel methodology based on recursive Bayesian inference of a reduced order model of the structure. Accuracy and power the proposed approach has been tested in the thesis through pseudo-experimental analysis. Online and real-time detection of the damage in the civil structural systems is a field that is still to be investigated. It is suggested to make use of other existing Bayesian filtering techniques for the purpose of the online real-time damage detection. This study does not provide experimental verification of the proposed methodology; hence it is suggested as a future research work.

Chapter 2: Recursive Bayesian estimation of partially observed dynamic systems

2.1 Introduction

Recursive inference of the dynamics of a system through noisy observations is usually pursued within a Bayesian framework. In this regard, provided that there is a-priori information available on probability distribution of observable quantities of the system and there is a correlation between observable and hidden quantities of the system, Bayes probability concept is used to estimate probability distribution of the hidden state variables. Such an approach is exploited in a wide variety of applications: in econometrics for estimation of volatility in the market (Ishihara, Omori 2010, Yang, Lee 2011, Miazhynskaia, Frühwirth-Schnatter & Dorffner 2006), for a review on the literature see (D. Creal 2009); in robotics for developing behaviors for robots (Lazkano et al. 2007), system identification of the robots (Ting, D'Souza & Schaal 2011), and their localization (Zhou, Sakane 2007); in biology for molecular characterization of diseases (Alvarado Mora et al. 2011), finding linkage in DNA (Allen, Darwiche 2008, Biedermann, Taroni 2008) and for characterization of genomic data (Caron, Doucet & Gottardo 2012); in image processing for diagnosis of diseases from medical images (Mitra, Lee & Goldbaum 2005), for image segmentation (Adelino R., Ferreira da Silva 2009), for image retrieval (Duan et al. 2005); in object tracking and radars (Jay et al. 2003, Velarde, Migon & Alcoforado 2008, White et al. 2009); in speech enhancement (Saleh, Niranjan 2001, Yahya, Mahmod & Ramli 2010); in mechanical characterization and parameter identification of materials (Corigliano, Mariani 2004, Corigliano, Mariani 2001a, Corigliano, Mariani 2001b), mechanical system identification (Mariani, Ghisi 2007, Mariani, Corigliano 2005) and many other fields that are not included for the sake of brevity. The mentioned instances are just a few fields of application of Bayesian inference schemes; their diversity proves the versatility of such approach in solving problems.

This Chapter of the thesis deals with simultaneous estimation of state and parameters of a structural system, in a recursive fashion. As new observations become available, the information concerning the current state of the system, which is obtained through a model of the system, is updated based on the measured observation. This goal is realized by making use of four recursive Bayesian filters, namely: the extended Kalman filter (EKF), the sigma-point Kalman filter (S-PKF), the particle filter (PF) and a newly proposed hybrid extended Kalman particle filter (EKPF). In this regard, to avoid shadowing effects of high dimensional structures, a single degree-of-freedom system has first been considered. The performances of the filters are benchmarked for simultaneous estimation for state and parameters of a nonlinear constitutive model of the system. After the performance of the filters dealing with a single degree-of-freedom structure has been verified, we move to the analysis of multi degree-of-freedom (DOF) structures. To this end, a shear type of the buildings has been considered. It has to be highlighted that, though the studied Bayesian filters have been adopted in the other fields like automatic control, their use in the field of structural engineering needs further investigations. The remainder of this Chapter is organized as follows: in Section 2.2, the dual estimation concept for simultaneous estimation of state and parameters of a state-space model is reviewed; in Section 2.3, general frames of the recursive Bayesian inference techniques are discussed; Section 2.4 is devoted to the Kalman filter, as the optimal filter of linear state-space models; Section 2.5 deals with approximate Bayesian filters for nonlinear systems; in Section 2.6 numerical results concerning dual estimation of states and parameters of single DOF and multi DOFs structures is presented; the Chapter is finally concluded in Section 2.7, where the limitations of studied filters, when applied to simultaneous state and parameter estimation of high dimensional problems, are discussed together with our remedy to solve the issue.

2.2 Dual estimation of states and parameters of mechanical systems

In this study the focus is on civil structures. Hence, we address mechanical systems whose dynamics is governed by the well-known set of ordinary differential equations governs evolution of their dynamic:

$$\boldsymbol{M}\ddot{\boldsymbol{u}} + \boldsymbol{D}\dot{\boldsymbol{u}} + \boldsymbol{R}(\boldsymbol{u}, t) = \boldsymbol{F}(t) \tag{2.1}$$

where: $\boldsymbol{M}$ is the mass matrix, $\boldsymbol{D}$ is the damping matrix; $\boldsymbol{R}(\boldsymbol{u}, t)$ stands for possibly displacement dependent internal force, whereas $\boldsymbol{F}(t)$ is the loading vector; $\boldsymbol{u}$, $\dot{\boldsymbol{u}}$ and $\ddot{\boldsymbol{u}}$ are the nodal displacements, velocities and accelerations, respectively. Since measurements are usually done in discrete time, we limit our attention to a discrete time formulation, where it is assumed that a part of displacements or accelerations of the system are measured in evenly spaced time grids.

To embed the mathematical model into algorithms designed for recursive Bayesian inference, we represent the dynamics of the system in a state-space form; details concerning the state-space representation of the mathematical model (2.1) is presented in the following Sections. Throughout the dissertation, by state we mean displacement, velocity and acceleration quantities of the response of the structure and by parameters we intend in the coefficients of the internal force term (in linear elastic case, components of the stiffness matrix). The state vector $\boldsymbol{z}$ thus contains $\boldsymbol{u}$, $\dot{\boldsymbol{u}}$ and $\ddot{\boldsymbol{u}}$, namely:

$$\boldsymbol{z}_k = \begin{bmatrix} \boldsymbol{u}_k \\ \dot{\boldsymbol{u}}_k \\ \ddot{\boldsymbol{u}}_k \end{bmatrix} \tag{2.2}$$

while parameter vector $\boldsymbol{\vartheta}_k$ gathers some unknown parameters of the system.

The state space representation of the system thus reads:

$$\boldsymbol{z}_k = \boldsymbol{f}_k^{\boldsymbol{z}}(\boldsymbol{z}_{k-1}; \boldsymbol{\vartheta}_{k-1}) + \boldsymbol{v}_k^{z} \tag{2.3}$$

$$\boldsymbol{y}_k = \boldsymbol{H}_k^{\boldsymbol{z}} \boldsymbol{z}_k + \boldsymbol{w}_k \tag{2.4}$$

where, for any time interval $[t_{k-1} \;\; t_k]$, $\boldsymbol{f}_k^{\boldsymbol{z}}(.)$ is a function of the state $\boldsymbol{z}_{k-1}$ and parameters $\boldsymbol{\vartheta}_{k-1}$ of the system, and evolves the state of the system $\boldsymbol{z}_{k-1}$ to obtain $\boldsymbol{z}_k$. $\boldsymbol{H}_k^{\boldsymbol{z}}$ quantifies the correlation between the state and the observable part of the system, at any given time instant; the name of Eq. (2.4), observation equation, stems from the aforementioned fact. $\boldsymbol{v}_k^{z}$ and $\boldsymbol{w}_k$ are zero mean, uncorrelated Gaussian processes with covariance matrices $\boldsymbol{V}^{\boldsymbol{z}}$ and $\boldsymbol{W}$, respectively. In general, observation equation may take any form; however, in the current study it is reasonably

assumed that observation process consists of a part of the state vector, say displacements and/or accelerations of some representative points. Consequently, the observation equation can be written as a sum of a linear mapping of the state through a Boolean matrix ($\boldsymbol{H}_k^z$) and an additive, uncorrelated Gaussian noise stemming from uncertainty of measurement sensor.

In this study the main mission of Bayesian filters, beyond estimating hidden part of the state vector, would be the calibration of system model parameters in an online fashion. At each time interval $[t_{k-1}\ t_k]$, on the basis of the information contained in the latest observation $\boldsymbol{y}_k$, the algorithms update previous knowledge of the parameter $\boldsymbol{\vartheta}_{k-1}$ to yield $\boldsymbol{\vartheta}_k$. To this end, dual estimation of states and parameters is considered; the parameter vector $\boldsymbol{\vartheta}_k$ is therefore augmented by defining the state vector (Mariani, Corigliano 2005):

$$\boldsymbol{x}_k = \begin{bmatrix} \boldsymbol{z}_k \\ \boldsymbol{\vartheta}_k \end{bmatrix} \tag{2.5}$$

Besides the conventional form of state-space equation, that is composed of evolution and observation equations, dual estimation is pursued via an extra vectorial equation that governs the evolution of the parameters over time according to:

$$\boldsymbol{\vartheta}_k = \boldsymbol{\vartheta}_{k-1} + \boldsymbol{v}_k^{\vartheta} \tag{2.6}$$

The intuitive idea behind this extra equation is to permit the unknown parameters of the system to vary over time, starting from an initial guess and hopefully converge onto an unbiased estimate. The possibility of variation to parameters is provided by white Gaussian fictitious noise $\boldsymbol{v}_k^{\vartheta}$, added to parameter evolution; the intensity of such a noise should be tuned, in order to have an unbiased and converging estimate for the parameters (Bittanti, Savaresi 2000). The state-space equation governing evolution of the augmented state thus reads:

$$\boldsymbol{x}_k = \boldsymbol{f}_k(\boldsymbol{x}_{k-1}) + \boldsymbol{v}_k \tag{2.7}$$

$$\boldsymbol{y}_k = \boldsymbol{H}_k \boldsymbol{x}_k + \boldsymbol{w}_k \tag{2.8}$$

where $\boldsymbol{f}_k(.)$, maps the extended state vector $\boldsymbol{x}_k$ over time, and therefore features both equations (2.3) and (2.6) in a unique equation.

2.3 Recursive Bayesian inference

The inference problem might be regarded as recursively estimating the expected value $E[\boldsymbol{x}_k|\boldsymbol{y}_{1:k}]$ of the state of the system, conditioned on the observations. Provided that the initial probability density function (PDF) $p(\boldsymbol{x}_0|\boldsymbol{y}_0) = p(\boldsymbol{x}_0)$ of the state vector is known, the problem consists in estimating $p(\boldsymbol{x}_k|\boldsymbol{y}_{1:k})$, assuming that the conditional PDF $p(\boldsymbol{x}_{k-1}|\boldsymbol{y}_{1:k-1})$ is available. The problem may be decomposed in two stages of prediction and update. As for the prediction stage, the Chapman-Kolmogorov equation furnishes the a-priory estimate of the state PDF at t_k (Arulampalam et al. 2002):

$$p(\boldsymbol{x}_k|\boldsymbol{y}_{1:k-1}) = \int p(\boldsymbol{x}_k|\boldsymbol{x}_{k-1})\, p(\boldsymbol{x}_{k-1}|\boldsymbol{y}_{1:k-1}) d\boldsymbol{x}_{k-1} \tag{2.9}$$

In the update stage, as soon as the new observation $\boldsymbol{y}_k$ becomes available, Bayes rule is profited to apply correction on the PDF of the state (Cadini, Zio & Avram 2009):

$$p(\boldsymbol{x}_k|\boldsymbol{y}_{1:k}) = \varsigma\, p(\boldsymbol{y}_k|\boldsymbol{x}_k) p(\boldsymbol{x}_k|\boldsymbol{y}_{1:k-1}) \tag{2.10}$$

where ς is a normalizing constant which depends on the likelihood function of the observation process. The Eqs. (2.9) and (2.10) together forge the basis for any Bayesian recursive inference scheme. The analytical solution of the integral in (2.9) is not possible except for a limited category of problems, namely systems formulated by linear state space equations and disturbed by uncorrelated white Gaussian noises (Eftekhar Azam, Bagherinia & Mariani submitted). In case of a general nonlinear problem one has to make recourse to approximate solutions, either by approximating the nonlinear evolution equations via linearization (Corigliano, Mariani 2004) or via discrete approximate representation of the PDF of the state vector (Mariani, Ghisi 2007, Doucet, Johansen 2009, Doucet, Johansen 2009). In the next Section, main features of the analytical solution available for linear Gaussian state space model is reviewed, and is followed by the Section 2.5 which deals with approximate solutions for nonlinear state-space models.

2.4 Linear dynamic state space equations: optimal closed form estimator

As mentioned in the preceding section, recursive Bayesian estimation of linear Gaussian state-space models can be handled analytically. Consider a linear discrete state-space model, that can be obtained by substituting the arbitrary evolution equation $\boldsymbol{f}_k(.)$ in Eqs. (2.7) and (2.8) by a linear operator $\boldsymbol{F}_k$. The state-space equations of such a system therefore read:

$$\boldsymbol{x}_k = \boldsymbol{F}_k\, \boldsymbol{x}_{k-1} + \boldsymbol{v}_k \tag{2.11}$$

$$\boldsymbol{y}_k = \boldsymbol{H}_k\, \boldsymbol{x}_k + \boldsymbol{w}_k \tag{2.12}$$

Provided that the initial probability distribution of the state is Gaussian, it is straight-forward to show that a linear operator does not change the Gaussian PDF over time (Kalman 1960). That is, in the Chapman-Kolmogorov integral at any arbitrary time instant t_k the functional form of both integrands is a priori known; $p(\boldsymbol{x}_{k-1}|\boldsymbol{y}_{1:k-1})$ is always a Gaussian probability density function, and also $p(\boldsymbol{x}_k|\boldsymbol{x}_{k-1})$ is by definition a Gaussian function. Consequently, the integral can be handled analytically. Kalman, in his seminal paper (Kalman 1960), introduced a well-known filter which is the optimal estimator for linear systems with uncorrelated Gaussian noise; the filter provides an online estimation of first and second order statistics of a state space model, and it includes a prediction stage which is simply an evolution of state over time. In the update stage, by calculating the Kalman gain $\boldsymbol{G}_k$, the filter enhances the predicted values furnished in previous stage. For a detailed description and algorithmic implementation of the Kalman filter (KF) readers are referred to Table 2-1.

In many real life problems, neither the dynamics of the system takes a linear form nor the uncertainties of transition equation might be regarded as Gaussian distributions. Even if the initial distribution of the uncertainties could be assumed Gaussian, a nonlinear state-space model would change the distribution over time (Mariani, Ghisi 2007). Hence, an optimal closed form solution would not be available for a general nonlinear problem (Doucet, Johansen 2009).

Table 2-1: Kalman Filter algorithm

- Initialization at time t_0: $$\hat{\boldsymbol{x}}_0 = \mathbb{E}[\boldsymbol{x}_0]$$ $$\boldsymbol{P}_0 = \mathbb{E}[(\boldsymbol{x}_0 - \hat{\boldsymbol{x}}_0)(\boldsymbol{x}_0 - \hat{\boldsymbol{x}}_0)^{\mathrm{T}}]$$
- At time t_k, for $k = 1, \dots, N_t$: • Prediction stage: 1. Evolution of state and prediction of covariance $$\boldsymbol{x}_k^- = \boldsymbol{F}_k\, \boldsymbol{x}_{k-1}$$ $$\boldsymbol{P}_k^- = \boldsymbol{F}_k \boldsymbol{P}_{k-1} \boldsymbol{F}_k^T + \boldsymbol{V}$$ • Update stage: 1. Calculation of Kalman gain: $$\boldsymbol{G}_k = \boldsymbol{P}_k^- \boldsymbol{H}_k^{\mathrm{T}} \left(\boldsymbol{H}_k \boldsymbol{P}_k^- \boldsymbol{H}_k^{\mathrm{T}} + \boldsymbol{W}\right)^{-1}$$ 2. Improve predictions using latest observation: $$\hat{\boldsymbol{x}}_k = \boldsymbol{x}_k^- + \boldsymbol{G}_k(\boldsymbol{y}_k - \boldsymbol{H}_k \boldsymbol{x}_k^-)$$ $$\boldsymbol{P}_k = \boldsymbol{P}_k^- - \boldsymbol{G}_k \boldsymbol{H}_k \boldsymbol{P}_k^-$$

In a mechanical system, the source of nonlinearity might be the material response to loading (Corigliano, Mariani 2001a, Corigliano, Mariani 2001b, Corigliano 1993); however, even if the material behavior would be linear, dual estimation of states and parameter will result in a bilinear (nonlinear) state space model (Ljung 1999). We illustrate this issue via an intuitive example, by considering the following linear state space model:

$$z_k = a\, z_{k-1} + \, b + v_k^z \tag{2.13}$$

$$y_k = H\, z_k + w_k \tag{2.14}$$

where: z_k and y_k denote the state and the observation of the system at a given time instant t_k; a and b represent the linear transition for the state in a given time interval $[t_{k-1} \;\; t_k]$, while H links

the hidden state z_k to the observation process. v_k^z and w_k denote the zero mean white Gaussian processes that quantify evolution and measurement inaccuracies, respectively. In case one is only interested in estimating the state of the system z_k, we already know the Kalman filter furnishes optimal estimation; however, let us imagine one is also interested in an online estimation of the parameters of the state space model. For the sake of simplicity we assume that only parameter a is of interest. As already mentioned the trick in dual estimation framework is to collect the unknown parameter a into the extended state vector $\boldsymbol{x}_k$ and try to track the dynamics of such system via recursive Bayesian inference algorithms. Note that, even though parameter a is stationary by definition, in the formulation of dual estimation the parameter is allowed to vary. In this regard, a transition equation governing evolution of the parameter is introduced:

$$a_k = a_{k-1} + v_k^a \tag{2.15}$$

Equation (2.15), together with (2.13) and (2.14), constitute the required state-space model for dual estimation of states and parameters. The augmented state vector $\boldsymbol{x}_k$ thus becomes $\boldsymbol{x}_k = [z_k \quad a_k]^T$, where $\boldsymbol{x}_k(1) = z_k$ and $\boldsymbol{x}_k(2) = a_k$; consequently Eqs. (2.13 − 2.15) become:

$$\boldsymbol{x}_k(1) = \boldsymbol{x}_{k-1}(2)\, \boldsymbol{x}_{k-1}(1) + \ b \tag{2.16}$$

$$\boldsymbol{x}_k(2) = \boldsymbol{x}_{k-1}(2) + v_k^a \tag{2.17}$$

$$y_k = H\, \boldsymbol{x}_k(1) + w_k \tag{2.18}$$

or, in matrix form:

$$\begin{bmatrix} \boldsymbol{x}_k(1) \\ \boldsymbol{x}_k(2) \end{bmatrix} = \begin{bmatrix} \boldsymbol{x}_{k-1}(2)\, \boldsymbol{x}_{k-1}(1) \\ \boldsymbol{x}_{k-1}(2) \end{bmatrix} + \begin{bmatrix} v_k^z \\ v_k^a \end{bmatrix} + \begin{bmatrix} b \\ 0 \end{bmatrix} \tag{2.19}$$

$$y_k = \ [H \quad 0] \begin{bmatrix} \boldsymbol{x}_k(1) \\ \boldsymbol{x}_k(2) \end{bmatrix} + w_k \tag{2.20}$$

It is evident that Eq. (2.19) is a nonlinear mapping over the given time interval $[t_{k-1} \ \ t_k]$. The above mentioned fact, together with consideration that many real life problems are nonlinear, substantiates the need for Bayesian inference algorithms targeting general nonlinear, non-

Gaussian problems. The following Section is devoted to reviewing the approximate solutions available in the literature to deal recursive Bayesian estimation of nonlinear state-space models.

2.5 Nonlinear dynamic state space equations: approximate Bayesian estimators

A simple remedy for dealing with nonlinear state-space models is through an extension of the Kalman filter, where for each time instant t_k the nonlinear state mapping $\boldsymbol{f}_k(\boldsymbol{x}_{k-1})$ is linearized by a first order truncation of a Taylor series expansion around $\boldsymbol{x}_{k-1}$. To this end, the Jacobian of the evolution equation is used as a surrogate for linear transition matrices in order to update covariance (Gelb 1974); then, the Kalman gain is used to update state statistics. This procedure is the extension of the Kalman filter for nonlinear state space models, hence its name extended Kalman filter (EKF). The extended Kalman filter assumes the prior $p(\boldsymbol{x}_{k-1}|\boldsymbol{y}_{1:k-1})$ to be Gaussian; however, even if initially Gaussian, a nonlinear mapping will change its probability distribution. Moreover, a severely nonlinear mapping of state might change the probability distribution into a tailed or a bimodal distribution (Adelino R., Ferreira da Silva 2009, Van der Merwe 2004) and cause bias in the estimates furnished by the EKF. Also, the approximation of the state mapping via its Jacobian is not accurate enough in some cases; it does not consider the stochastic nature of the state vector, and the effect of the neglected terms may become considerable. As a consequence, the approximation might lead to an inconsistent estimation of the covariance, hence a bias or divergence might occur in estimation of the state (Julier, Uhlmann 1997). For a detailed description of EKF algorithm see Table 2-2, where $\nabla_x \boldsymbol{f}_{\boldsymbol{k}}(\boldsymbol{x})|_{\boldsymbol{x}=\boldsymbol{x}_{\boldsymbol{k}-\boldsymbol{1}}}$denotes the Jacobian of $\boldsymbol{f}_{\boldsymbol{k}}(\boldsymbol{x})$ at $\boldsymbol{x} = \boldsymbol{x}_{\boldsymbol{k}-\boldsymbol{1}}$.

Table 2-2: Extended Kalman Filter algorithm

- Initialization at time t_0: $$\hat{\boldsymbol{x}}_0 = \mathbb{E}[\boldsymbol{x}_0]$$ $$\boldsymbol{P}_0 = \mathbb{E}[(\boldsymbol{x}_0 - \hat{\boldsymbol{x}}_0)(\boldsymbol{x}_0 - \hat{\boldsymbol{x}}_0)^{\mathrm{T}}]$$
- At time t_k, for $k = 1, \dots, N_t$: • Prediction stage: 1. Computing process model Jacobian: $$\boldsymbol{F}_k = \nabla_x \boldsymbol{f}_{\boldsymbol{k}}(\boldsymbol{x})\|_{\boldsymbol{x} = \boldsymbol{x}_{\boldsymbol{k-1}}}$$ 2. Evolution of state and prediction of covariance: $$\boldsymbol{x}_k^- = \boldsymbol{F}_k\, \boldsymbol{x}_{k-1}$$ $$\boldsymbol{P}_k^- = \boldsymbol{F}_k \boldsymbol{P}_{k-1} \boldsymbol{F}_k^T + \boldsymbol{V}$$ • Update stage: 1. Calculation of Kalman gain: $$\boldsymbol{G}_k = \boldsymbol{P}_k^- \boldsymbol{H}_k^{\mathrm{T}} \left(\boldsymbol{H}_k \boldsymbol{P}_k^- \boldsymbol{H}_k^{\mathrm{T}} + \boldsymbol{W}\right)^{-1}$$ 2. Improve predictions using latest observation: $$\hat{\boldsymbol{x}}_k = \boldsymbol{x}_k^- + \boldsymbol{G}_k(\boldsymbol{y}_k - \boldsymbol{H}_k \boldsymbol{x}_k^-)$$ $$\boldsymbol{P}_k = \boldsymbol{P}_k^- - \boldsymbol{G}_k \boldsymbol{H}_k \boldsymbol{P}_k^-$$

In case of severely nonlinear systems, the successive linearization approach might be inaccurate (Mariani 2009b). For certain problems it might be practically difficult to adopt: in case of a non holonomic material behavior, to calculate the Jacobian one has to know if the current state of the system proceeds toward loading or unloading (Mariani, Ghisi 2007). The difficulty in estimation of the Jacobian and also its inadequate accuracy has led to development of a category of derivative-free filters, called sigma-point Kalman filters, SPKF (Julier, Uhlmann & Durrant-Whyte 1995, Julier, Uhlmann & Durrant-Whyte 2000). The basic idea behind these filters is that it is easier to approximate a probability distribution than a nonlinear state-space model. A SPKF

uses a deterministic set of quadrature points, called sigma-points, to handle the Chapman-Kolmogorov integral (Ito, Xiong 2000); this set of deterministic points can be used since a-prior distribution of the state is assumed to have a Gaussian functional form for all the time instants. Hence, it is possible to approximate it through a set of deterministic points which are parameterized through the mean and covariance of the state vector. The distribution of the state vector, a multivariate Gaussian probability distribution, at time t_{k-1} reads:

$$p(\boldsymbol{x}_{k-1}|\boldsymbol{y}_{1:k-1}) = \frac{1}{((2\pi)^n|\boldsymbol{P}_{k-1}|)^{1/2}} \exp[-\frac{1}{2}(\boldsymbol{x}_{k-1} - \hat{\boldsymbol{x}}_{k-1})^T \boldsymbol{P}_{k-1}^{-1}(\boldsymbol{x}_{k-1} - \hat{\boldsymbol{x}}_{k-1})] \quad (2.21)$$

where: $\hat{\boldsymbol{x}}_{k-1}$and $\boldsymbol{P}_{k-1}$ are the associated mean vector and covariance matrix of the state vector, respectively.

Once it is established that the a-priori distribution of the state vector is a known Gaussian one, the Chapman-Kolmogorov integral can be recast as a Gaussian integral of the form $\int_{\mathbb{R}^n} \mu(\boldsymbol{x})\omega(\boldsymbol{x})d\boldsymbol{x}$, where $\mu(.)$ is an arbitrary probability distribution, whereas $\omega(.)$ denotes the a-priori probability distribution of state vector. Hence (2.9) becomes (Ito, Xiong 2000):

$$\int \mu(\boldsymbol{x}_{k-1}) \frac{1}{((2\pi)^n|\boldsymbol{P}_{k-1}|)^{1/2}} \exp[-\frac{1}{2}(\boldsymbol{x}_{k-1} - \hat{\boldsymbol{x}}_{k-1})^T \boldsymbol{P}_{k-1}^{-1}(\boldsymbol{x}_{k-1} - \hat{\boldsymbol{x}}_{k-1})]d\boldsymbol{x}_{k-1} \quad (2.22)$$

where $\omega(.)$ is an arbitrary function of state vector. To numerically handle the Gaussian integral in (2.22), a discrete representation of (2.21) is necessary, as done by a set of points that feature the same statistics of the original Gaussian distribution (Ito, Xiong 2000):

$$\boldsymbol{\chi}_j = \begin{cases} \sqrt{n+\rho}\boldsymbol{e}_j, & 1 \le j \le n \\ -\sqrt{n+\rho}\boldsymbol{e}_{j-n}, & n+1 \le j \le 2n \\ \mathbf{0}, & 2n+1 \end{cases} \quad (2.23)$$

and

$$\omega(\boldsymbol{\chi}_j) = \begin{cases} \frac{2\rho}{2(n+\rho)} & j = 2n+1 \\ \frac{1}{2(n+\rho)} & 1 \le j \le 2n \end{cases} \quad (2.24)$$

where $\rho > 0$ is a constant and $\boldsymbol{e}_k$ is the kth unit vector in $\mathbb{R}^n$. Julier and co-workers (Julier, Uhlmann & Durrant-Whyte 1995) proposed their S-PKF based on a quadrature rule which, for scalar functions, is identical to the Gauss-Hermit quadrature rule (Ito, Xiong 2000):

$$\int_{\mathbb{R}^n} \mu(\boldsymbol{x})\omega(\boldsymbol{x})d\boldsymbol{x} \approx \sum_{i=1}^{2n+1} \mu(\boldsymbol{\chi}_i)\omega(\boldsymbol{\chi}_i) \tag{2.25}$$

The $2n+1$ quadrature points are the minimal number of points necessary to preserve first and second moments of a multivariate normal distribution (Julier, Uhlmann & Durrant-Whyte 1995). One can assume $\omega(\boldsymbol{\chi}_i)$ as quadrature weights, which in this case are constant in all time instants, while the quadrature points are varying over time on the basis of the information contained in the covariance of the state, at $t = t_k$ the set of sigma-points are:

$$\boldsymbol{\chi}_{k,j} = \begin{cases} \hat{\boldsymbol{x}}_{k-1} & j = 2n+1 \\ \hat{\boldsymbol{x}}_{k-1} + \psi\sqrt{\boldsymbol{P}_{k-1,j}} & 1 \le j \le n \\ \hat{\boldsymbol{x}}_{k-1} - \psi\sqrt{\boldsymbol{P}_{k-1,(j-n)}} & n+1 \le j \le 2n \end{cases} \tag{2.26}$$

where $\hat{\boldsymbol{x}}_{k-1}$ denotes the expected value of the state and $\sqrt{\boldsymbol{P}_{k-1,j}}$ stands for j^{th} column of square root of its associated covariance at $t = t_{k-1}$. This scheme outperforms the extended Kalman filter (Mariani, Ghisi 2007); for a detailed description of SPKF algorithm, see Table 2-3.

In Table 2-3, ω^{*j} and ω^{j} are weights adopted in the merging stage at the end of the time step, to build mean and covariance of the current state. ψ instead denotes, a time invariant scaling factor that renders possible capturing local effects of nonlinear functions. To enhance the performance, the scaling factor ψ should be carefully calibrated to allow appropriate capturing of local nonlinearity effects, by tuning the distances of each sigma-point from the mean of a-priori distribution of the variable. In the SPKF, the square root $\sqrt{\boldsymbol{P}_{k-1}}$ is calculated by a Choleski factorization. The subscript j refers to the jth column of the Choleski factor of the covariance.

The SPKF approach, similarly to the EKF, is based on the assumption that at each time instant the a-priori distribution of the state is Gaussian.

Table 2-3: Sigma-Point Kalman Filter algorithm

- Initialization at time t_0:

$$\hat{\boldsymbol{x}}_0 = \mathbb{E}[\boldsymbol{x}_0]$$
$$\boldsymbol{P}_0 = \mathbb{E}[(\boldsymbol{x}_0 - \hat{\boldsymbol{x}}_0)(\boldsymbol{x}_0 - \hat{\boldsymbol{x}}_0)^{\mathrm{T}}]$$

- At time t_k, for $k = 1, \dots, N_t$:

- Prediction stage:
  1. Deploying Sigma-Points:

$$\boldsymbol{\chi}_{k,j}^{-} = \begin{cases} \hat{\boldsymbol{x}}_{k-1} & j = 2n+1 \\ \hat{\boldsymbol{x}}_{k-1} + \psi\sqrt{\boldsymbol{P}_{k-1,j}} & 1 \le j \le n \\ \hat{\boldsymbol{x}}_{k-1} - \psi\sqrt{\boldsymbol{P}_{k-1,(j-n)}} & n+1 \le j \le 2n \end{cases}$$

  2. Evolution of the sigma points:

$$\boldsymbol{\chi}_{k,j} = \boldsymbol{f}_k(\boldsymbol{\chi}_{k,j}^{-})$$

  3. Estimation of the statistics:

$$\boldsymbol{x}_k^{-} = \sum_{j=1}^{2n+1} \omega^j \boldsymbol{\chi}_{k,j}$$

$$\boldsymbol{P}_k^{-} = \boldsymbol{R}_k + \boldsymbol{V}$$

Where:

$$\boldsymbol{R}_k = \sum_{j=1}^{2n+1} \omega^{*j}(\boldsymbol{\chi}_{k,j} - \boldsymbol{x}_k^{-})(\boldsymbol{\chi}_{k,j} - \boldsymbol{x}_k^{-})^T$$

- Update stage:
  1. Calculation of Kalman gain:

$$\boldsymbol{G}_k = \boldsymbol{P}_k^{-}\boldsymbol{H}_k^{\mathrm{T}}(\boldsymbol{H}_k\boldsymbol{P}_k^{-}\boldsymbol{H}_k^{\mathrm{T}} + \boldsymbol{W})^{-1}$$

  2. Improve predictions using latest observation:

$$\hat{\boldsymbol{x}}_k = \boldsymbol{x}_k^{-} + \boldsymbol{G}_k(\boldsymbol{y}_k - \boldsymbol{H}_k\boldsymbol{x}_k^{-})$$
$$\boldsymbol{P}_k = \boldsymbol{P}_k^{-} - \boldsymbol{G}_k\boldsymbol{H}_k\boldsymbol{P}_k^{-}$$

To deal with more general problems, it is a common practice to make recourse to Sequential Monte Carlo methods (Doucet, Johansen 2009) for handling the Chapman-Kolmogorov integral by numerical approximations. Sequential Monte-Carlo methods make no explicit assumptions concerning the form of the posterior density $p(\boldsymbol{x}_{0:k}|\boldsymbol{y}_{1:k})$. These methods approximate the Chapman-Kolmogorov integrals in (2.9) through finite sums, adopting a sequential importance sampling on an adaptive stochastic grid. Within this frame, the particle filter implements an optimal recursive Bayesian estimation by recursively approximating the complete posterior state density. A set of N_P weighted particles $\boldsymbol{x}_k^{(i)}$, drawn from the posterior distribution $p(\boldsymbol{x}_{0:k}|\boldsymbol{y}_{1:k})$, is used to map the integrals. To this end, the main trick is to represent the posteriori PDF via Dirac delta functions pond at discrete sample points, namely the so-called particles. Without loss of generality, one can write (Cadini, Zio & Avram 2009):

$$p(\boldsymbol{x}_{0:k}|\boldsymbol{y}_{1:k}) = \int p(\boldsymbol{\varepsilon}_{0:k}|\boldsymbol{y}_{1:k})\, \delta(\boldsymbol{\varepsilon}_{0:k} - \boldsymbol{x}_{0:k}) d\boldsymbol{\varepsilon}_k \tag{2.27}$$

where $\delta(.)$ denotes the Dirac function.

Assuming the true posterior $p(\boldsymbol{x}_{1:k}|\boldsymbol{y}_{1:k})$ is known and can be sampled, an estimated of (2.27) is given by:

$$p(\boldsymbol{x}_{0:k}|\boldsymbol{y}_{1:k}) \approx \frac{1}{N_P} \sum_{i=1}^{N_P} \delta(\boldsymbol{x}_{0:k} - \boldsymbol{x}_{0:k}^i) \tag{2.28}$$

where $\boldsymbol{x}_k^i$ are a set of random samples drawn from true posterior $p(\boldsymbol{x}_{0:k}|\boldsymbol{y}_{1:k})$. In practice, it is impossible to efficiently sample from the true posterior; a remedy is built by making recourse to the importance sampling, i.e. to sample state sequences from an arbitrarily chosen distribution $\pi(\boldsymbol{x}_{0:k}|\boldsymbol{y}_{1:k})$ called importance function. An unbiased estimate of $p(\boldsymbol{x}_{0:k}|\boldsymbol{y}_{1:k})$ can then still be made as (Cadini, Zio & Avram 2009):

$$\begin{aligned} p(\boldsymbol{x}_{0:k}|\boldsymbol{y}_{1:k}) &= \int \pi(\boldsymbol{\varepsilon}_{0:k}|\boldsymbol{y}_{1:k}) \frac{p(\boldsymbol{\varepsilon}_k|\boldsymbol{y}_{1:k})}{\pi(\boldsymbol{\varepsilon}_{0:k}|\boldsymbol{y}_{1:k})}\, \delta(\boldsymbol{\varepsilon}_{0:k} - \boldsymbol{x}_{0:k}) d\boldsymbol{\varepsilon}_k \\ &\approx \frac{1}{N_s} \sum_{i=1}^{N_s} \omega_k^{*i} \delta(\boldsymbol{x}_{0:k} - \boldsymbol{x}_{0:k}^i) \end{aligned} \tag{2.29}$$

where:

$$\omega_k^{*i} = \frac{p(\boldsymbol{y}_{1:k}|\boldsymbol{x}_{0:k}^i)p(\boldsymbol{x}_{0:k}^i)}{p(\boldsymbol{y}_{1:k})\pi(\boldsymbol{x}_{0:k}^i|\boldsymbol{y}_{1:k})} \tag{2.30}$$

is the importance weight associated to the state process $\boldsymbol{x}_k^i$. In practice, these weights are difficult to calculate, due to the need of evaluating the integral for normalizing constant $p(\boldsymbol{y}_{1:k})$. Instead, the following weights are used (Gordon, Salmond & Smith 1993):

$$\omega_k^i = \frac{p(\boldsymbol{y}_{1:k}|\boldsymbol{x}_{0:k}^i)p(\boldsymbol{x}_{0:k}^i)}{\pi(\boldsymbol{x}_k^i|\boldsymbol{y}_{1:k})} \tag{2.31}$$

which are subsequently normalized according to:

$$\widetilde{\omega}_k^i = \frac{\omega_k^i}{\sum_{j=1}^{N_S} \omega_k^j} \tag{2.32}$$

Thus, estimate of the posterior distribution reads:

$$p(\boldsymbol{x}_{0:k}|\boldsymbol{y}_{1:k}) \approx \sum_{i=1}^{N_s} \widetilde{\omega}_k^i \delta(\boldsymbol{x}_{0:k} - \boldsymbol{x}_{0:k}^i) \tag{2.33}$$

If the current state of the importance sampling function do not depend on future observations, i.e., if the importance sampling function satisfies the following condition (Van der Merwe 2004):

$$\begin{aligned} \pi(\boldsymbol{x}_{1:k}|\boldsymbol{y}_{1:k}) &= \pi(\boldsymbol{x}_1|\boldsymbol{y}_1) \prod_{j=1}^{k} \pi(\boldsymbol{x}_j|\boldsymbol{x}_{1:j-1}, \boldsymbol{y}_{1:j}) \\ &= \pi(\boldsymbol{x}_k|\boldsymbol{x}_{1:k-1}, \boldsymbol{y}_{1:k})\pi(\boldsymbol{x}_{1:k-1}|\boldsymbol{y}_{1:k-1}) \end{aligned} \tag{2.34}$$

and if states can be considered as a Markov process, through the assumption that the observations are conditionally independent given the states we get (Van der Merwe 2004):

$$p(\boldsymbol{x}_{0:k}) = p(\boldsymbol{x}_{0:k}) \prod_{j=1}^{k} p\left(\boldsymbol{x}_j|\boldsymbol{x}_{j-1}\right) \tag{2.35}$$

$$p(\boldsymbol{y}_{1:k}|\boldsymbol{x}_{0:k}) = \prod_{j=1}^{k} p\left(\boldsymbol{y}_j|\boldsymbol{x}_j\right) \tag{2.36}$$

So, by using Eqs. $(2.34 - 36)$ in (2.30), the recursive formula for the update of importance weights becomes (Van der Merwe 2004):

$$\omega_k^i = \omega_{k-1}^i \frac{p(\boldsymbol{y}_k|\boldsymbol{x}_k^i)p(\boldsymbol{x}_k^i|\boldsymbol{x}_{k-1}^i)}{\pi(\boldsymbol{x}_k^i|\boldsymbol{x}_{0:k-1}^i,\boldsymbol{y}_{1k})} \tag{2.37}$$

For filtering purposes, the estimation of the marginal probability density $p(\boldsymbol{x}_k|\boldsymbol{y}_k)$ of the full posterior is enough, that is, if $\pi(\boldsymbol{x}_k|\boldsymbol{x}_{1:k-1},\boldsymbol{y}_{1:k})$ is substituted by $\pi(\boldsymbol{x}_k|\boldsymbol{x}_{k-1},\boldsymbol{y}_k)$, the sampling proposal will only depend on $\boldsymbol{x}_{k-1}$ and $\boldsymbol{y}_k$ (Arulampalam et al. 2002). Consequently, the recursive formula for estimation and update of the non-normalized weights reads (Arulampalam et al. 2002):

$$\omega_k^i = \omega_{k-1}^i \frac{p(\boldsymbol{y}_k|\boldsymbol{x}_k^i)p(\boldsymbol{x}_k^i|\boldsymbol{x}_{k-1}^i)}{\pi(\boldsymbol{x}_k^i|\boldsymbol{x}_{k-1}^i,\boldsymbol{y}_k)} \tag{2.38}$$

The (2.38) provides a way to sequentially update the importance weights, given an appropriate choice of the proposal distribution $\pi(\boldsymbol{x}_k|\boldsymbol{x}_{k-1},\boldsymbol{y}_k)$. Consequently, any expectations of the form $E[g(\boldsymbol{x}_k)] = \int g(\boldsymbol{x}_k)p(\boldsymbol{x}_{0:k}|\boldsymbol{y}_{1:k})d\boldsymbol{x}_k$, $g(.)$ being any given function, can be approximated through $E[g(\boldsymbol{x}_k)] \approx \sum_{j=1}^{N_P} \omega_k^i g(\boldsymbol{x}_k^i)$.

In (Doucet 1997), it was shown that the proposal distribution $\pi(\boldsymbol{x}_k|\boldsymbol{x}_{k-1},\boldsymbol{y}_k)$ minimizes the variance of the importance weights, conditional on $\boldsymbol{x}_{k-1}$ and $\boldsymbol{y}_k$. Nonetheless, the distribution $p(\boldsymbol{x}_j|\boldsymbol{x}_{j-1})$ (i.e. the transition prior) is the most popular choice for the proposal distribution. Although it results in a Monte-Carlo variation higher than that obtained using the optimal proposal $\pi(\boldsymbol{x}_k|\boldsymbol{x}_{k-1},\boldsymbol{y}_k)$, the importance weights are easily updated by simply evaluating the observation likelihood density $\pi(\boldsymbol{x}_k|\boldsymbol{x}_{k-1})$ for the sampled particle set, through (Cadini, Zio & Avram 2009):

$$\omega_k^i = \omega_{k-1}^i p(\boldsymbol{y}_k|\boldsymbol{x}_k^i) \tag{2.39}$$

The variance of these importance weights increases stochastically over time (Doucet 1997); after a few time steps, one of the normalized importance weights tends to one, while the remaining weights tend to zero. To address this rapid degeneracy, a resampling stage may be used to eliminate samples with low importance weights, and duplicate samples with high importance

weights. An intuitive explanation of particle filtering technique reads: each sample $\boldsymbol{x}_k^i$ might be a solution of the problem, and its associated weight ω_k^i signifies its probability of being the correct solution. In the resampling stage, the particles with higher probability are duplicated and in turn the ones with lower probability are discarded. Such an approach somehow permits the filter to condense the cloud of particles around the peak probability zone. An algorithm built in this way was first proposed by (Gordon, Salmond & Smith 1993), and has been called in different names like bootstrap filter, condensation algorithm etc.; for a detailed algorithmic specification see Table 2-4.

It is worth underlining that the update stage in the particle filter algorithm is conducted via evolution of particle weights, based on the probability of occurrence of each particle conditioned on latest observation a weight. After such weight evolution, the resampling stage is prescribed to alleviate the degeneracy issue, where ensemble of the samples is refined to increase the population of the samples which are more likely and decrease the lower probability population. To this end, different algorithms were proposed in the literature, like e.g. stratified, systematic, or residual resampling. Accounting for sampling quality and computational complexity, the systematic resampling scheme here adopted turns out to be the most favorable one (Hol, Schon & Gustafsson 2006). The resampling stage is performed by drawing a random sample ζ_j from the uniform distribution over (0,1]; then, the Mth particle for which the value of the random number ζ_j is between values of the empirical cumulative distribution of particles at $M-1$ and M is duplicated by resampling stage. Details of the systematic resampling (Kitagawa 1996) algorithm are shown in Table 2-5.

Since particle filter handles the current, actual PDF of the state to draw particles in prediction stage, it can appropriately account for non-Gaussian densities. However, as the dimension of the state vector increases, computational costs associated with numerical integrations increase drastically. It is suggested, as a rough rule of thumb, not to apply paticle filter to problems with dimension of state vector more than five (Li, Goodall & Kadirkamanathan 2004).

Table 2-4: Particle filter algorithm

- Initialization at time t_0:

$\widehat{\boldsymbol{x}}_0 = \mathbb{E}[\boldsymbol{x}_0]$ $\qquad$ $\boldsymbol{x}_0^{(i)} = \widehat{\boldsymbol{x}}_0$

$\boldsymbol{P}_0 = \mathbb{E}[(\boldsymbol{x}_0 - \widehat{\boldsymbol{x}}_0)(\boldsymbol{x}_0 - \widehat{\boldsymbol{x}}_0)^{\mathrm{T}}]$ $\qquad$ $\omega_0^{(i)} = p(\boldsymbol{y}_0|\boldsymbol{x}_0) \quad i = 1, \dots, N_{\mathrm{P}}$

- At time t_k, for $k = 1, \dots, N_t$:

- Prediction stage:
  1. Draw particles:

$$\boldsymbol{x}_k^{(i)} \sim p\left(\boldsymbol{x}_k|\boldsymbol{x}_{k-1}^{(i)}\right) \qquad i = 1, \dots, N_{\mathrm{P}}$$

- Update stage:
  1. Evolve weights:

$$\omega_k^{(i)} = \omega_{k-1}^{(i)}\, p\left(\boldsymbol{y}_k|\boldsymbol{x}_k^{(i)}\right) \qquad i = 1, \dots, N_{\mathrm{P}}$$

  2. Resampling, see Table 2-5.
  3. Compute expected value:

$$\widehat{\boldsymbol{x}}_k = \sum_{i=1}^{N_{\mathrm{P}}} \omega_k^{(i)}\, \boldsymbol{x}_k^{(i)}$$

Table 2-5: Systematic resampling algorithm

- At time t_k, for $j = 1, \dots, N_P$:
  - draw a random sample ζ_j from uniform distribution over $(0, 1]$
  - find M that satisfies:

$$\sum_{i=1}^{M-1} \omega_k^{(i)} < \zeta_j \leq \sum_{i=1}^{M} \omega_k^{(i)}$$

  - $\boldsymbol{x}_k^{(j)} \leftarrow \boldsymbol{x}_k^{(M)}$

The sampling distribution used in the generic particle filter can cause serious problems, since it is not the optimal one, conditioned on the latest observation. This fact leads to high computational costs, since the cloud of the samples fall far from the zones with high probability; many samples has therefore to be drawn in order to make the algorithm to converge. To alleviate the aforementioned issue, our remedy is to keep using the same sampling distribution; however, after the samples are drawn we improve the quality of the ensemble of the samples. Roughly speaking, once the samples are drawn, they are pushed by an extended Kalman filter toward the zones of higher probability in order to incorporate data from the latest observations into each sample.

The reason for exploiting the EKF instead of the SPKF, for enhancing the quality of sample ensemble, is twofold: first, the difficulty in tuning it in a way to have all the particles moved appropriately; second, the computational cost of the SPKF combined with particle filter can be significant, since both adopt numerical approximations to handle the quadrature. That is, the EKF is combined with particle filter frames to update each particle based on the information that is contained in the latest observation, see Table 2-6.

In Table 2-6 , $\boldsymbol{F}_k$ represents the current Jacobians of mappings $\boldsymbol{f}_k(\blacksquare)$.

In what follows, we will assess performance of the filters through numerical examples. In the absence of experimental data, for validation of the algorithms we rely on pseudo experimental data, i.e. numerical data resulting from direct analysis contaminated by white Gaussian processes substitute noisy measurements of the observable part of the state vector.

Table 2-6: Hybrid extended Kalman particle filter algorithm

- Initialization at time t_0:

$$\hat{\boldsymbol{x}}_0 = \mathbb{E}[\boldsymbol{x}_0] \qquad \boldsymbol{x}_0^{(i)} = \hat{\boldsymbol{x}}_0$$

$$\boldsymbol{P}_0 = \mathbb{E}[(\boldsymbol{x}_0 - \hat{\boldsymbol{x}}_0)(\boldsymbol{x}_0 - \hat{\boldsymbol{x}}_0)^{\mathrm{T}}] \qquad \omega_0^{(i)} = p(\boldsymbol{y}_0|\boldsymbol{x}_0) \quad i = 1, \dots, N_{\mathrm{P}}$$

- At time t_k, for $k = 1, \dots, N_t$:

- Prediction stage:

1. Draw particles:

$$\boldsymbol{x}_k^{(i)} \sim p\left(\boldsymbol{x}_k|\boldsymbol{x}_{k-1}^{(i)}\right) \qquad i = 1, \dots, N_{\mathrm{P}}$$

2. Push the particles toward the region of high probability through an EKF:

$$\begin{aligned} \boldsymbol{P}_k^{(i)-} &= \boldsymbol{F}_k \boldsymbol{P}_{k-1}^{(i)} \boldsymbol{F}_k^{\mathrm{T}} + \boldsymbol{V} \\ \boldsymbol{G}_k^{(i)} &= \boldsymbol{P}_k^{(i)-} \boldsymbol{H}_k^{\mathrm{T}} \left(\boldsymbol{H}_k \boldsymbol{P}_k^{(i)-} \boldsymbol{H}_k^{\mathrm{T}} + \boldsymbol{W}\right)^{-1} \\ \boldsymbol{x}_k^{(i)} &= \boldsymbol{x}_k^{(i)-} + \boldsymbol{G}_k^{(i)} \left(\boldsymbol{y}_k - \boldsymbol{H}_k \boldsymbol{x}_k^{(i)-}\right) \\ \boldsymbol{P}_k^{(i)} &= \boldsymbol{P}_k^{(i)-} - \boldsymbol{G}_k^{(i)} \boldsymbol{H}_k \boldsymbol{P}_k^{(i)-} \end{aligned} \qquad i = 1, \dots, N_{\mathrm{P}}$$

- Update stage:

1. Evolve weights:

$$\omega_k^{(i)} = \omega_{k-1}^{(i)}\, p\left(\boldsymbol{y}_k|\boldsymbol{x}_k^{(i)}\right) \qquad i = 1, \dots, N_{\mathrm{P}}$$

2. Resampling, see Table 2-5.
3. Compute expected value or other required statistics:

$$\hat{\boldsymbol{x}}_k = \sum_{i=1}^{N_{\mathrm{P}}} \omega_k^{(i)}\, \boldsymbol{x}_k^{(i)}$$

2.6 Numerical Results for dual estimation of single degree and multi degrees of freedom dynamic systems

To numerically solve the set of ordinary differential equations that govern the dynamics of the system, a Newmark explicit integration scheme has been adopted. According to (Hughes 2000), the time marching algorithm within the time step $[t_{k-1}\ \ t_k]$ can be partitioned into:

- predictor stage:

$$\widetilde{\boldsymbol{u}}_k = \boldsymbol{u}_{k-1} + \Delta t\, \dot{\boldsymbol{u}}_{k-1} + \Delta t^2(\tfrac{1}{2} - \beta)\ddot{\boldsymbol{u}}_{k-1} \tag{2.40}$$

$$\dot{\widetilde{\boldsymbol{u}}}_k = \dot{\boldsymbol{u}}_{k-1} + \Delta t(1-\gamma)\ddot{\boldsymbol{u}}_{k-1} \tag{2.41}$$

- explicit integrator:

$$\ddot{\boldsymbol{u}}_k = \boldsymbol{M}^{-1}(\boldsymbol{R}_k - (\boldsymbol{D}\,\dot{\widetilde{\boldsymbol{u}}}_k + \boldsymbol{K}\,\widetilde{\boldsymbol{u}}_k)) \tag{2.42}$$

- corrector stage:

$$\boldsymbol{u}_k = \widetilde{\boldsymbol{u}}_k + \Delta t^2\beta\ddot{\boldsymbol{u}}_k \tag{2.43}$$

$$\dot{\boldsymbol{u}}_k = \dot{\widetilde{\boldsymbol{u}}}_k + \Delta t\,\gamma\ddot{\boldsymbol{u}}_k \tag{2.44}$$

where $\Delta t = t_k - t_{k-1}$ denotes the time step size. To ensure numerical stability in the linear regime, Δt needs to be upper bounded by (Bathe 1996):

$$\Delta t_{cr} = \frac{T_n}{\pi} \tag{2.45}$$

where T_n is the period associated with the highest oscillation frequency. Even if Δt_{cr} can be increased in the reduced model, since higher order oscillations are filtered out of the numerical solution, in what follows we are keeping Δt constant in all the simulations. Hence, the speedup reported is therefore to be mainly linked to the reduction of the number of handled DOFs.

In (Corigliano, Mariani 2001b) it was shown that structural effects may play a prominent role in system identification. They typically lead to shadowing effects, arising when the sensitivity of

measurable variables (like, e.g. displacements or velocities) to constitutive parameters becomes negligible or falls out of the measurement range (i.e. they become comparable to round-off errors). Such structural effects practically lead to multiple solutions of the inverse problem in terms of model parameters update (all difficult to distinguish in the noisy environment), and filters provide biased or divergent calibrations, see e.g. (Corigliano, Mariani 2004, Corigliano, Mariani 2001a, Corigliano, Mariani 2001b). To solely benchmark performance of the filters we first focus on dynamics of a single degree-of-freedom structure. Once the performances of the filters are benchmarked by analyses concerning a single degree-of-freedom, then we move to the multi degrees of freedom structures to study the applicability of these methods to more realistic scenarios.

2.6.1 Single degree-of-freedom dynamic system

Since we are interested in benchmarking the extended Kalman particle filter (EK-PF) when compared to other Bayesian filters here tested (i.e. the EKF, the SPKF and the PF), the aforementioned structural effects are avoided by focusing on an undamped single DOF system constituted by a mass (or rigid block) connected to the reference frame through a spring, see Figure 2-1. The equation of motion of the system reads:

$$M\ddot{u} + R(u) = F(t) \tag{2.46}$$

where: m is the block mass; $R(u)$ is the spring force; $F(t)$ is the external load, which evolves in time; u and $\ddot{u}$ are the displacement and acceleration of the block, respectively. Results can be easily extended to the damped case; in such situation, it is however important to have the system continuously (or permanently) excited, so as to avoid vibration amplitudes to progressively decrease in time, thereby loosing filter efficiency, see (Corigliano and Mariani, 2004).

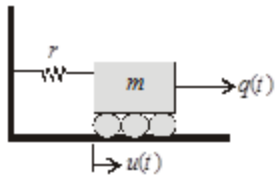

Figure 2-1: Single degree-of-freedom structural system

All the filters here studied perform well for dual estimation of a linear SDOF structure, hence the results are not discussed here for the sake of brevity. Instead, to assess the filter performance r is assumed to be a highly nonlinear, RFS-type function of the displacement u, i.e. of the spring elongation (Rose, Ferrante & Smith 1981, Corigliano, Mariani & Pandolfi 2006):

$$R(u) = a\,u\,\exp[-n\,u] \tag{2.47}$$

where a and n are unknown model parameters in need of tuning. Even if inspired by tight binding studies in atomistic simulations, law (2.47) is to be considered as phenomenological description of damaging processes taking place inside the spring: once a peak reaction is attained, softening (i.e. strength degradation) sets in and drives the state toward a smooth failure, occurring when $u \to +\infty$. The two parameters a and n in (2.47) can therefore be related to the strength r^M and the toughness G of the spring, through:

$$\begin{aligned} R^M &= \frac{a}{en} \\ G &= \int_0^\infty R\,\mathrm{d}u = \frac{a}{n^2} \end{aligned} \tag{2.48}$$

where e is the Nepero number.

Law (2.47) can be handled as a tensile envelope, with damage activation/deactivation conditions to be adopted to properly describe unloading/reloading paths, see e.g. (Mariani, Ghisi 2007). In accordance with previous papers (Mariani 2009b, Mariani 2009a), we instead assume here that

damage evolution is captured by strength degradation only, and model (2.45) is managed as a holonomic (nonlinear elastic) law.

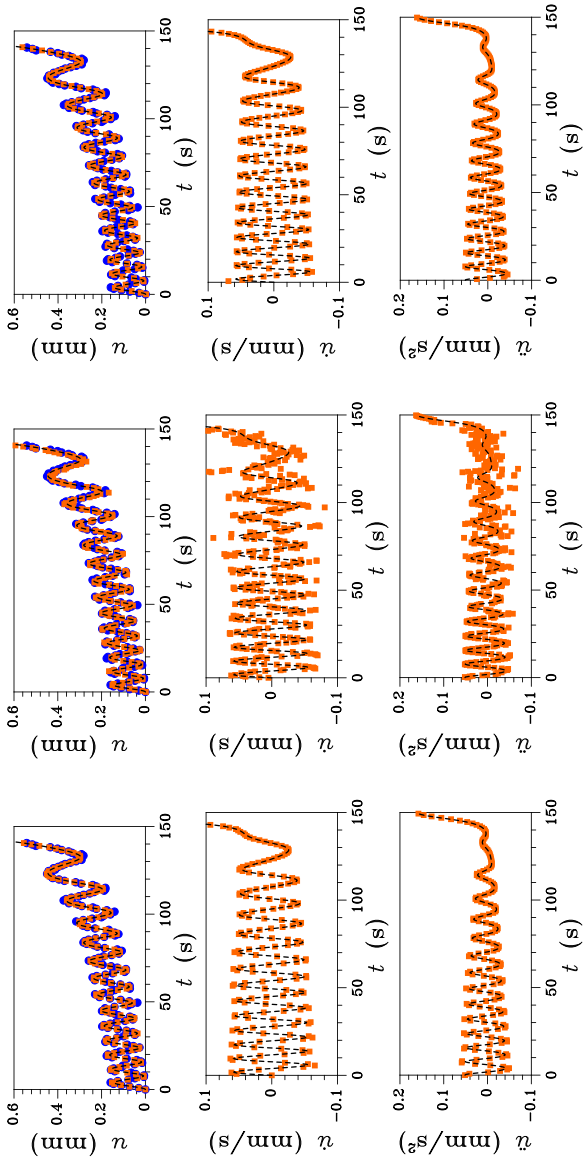

Figure 2-2: State tracking. Comparison between target (dashed lines) and tracked (orange squared symbols) system evolution, in terms of: (left column) displacement u; (central column) velocity u̇; (right column) acceleration ü. Results obtained by running: (top row) EK-PF; (middle row) PF, and (bottom row) S-PKF.

As mentioned before, we focus on pseudo-experimental (numerical) tests only. They consist in running direct analyses with known (target) values of model parameters, and then adding a white noise of assigned variance to the system output. This procedure allows to obtain scattered measurements, which are then used to feed the filters.

In order to handle a stable system dynamics, followed by divergence (i.e. by $u \to +\infty$) due to the inception and growth of damage in the spring, the applied load $F(t)$ (see Eq. 47) has been assumed to monotonically increase in time according to:

$$F(t) = 0.5 + 0.0075t \quad \text{(N)} \tag{2.49}$$

see also (Corigliano, Mariani 2004). With the mass initially at rest, this loading condition allows the system to be stable up to $t \cong 150$ s; beyond this threshold, softening in the spring becomes dominant (i.e. the transmitted force gets vanishing), and displacement u diverges.

In the analyses, the mass has been assumed $m = 9.72$ Ns^2/mm, see also (Corigliano, Mariani 2004). Measurements consist of the current mass displacement only, featuring a noise level characterized by a standard deviation $w = 0.05$ mm.

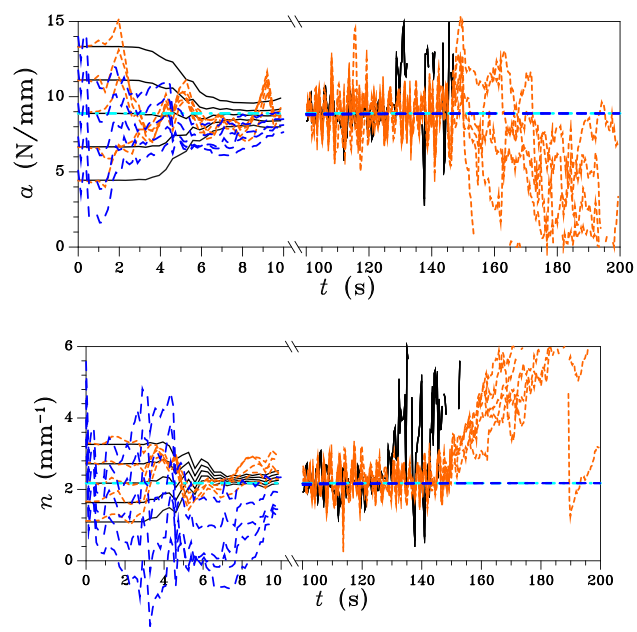

Figure 2-3: Model calibration. Time evolution of estimated model parameters (top row) a and (bottom row) n, at varying initialization values. Results obtained by running: EK-PF (long-dashed blue lines), PF (dashed orange lines) and S-PKF (continuous black lines).

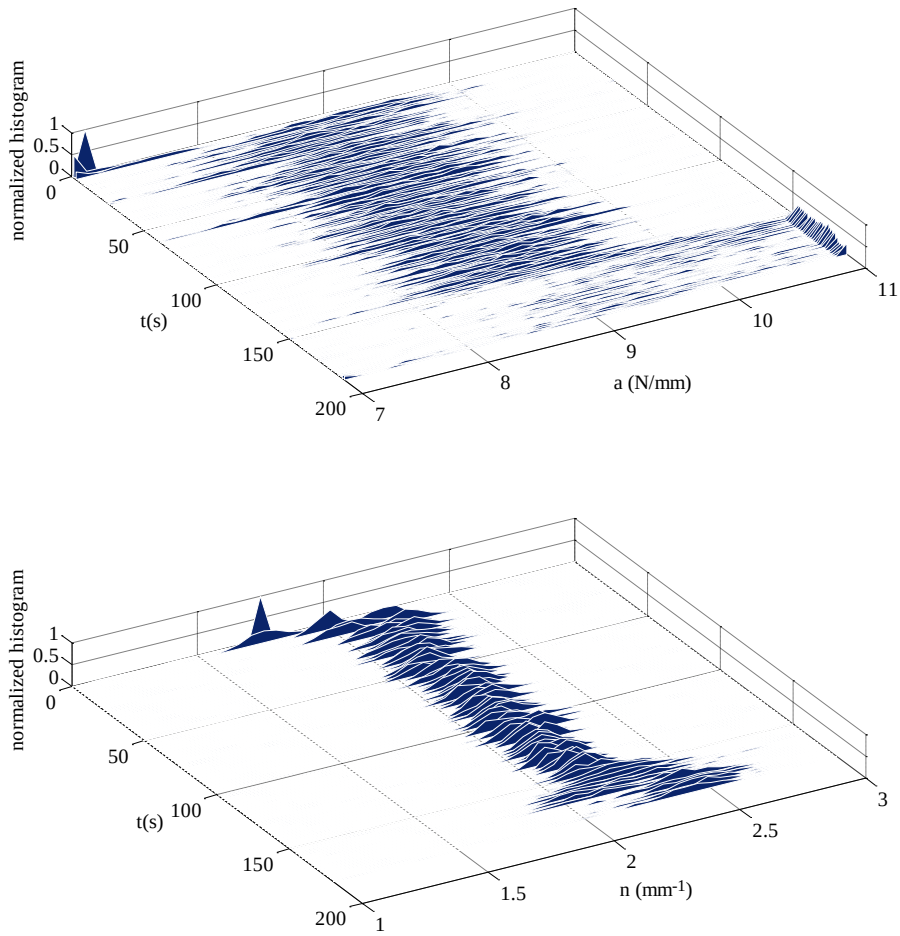

Figure 2-4: PF, projections onto the parameters (top) a and (bottom) n axes of the evolution of particles.

Results relevant to the tracking of the whole system state (i.e. u, $\dot{u}$ and $\ddot{u}$) are reported in Figure 2-2, as obtained by running the EK-PF and, for comparison purposes, the PF and the S-PKF. In these plots, the dashed lines represent the target system response; the orange squared symbols are instead the discrete-time estimations furnished by the filters, and the blue circular symbols stand for the measurements (that are displacement values only). The figure shows that the three filters are all capable to track the initial, stable oscillations and the transition to the unstable regime due to inception of softening. Even if a high number of particles (500 in this analysis) has been adopted, the PF is not able to attain the same accuracy of the S-PKF; the EK-PF (run using 5 particles) is instead very accurate, performing slightly better than the S-PKF.

We now move to the system identification task. As usual (see, e.g., (Ljung 1999)), results to follow have been obtained by setting the pivotal entries of $\boldsymbol{P}_0$ relevant to model parameters to be (at least) two orders of magnitude larger than those relevant to state variables. This way, model calibration is enhanced, since information (actually, innovation) brought by measurements is trusted much more than current estimates.

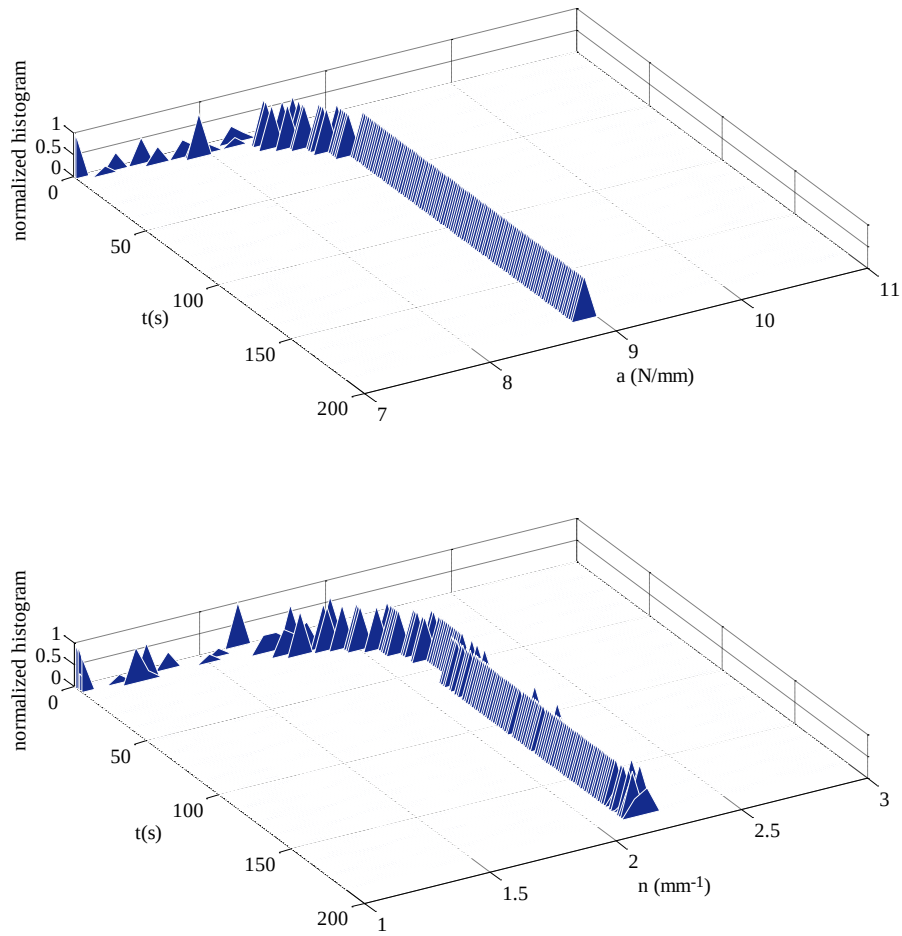

Figure 2-5: EK-PF, projections onto the parameters (top) a and (bottom) n axes of the evolution of particles.

In terms of time evolution of the estimates of model parameters a and n, it is shown in Figure 2-3 shows that they rapidly converge to the target values in the stable dynamic regime, independently of the initialization guess (here in the range between 50% and 150% of the target

values). The SPKF and the PF perform better than the EK-PF in the short-term time interval, featuring higher convergence rates without excessive oscillations of the estimates. But, as soon as the system stability threshold is approached, wild oscillations of increasing amplitude set in, and lead to diverging model calibration furnished by SPKF and PF. On the contrary, the EK-PF does not show such wild oscillations, and always provides stable, unbiased estimates.

To get insights into the superior performance of the EK-PF, Figures 2-4 and 2-5 report the projections onto the two model parameter axes of the time evolution of the (smoothed) distribution of particles deployed by PF and EK-PF, respectively. It can be seen that step #2 of prediction stage of the Table 2-6 proves very efficient in moving the particles toward the region of major interest, with distributions that are not spread over a wide range of values. This eventually helps avoid divergence of the estimates.

Next, we study the performance of Bayesian filters for a slightly more difficult task: the dual estimation of a system having a bilinear constitutive model for its spring. The system is the same as before, but now the relationship between the force in spring R and the displacement u reads:

$$R = \begin{cases} k_1 u & \text{if } u < u_M \\ k_1 u_M + k_2 (u - u_M) & \text{if } u > u_M \end{cases} \tag{2.50}$$

where k_1 denotes initial slope of the constitutive model of the spring; u_M is the limit at which spring constitutive model starts its bilinear behavior; and k_2 denotes the gradient of force-displacement after the displacement has exceeded u_M.

The strength of the constitutive law (2.50) lies in the versatility in simulating three different material behaviors, namely the linear-hardening, linear-perfect plastic and linear-softening. Under monotonically increasing loadings, depending on the k_2 value this bilinear constitutive law can be adopted to deal with identification of parameters of a structure whose behavior may not be known a-priori.

While dealing with joint state and parameter estimation, the main drawback of such constitutive law is the intricate interrelation of components of the state vector, when the parameter of the

constitutive model are included into the state vector. Consider the state-space representation of the system, augmented state vector incorporates k_1, k_2 and u_M so as:

$$\boldsymbol{\vartheta} = \begin{bmatrix} k_1 \\ k_2 \\ u_M \end{bmatrix} \tag{2.51}$$

At each time iteration, the evolution equation, based on the value of u_M may find two different functional form: if displacement of the spring is less than u_M, only the initial linear behavior of the spring gets involved; if displacement of the spring exceeds u_M, nonlinearity of spring affects the spring force. Filter thus has to decide which path to follow, as long as deterministic information is not available for u_M. In what follows results of application of nonlinear versions of Kalman filters and Particle filter and also a hybrid extended Kalman particle would be presented. The results are organized in three sets, each one of the filtering algorithms are assessed when dealing with reference problems of each scenario: linear hardening, linear-perfectly plastic and linear-softening constitutive laws.

Like before, in all the analyses pseudo-experimental data are used instead of data coming from experiments; the numerical data contaminated by a zero mean additive white noise are therefore taken as observations of the system. The initial slope k_1 is always assumed to be $3.27\ \mathrm{N/mm}$, while $k_2 = k_1/10$ for hardening, $k_2 = 0$ for plasticity and $k_2 = -k_1$ to mimic softening behavior. The value of the threshold of linear behavior u_M is set to 0.46 mm; the mass has been assumed $m = 9.72$ $\mathrm{Ns^2/mm}$, see also (Corigliano, Mariani 2004, Eftekhar Azam, Bagherinia & Mariani submitted). Measurements consist of the current mass displacement only, featuring a noise level characterized by a standard deviation $w = 0.01$ mm. In order to incept a nonlinear behavior due to damage in the spring, the applied load q has been assumed to monotonically increase in time according to (2.49). Since the main objective of this study is the calibration of constitutive parameters, we just include the plots of parameter estimation unless there is a specific reason for presenting state estimate plots.

Figures 2-6, 2-7 and 2-8 show the performance of the EKF in simultaneous calibrating the three constitutive parameters of linear hardening, linear plastic and linear softening case, respectively. The filter is run for different initialization values; it is seen that, except for the initializations from target values, in none of the scenarios the EKF is able to identify the constitutive parameters. As mentioned before, the EKF is a straight-forward extension of the Kalman filter, based on linearization of the evolution equation. It is suitably adopted for weakly nonlinear problems; however, if the nonlinearity is severe, such linearization is not accurate enough and poor performance is expected. It has to be underlined that tuning of the filter, in order to obtain unbiased estimate of parameters is not always easy, and we do not claim that we have tuned optimally the filters for different initializations and constitutive laws. In essence, three noise covariances associated with each parameter are tuning knobs of the system (Bittanti, Savaresi 2000). One has to notice that, as the number of the parameters increase the simultaneous tuning of them might become more difficult and algorithm appears to be practically inefficient.

Next, results relevant to the performance of the SPKF are presented; even though SPKF has proved to outperform EKF in many cases, it suffers from problem of positive definiteness of covariance matrix when dealing with parameter identification (Holmes, Klein & Murray 2008), and also the tuning of the scale factor might become critical (Mariani 2009b). Figures 2-9, 2-10 and 2-11 present the results obtained by SPKF when dealing with the three different scenarios of constitutive laws. Like in the previous case, the filter is run with different initializations to see whether convergence is triggered from different starting points. It is seen that the performance of SPKF is quite poor, as it is not able to furnish unbiased estimates of the parameters, except for the case that the initial guess are set at the target values of parameters. We remind that, in excess of three fictitious noise covariance to be tuned, within the SPKF algorithm also the scale factor should be tuned accurately; such a factor is used to let the filter capture local effects of nonlinearities of the evolution equation. Adding this to the three former parameters one can see how delicate could become the task of tuning.

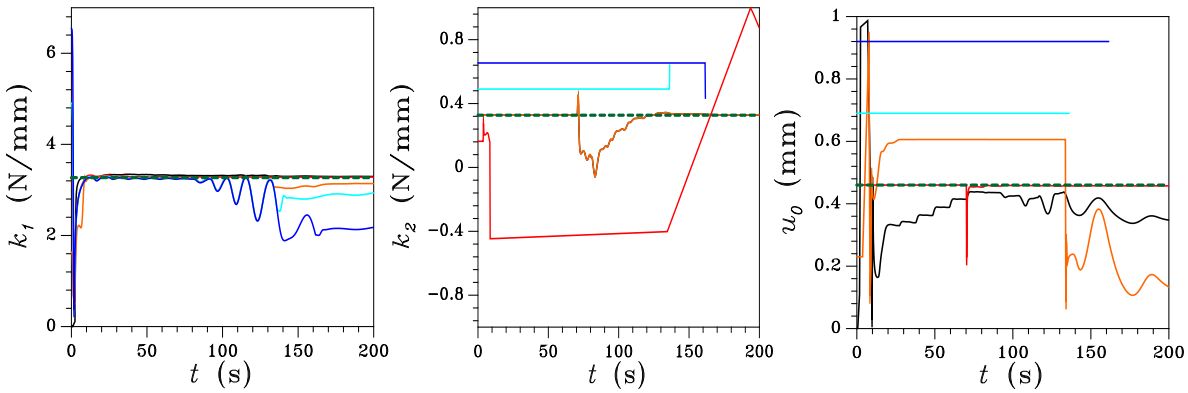

Figure 2-6: results of EKF for estimation of parameters of linear-hardening constitutive law

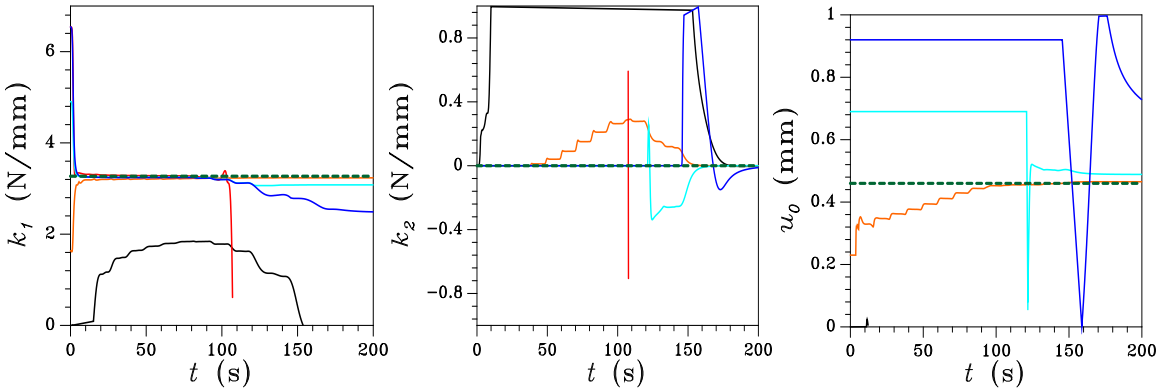

Figure 2-7: results of EKF for estimation of parameters of linear-plastic constitutive law

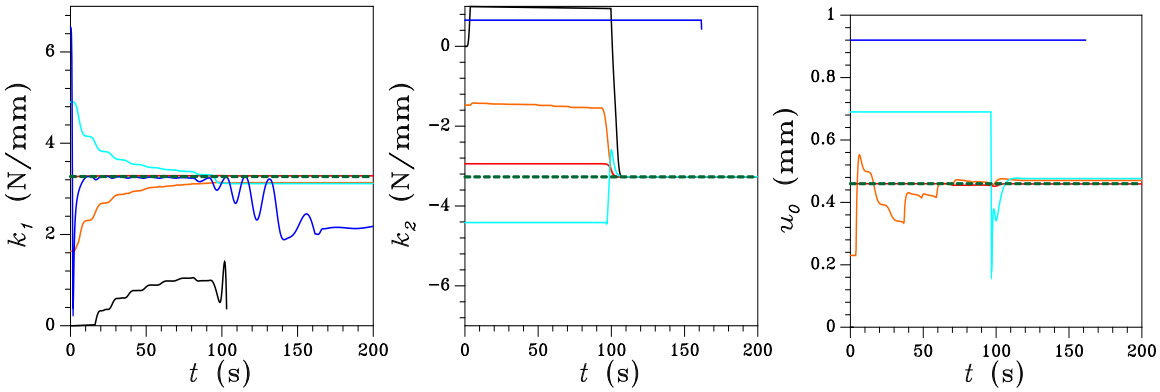

Figure 2-8: results of EKF for estimation of parameters of linear-softening constitutive law

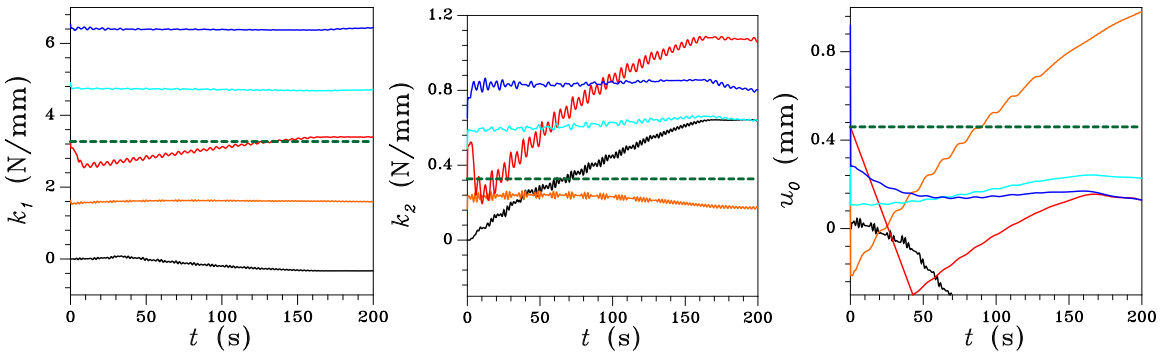

Figure 2-9: results of SPKF for estimation of parameters of linear-hardening constitutive law

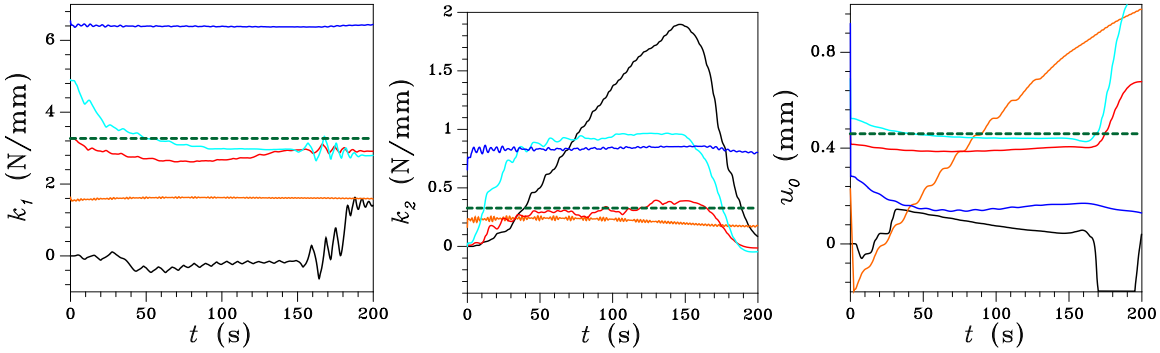

Figure 2-10: results of SPKF for estimation of parameters of linear-plastic constitutive law

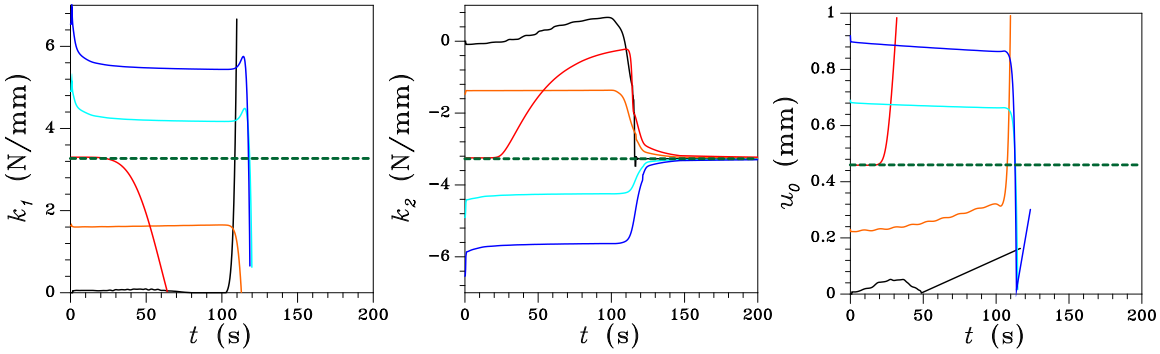

Figure 2-11: results of SPKF for estimation of parameters of linear-softening constitutive law

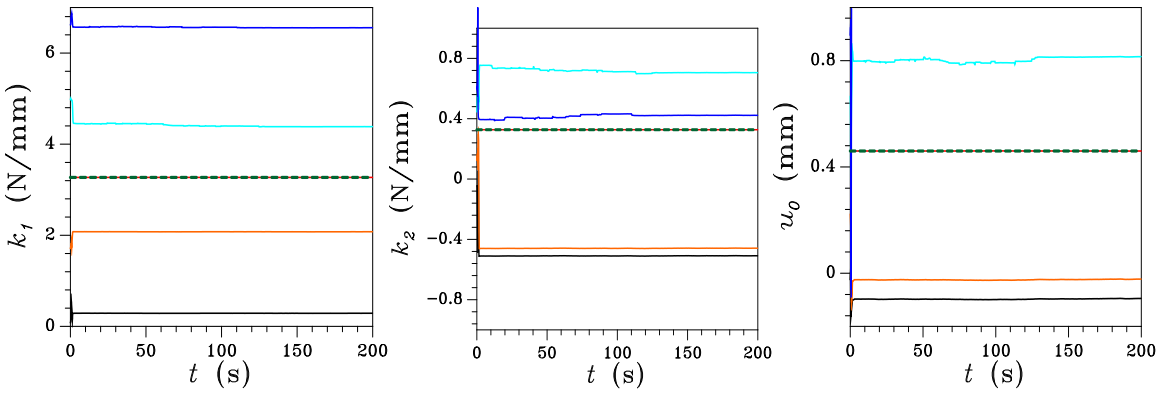

Figure 2-12: results of PF for estimation of parameters of linear-hardening constitutive law

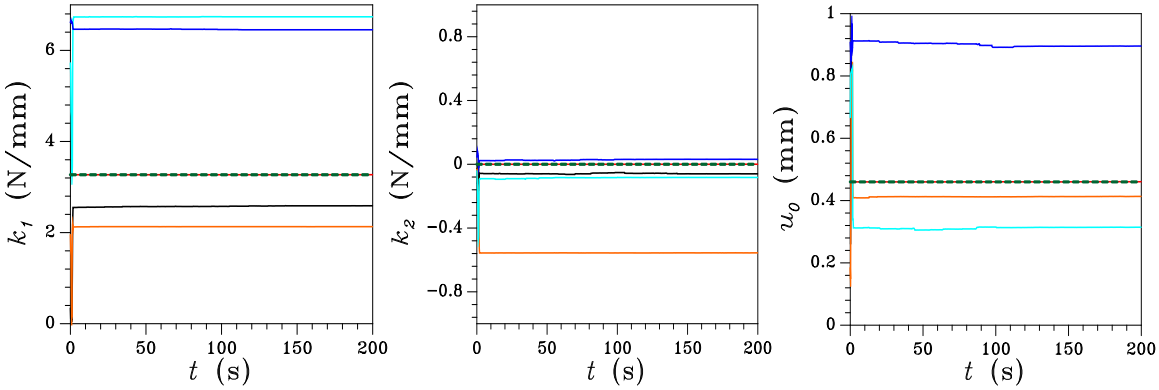

Figure 2-13: results of PF for estimation of parameters of linear-plastic constitutive law

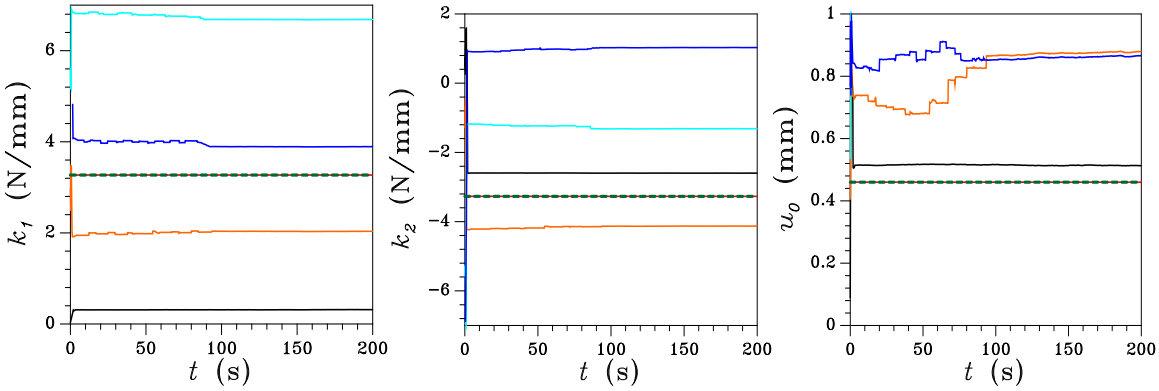

Figure 2-14: results of PF for estimation of parameters of linear-softening constitutive law

Since common extensions of the KF could not furnish unbiased estimates of constitutive parameters, we make recourse to Particle filters, as they are basically designed for nonlinear

systems with arbitrary uncertainty associated with them. Figures 2-12, 2-13 and 2-14 show the results of estimation of the parameters of linear-hardening, linear-perfect plastic and linear-softening constitutive model. Even though the particle filter is devised for nonlinear/non-Gaussian systems, it is seen through the graphs that it fails to estimate the parameters appropriately.

In designing a PF, it should be noticed that an appropriate initial guess of the distribution of the state of the system is essential to enhance the performance of the filter. Never the less, the value of the covariance of the noise for calibrating the parameters plays an important role (Arulampalam et al. 2002); they should be appropriately adjusted in order to let scattering of the samples in the feasible range of the parameter. We illustrate these issues via numerical examples. For ease of tuning, firstly it is assumed that we have quite good a priori knowledge of k_1 and u_0 and aim to estimate only k_2. Figures 2-15 to 2-20 show the results of analysis for estimation of k_2. Looking at Figures 2-15 and 2-18, they plot the time histories of estimation of the parameter k_2, supposing that the values of k_1 and u_M are a-priori known. Moving from Figure 2-15 to 2-18, we have changed the intensity if the tuning noise to highlight its importance in the parameter estimation. In both cases the initial value of the parameter is set to 50% of the target value. In the graph shown in Figure 2-15, the value of the noise for tuning k_2 is set to $10^{-2}\frac{\mathrm{N}^2}{\mathrm{mm}^2}$, which permit the evolution of the particles finally converge to the target value. On the contrary, the noise value equal to $10^{-4}\frac{\mathrm{N}^2}{\mathrm{mm}^2}$ which is used to obtain the results shown in Figures 2-18 to 2-20, does not let the algorithm to sample efficiently, and the ensemble of the particles does not finally converge to the target values of the parameters.

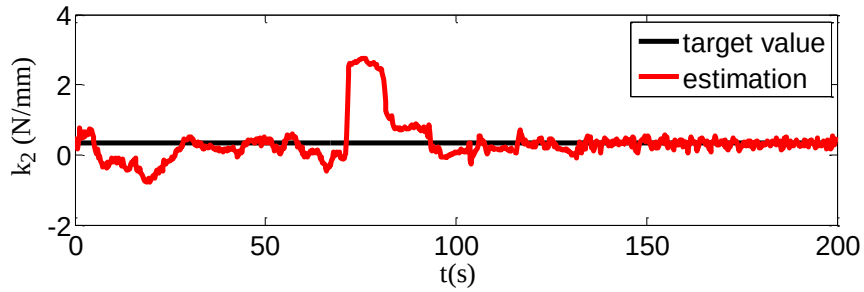

Figure 2-15: parameter estimates while noise covariance is set appropriately ($10^{-2}\frac{\mathrm{N}^2}{\mathrm{mm}^2}$)

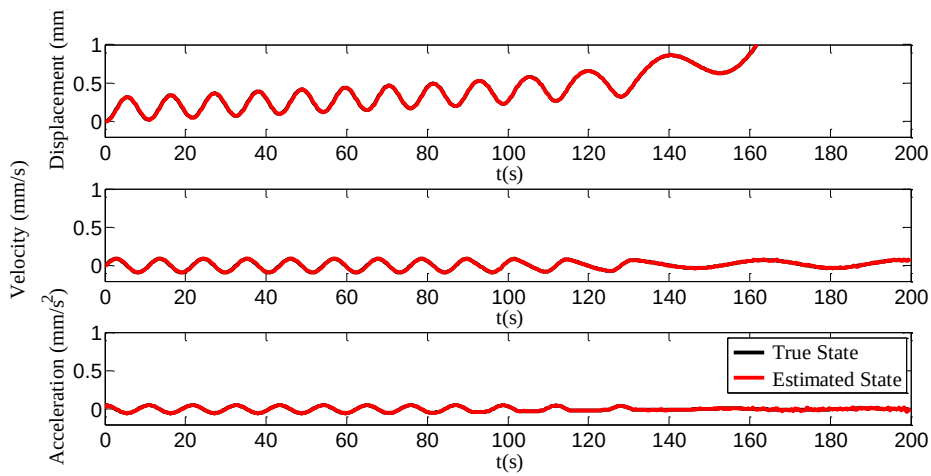

Figure 2-16: state estimates when noise covariance is set appropriately ($10^{-2}\frac{\mathrm{N}^2}{\mathrm{mm}^2}$)

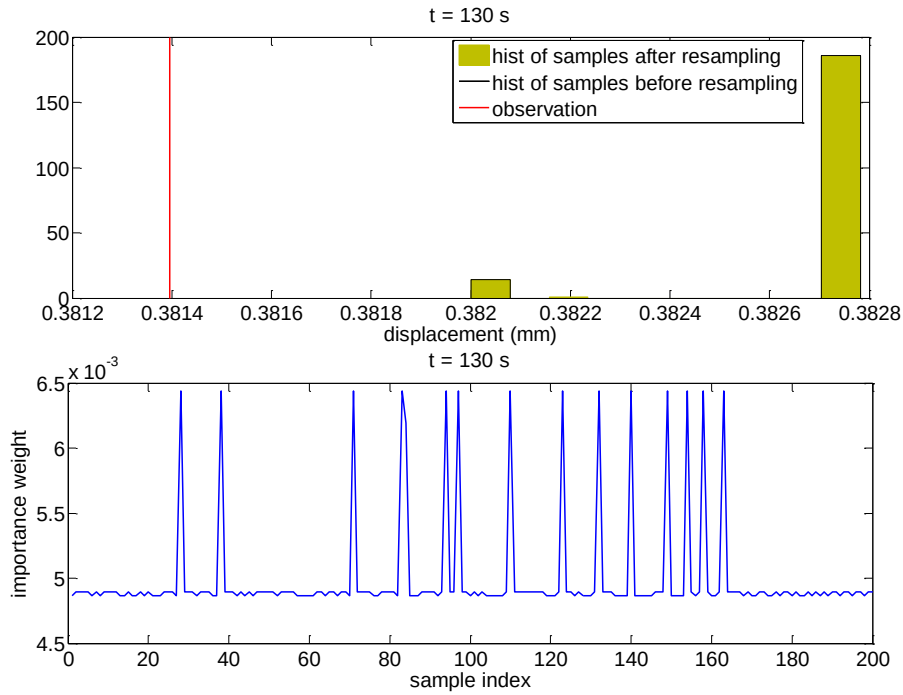

Figure 2-17: histogram of observable part of state vector (top) and associated sample weights (bottom) though through the top figure it seems that the sample has degenerated, through the bottom it is seen that many samples have significant weights. Also notice that samples are distributed in a close neighborhood of observation (red vertical line)

To compare the performance of the particle filter when the tuning noise intensity varies one can confront Figures 2-16 and 2-19. At $t = 100$ s, as the parameter k_2 enters in the system evolution due to the inception of nonlinearity, for the case with the noise equal to $10^{-4}\frac{\mathrm{N}^2}{\mathrm{mm}^2}$, estimates of the states of the system diverge, while in with the noise equal to $10^{-2}\frac{\mathrm{N}^2}{\mathrm{mm}^2}$ states are estimated un-biasedly. This corroborates the idea that a small value for tuning noise intensity prevents the cloud of the particles to efficiently approximate the a-posteriori distribution of the state. To investigate this issue in more details, we have focused on the histograms of the particles and their associated weights at $t = 130$ s, where there is a sharp change in the estimation of displacements (see Figure 2-17). Looking at the histograms and particle weights shown in Figure 2-20, it is seen that the cloud of the particles, shown via histogram, are far from the observation vicinity (the red

vertical line), where the distance of the closest bin to the observation is about 0.15 mm. As a consequence, in Figure 2-20 all of the particles have found equal normalized weights; their distance from the observation vicinity is too far, as a consequence the associated probability with each particle becomes less than the round-off errors. On the contrary, looking at the same time instant in the case in which estimates are converging target values, it is seen that the distance of the closest been to the observation is about 0.004 mm.; thus, in Figure 2-18 the particles closer to observation have found a more significant normalized weight whereas other have smaller weights. Such diversity of weights shows that the particles are distributed in a zone which is close to the observation.

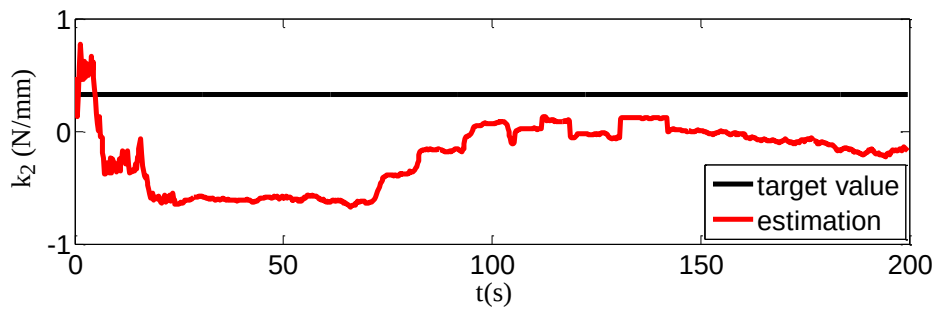

Figure 2-18: parameter estimates when noise covariance is not set appropriately ($10^{-4}\frac{\mathrm{N}^2}{\mathrm{mm}^2}$)

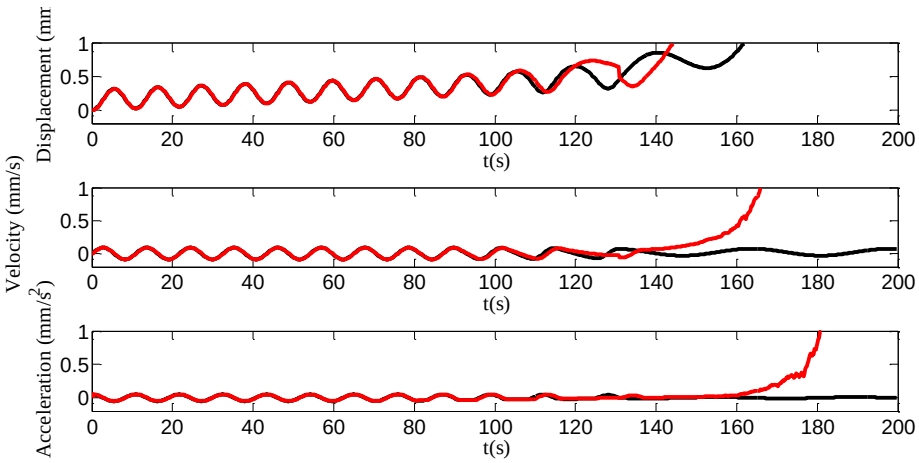

Figure 2-19: state estimates when noise covariance is not set appropriately ($10^{-4}\frac{\mathrm{N}^2}{\mathrm{mm}^2}$)

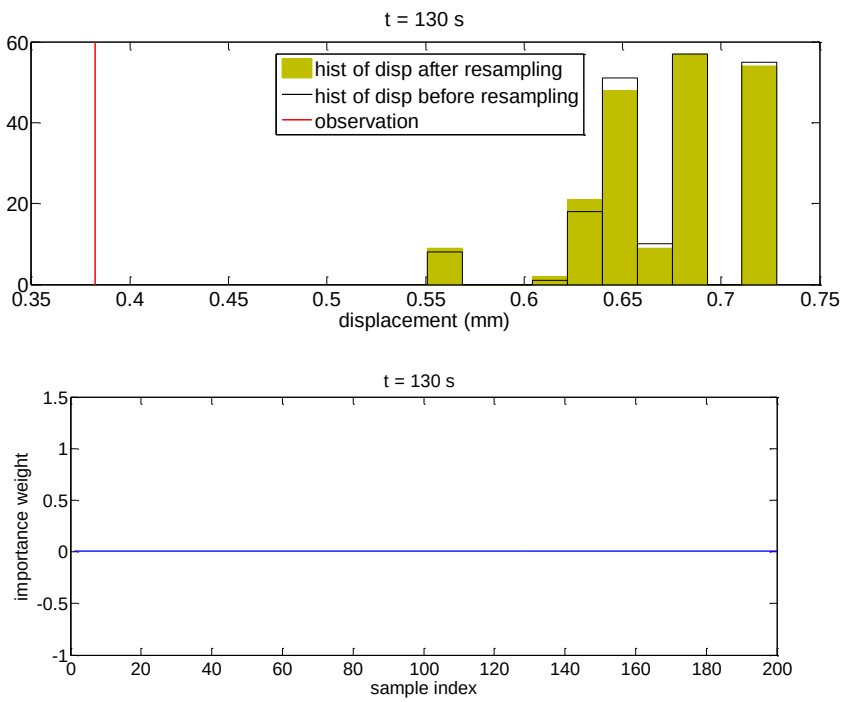

Figure 2-20: histogram of observable part of state vector (top) and associated samples weights (bottom) though from top it is seen that the sample cloud is quite far from observation neighborhood (vertical red line) consequently none of the particles find significant weights.

In what precedes, it has been shown that the proper choice of noise covariance has fundamental effects on the performance of PF. In case of dealing with one single parameter, it is not difficult to tune the filter; however, while dealing with more parameters, finding the right combination might become difficult. To address the issues induced by simultaneous track of the three parameters shown in Figures 2-11 to 2-14, for instance the step-function like behavior seen in Figure 2-14 when calibrating u_0, we focus on the state estimation time histories, see Figure 2-21, and consider the jump at $t = 34$ s. To have a closer look at what happens while this jump occurs, once again we make use of histogram of the distribution of the particles in two time instants: the beginning of the time step; the end of the time step. Before proceeding with this objective, let us review again the particle filter algorithm. The procedure is triggered by drawing a number of N_{P} samples from a Gaussian distribution, then at each time instant t_k the same number of samples are drawn from transition prior. By transition prior we mean a Gaussian distribution which it's mean equals to the value of evolved estimated state at previous time step t_{k-1} while it's

covariance equals to the covariance of the process noise. This procedure practically is equal to generation of N_{P} Gaussian random numbers, and adding to them the value of $\boldsymbol{x}_k$ which is evolved through evolution function. In the next stage, the probability of realization of each sample is computed. In this study, it is assumed that observation equation is contaminated by a white Gaussian process, hence calculation of the probability of realization of each particle would be a function of a norm of the distance of the particle from the observation. The functional form of a multivariate Gaussian distribution reads:

$$p(\boldsymbol{z}) = \frac{1}{\sqrt{2\pi|\boldsymbol{\Sigma}|}} e^{-\frac{1}{2}(\boldsymbol{z}-\boldsymbol{\mu})^T \boldsymbol{\Sigma}^{-1}(\boldsymbol{z}-\boldsymbol{\mu})} \tag{2.52}$$

where: $\boldsymbol{\mu}$ and $\boldsymbol{\Sigma}$ denote mean and covariance of the state vector, respectively; $|\,.\,|$ stands for the determinant of the matrix. Within the PF algorithm, the above mentioned formula is used to compute the probability of realization associated with each particle $\boldsymbol{x}_k^{(i)}$, according to:

$$p\left(\boldsymbol{y}_k|\boldsymbol{x}_k^{(i)}\right) = \frac{1}{\sqrt{2\pi|\boldsymbol{W}|}} e^{-\frac{1}{2}\left(\boldsymbol{y}_k-\boldsymbol{h}_k\left(\boldsymbol{x}_k^{(i)}\right)\right)^T \boldsymbol{W}^{-1}\left(\boldsymbol{y}_k-\boldsymbol{h}_k\left(\boldsymbol{x}_k^{(i)}\right)\right)} \tag{2.53}$$

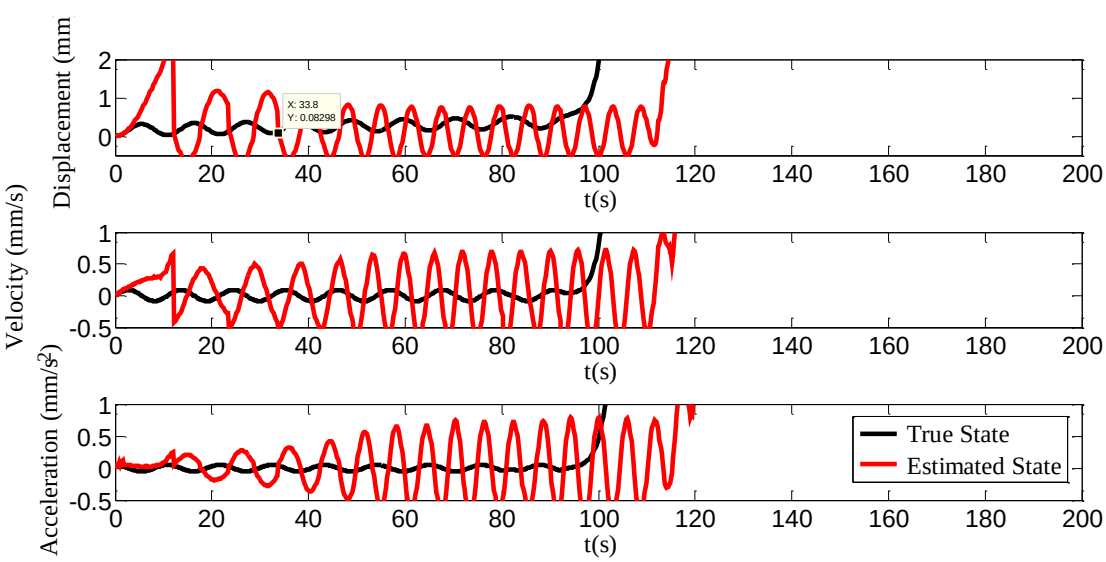

Figure 2-21: state estimation by PF, linear softening CL

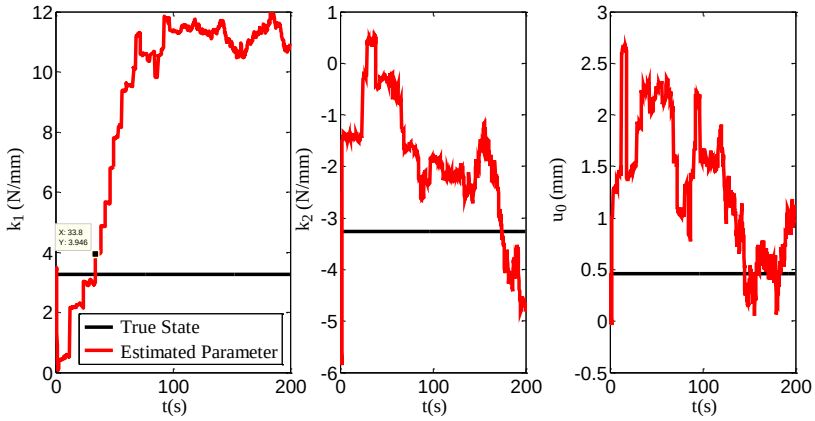

Figure 2-22: state estimation by PF, linear softening constitutive law

However, in case the observable part of the cloud of particles is too far from the observation $\boldsymbol{y}_k$, the calculated probability will equal zero due to round off errors. To cope with ill-conditioning, it is set to a small value. As a result, all the particles will find an equal weight. In this condition, at the resampling stage the resampled cloud will not change considerably, and would be like the already existing cloud of particles. If the observable part of the cloud of particles approaches to observation vicinity (i.e. the zone in which at least some of the probabilities are not affected by round-off error) a sharp change in the estimation of the state will occur. The gradient of such change in estimation of the observable part of state vector is obviously toward improvement in the estimate; however, the hidden (unobserved) part of state entries may or may not change in the direction to converge to an unbiased estimate, as seen in Figure 2-23.

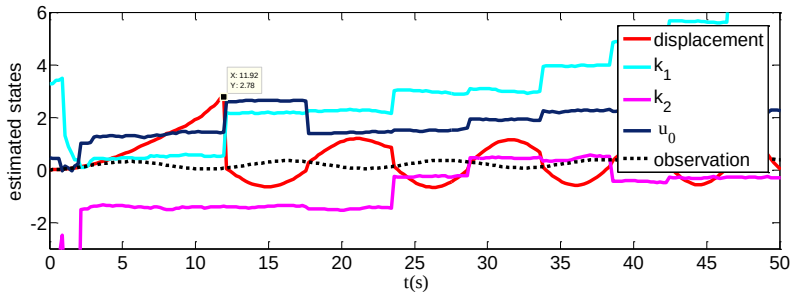

Figure 2-23: state and parameter estimation by use of PF

To visualize the phenomenon, the time evolution of displacement and parameters of the system are shown in the same plot, see Figure 2-23. Now we regard a few time intervals of interest, and look at the histograms of particles at some time instants picked before and after the jump, we keep the time instant $t = 11.92$ s as reference instant.

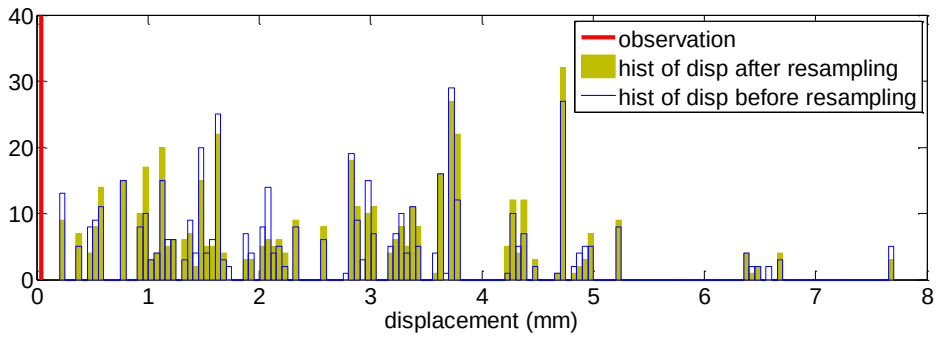

Figure 2-24: histogram of estimated displacements @ $t = 11.7$ s

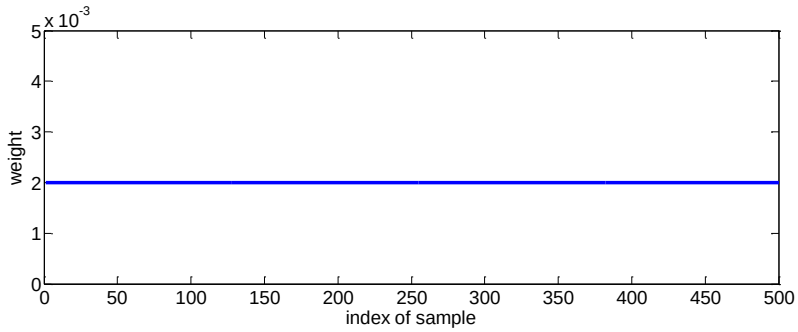

Figure 2-25: weights associated with each particle @ $t = 11.7$ s before resampling

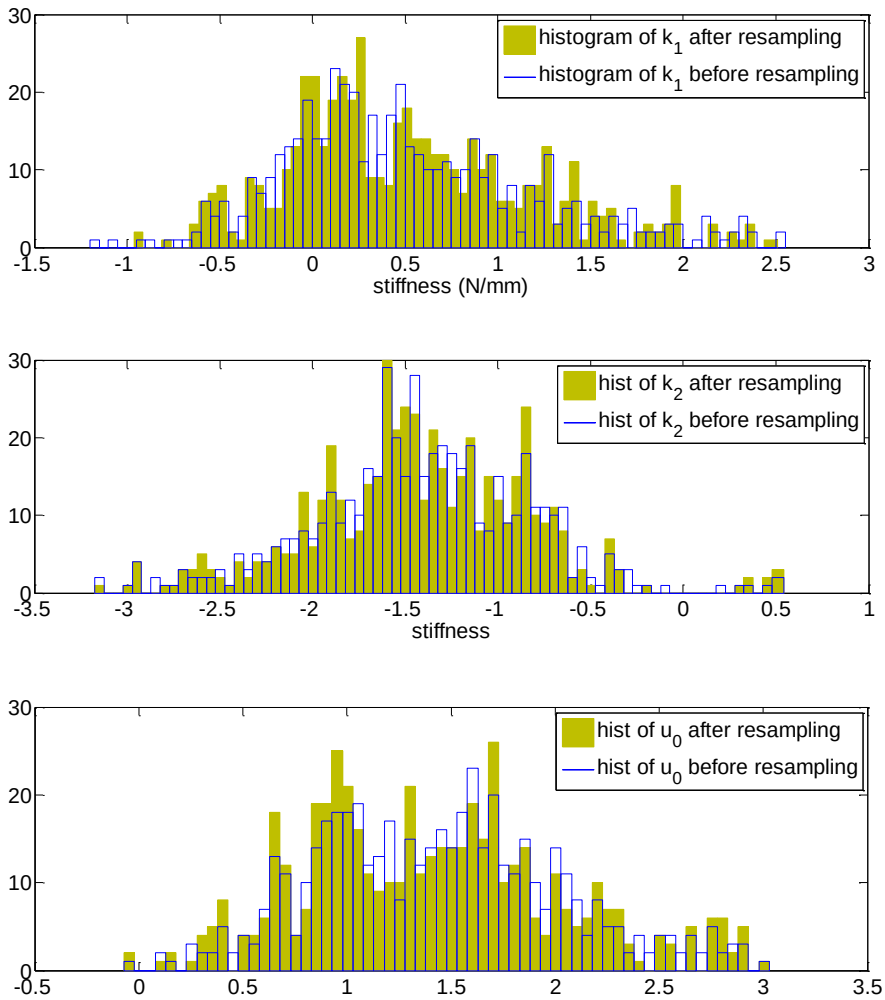

Figure 2-26: histogram of estimated parameters before and after resampling stage @ $t = 11.7$ s, top: k_1; middle: k_2; bottom: u_0

In Figure 2-24 it is seen that cloud of particles is not including the observation and the distance of the closest bin to the observation is about 0.2 mm. (the value of the observation is indicated by a red vertical bar in the graph). Consequently, all the probabilities become zero, due to the round-off errors. To cope with the problem of ill-conditioning caused by the zero probabilities, in case of a zero probability, it is set to the smallest value that the computer program used accounts for it. That is, all the particles find the same weight. Figures 2-26 shows the histograms of k_1, k_2 and u_0 respectively. As a consequence of the equal weights of the particles; it is seen that, before and after resampling stage, the histograms are not changed.

Now let us look at $t = 11.92$, plots included in Figures 2-27 to 2-29 look much like previous time instant $t = 11.7$ s, however it seems that the cloud of samples is now closer to observation, as seen Figure 2-27.

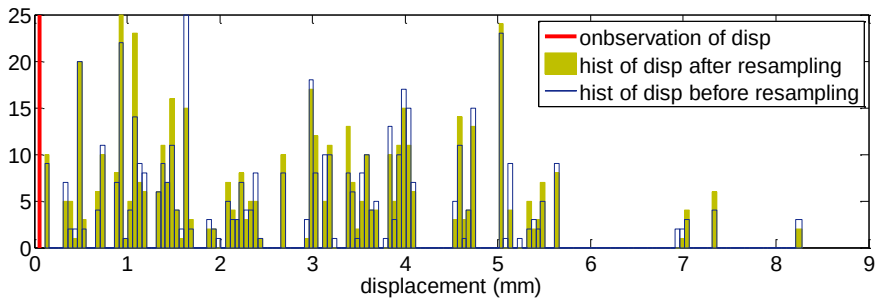

Figure 2-27: histogram of displacements @ $t = 11.92$ s

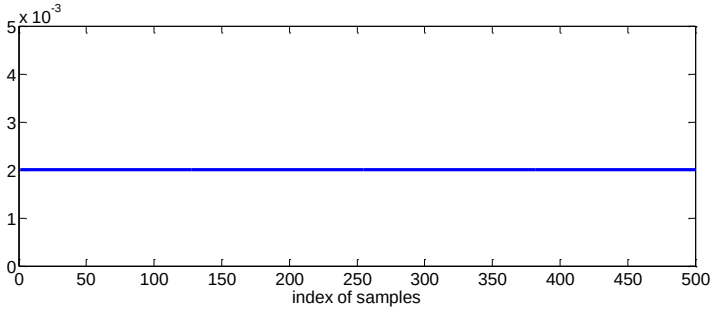

Figure 2-28: weights associated with each particle @ $t = 11.92$ s before resampling

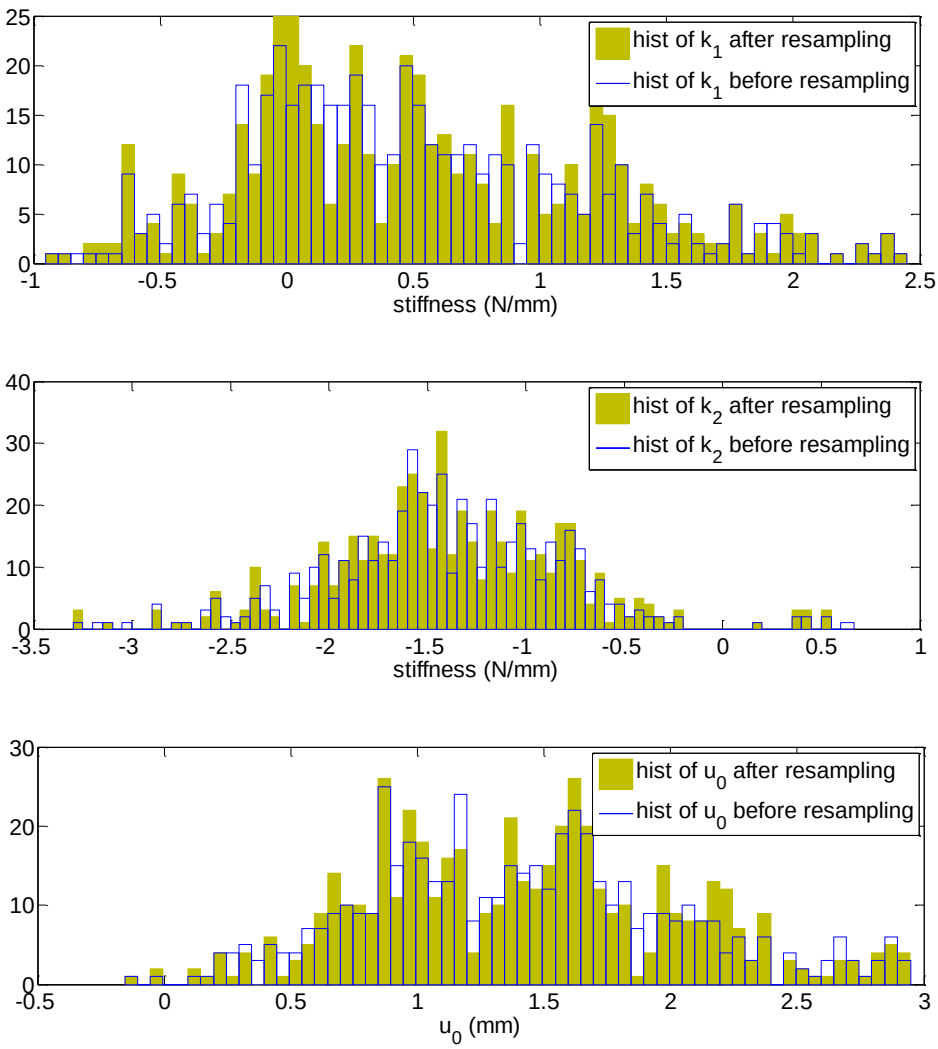

Figure 2-29: histograms of estimated parameters before and after resampling stage @ $t = 11.92$ s, top: k_1; middle: k_2; bottom: u_0

In what follows, histograms related to time instant $t = 12.13$ s are assessed. First see Figure 2-30, in which the histogram of displacements is shown. Again, the red bar signifies the value observation y_k at related time instant, at its intersection with horizontal axis. It is seen that they are scattered throughout a wide interval; however, some particles have approached observation vicinity, as close as required to have non-zero weights for a couple of the particles, see Figure 2-32.

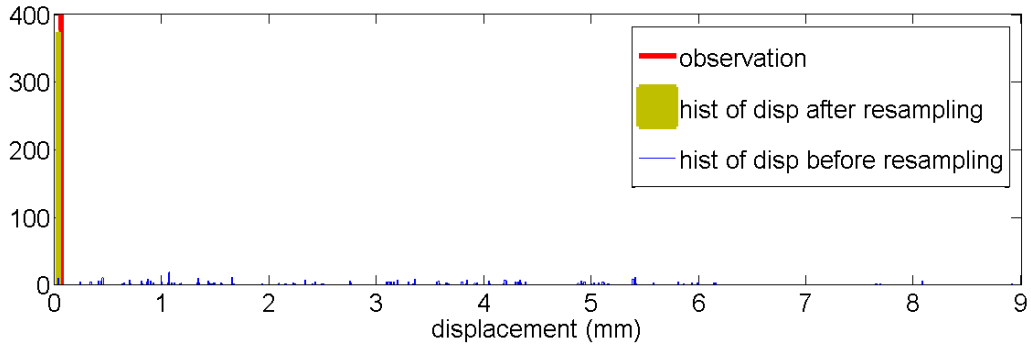

Figure 2-30: histogram of displacements @ $t = 12.13$ s

To have a more clear idea, in Figure 2-31 we have enlarged the vicinity of observation and histogram of resampled particles, in order to highlight the changes in the particle cloud after resampling stage. We have to remark that the plot is an enlargement also in ordinate. It is clearly seen that a few particles (represented via blue histogram) have reached quite close to observation (red bar) so that their associated weight has become significant (see Figure 2-32); as a consequence, in the resampling stage the particles far from observation neighborhood are eliminated, and the ones close to it are duplicated. Figure 2-32 shows the weights associated with each particle. The peaks in Figure 2-32 are the normalized weights associated with each particle, before the resampling stage. The closer ones have visible peaks; there are also some peaks which are not visible in Figure 2-32, once enlarged, also those become visible; however they are about ten (see Figure 2-33), almost negligible when compared with the number of particles, which in this case is 500.

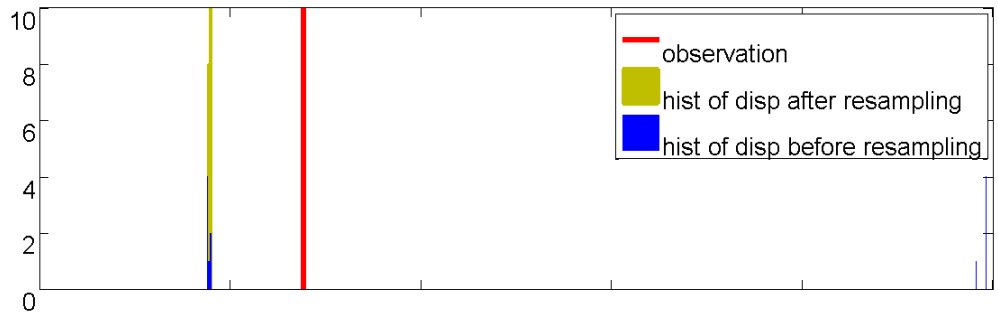

Figure 2-31: close up of histogram of displacements @ $t = 12.13$ s

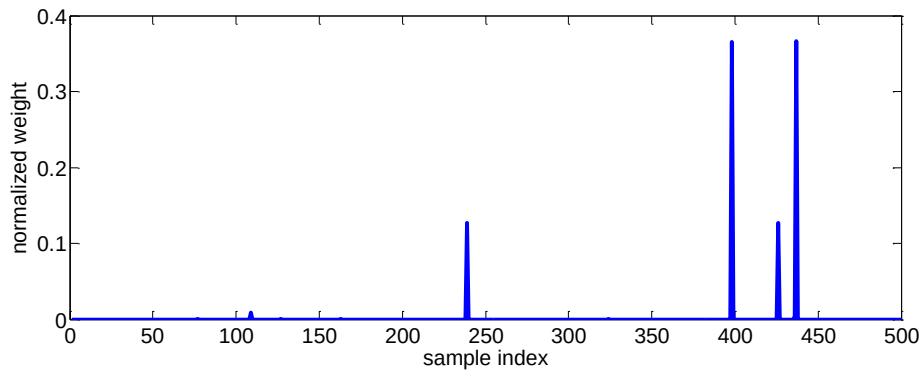

Figure 2-32: weights associated with each particle @ $t = 12.13$ s before resampling

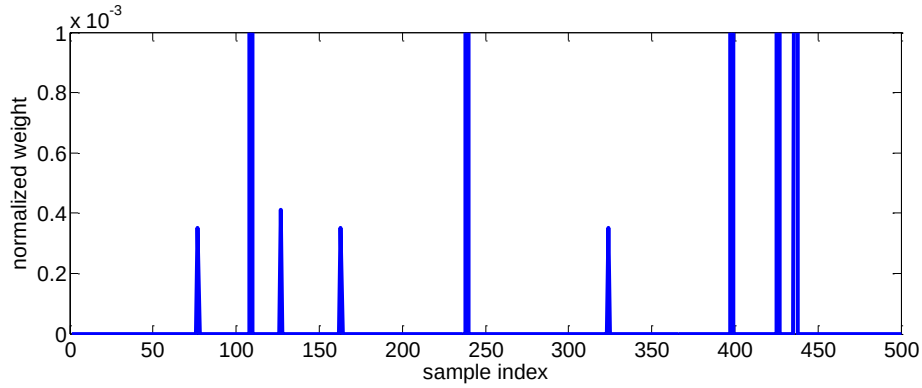

Figure 2-33: close up plot of weights associated with each particle @ $t = 12.13$ s before resampling

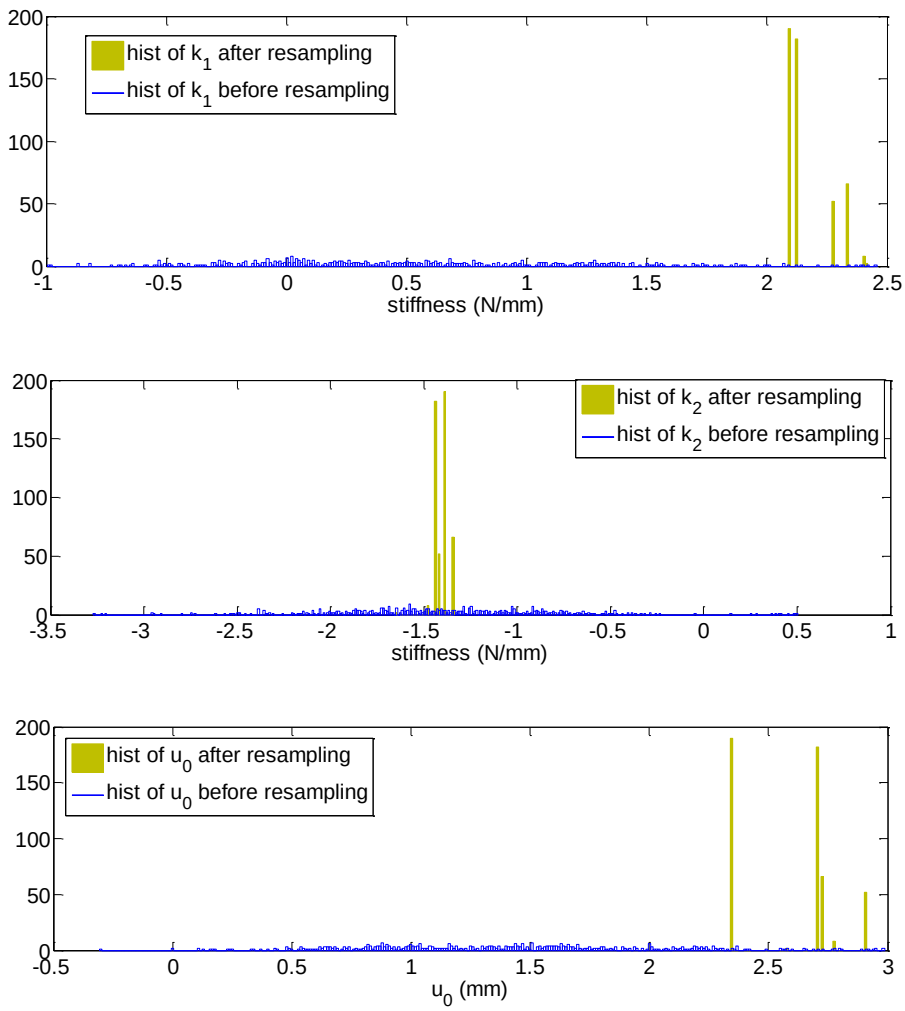

Figure 2-34: histogram of estimated parameters before and after resampling stage @ $t = 12.13$ s, top: k_1; middle: k_2; bottom: u_0

As it is seen in Figure 2-34, resampled particles do not necessarily move toward the target value; this is due to the fact that a wrong set of parameters has accompanied the shift of the samples toward the observation vicinity. Figure 2-34 well described the reason of failure of PF in estimating states and parameters, namely the distance of could of samples from observation vicinity. In order to alleviate such a problem, a remedy is to push the cloud of the samples toward observation vicinity. It can be done by use of the EKF: in each iteration, the EKF is used to update each particle by considering the information contained in the latest observation (de Freitas et al. 2000). More precisely, in the sampling stage, samples are drawn from the transition

prior; afterwards, each sample is updated by the EKF and so is pushed toward the observation vicinity. This approach alleviates to some extent the problems arouse by choosing a suboptimal sampling distribution, namely the transition prior. Figures 2-35, 2-36 and 2-37 show performance of a generic PF enhanced by EKF. It is seen that such approach substantially improves the estimate of the parameters of the system.

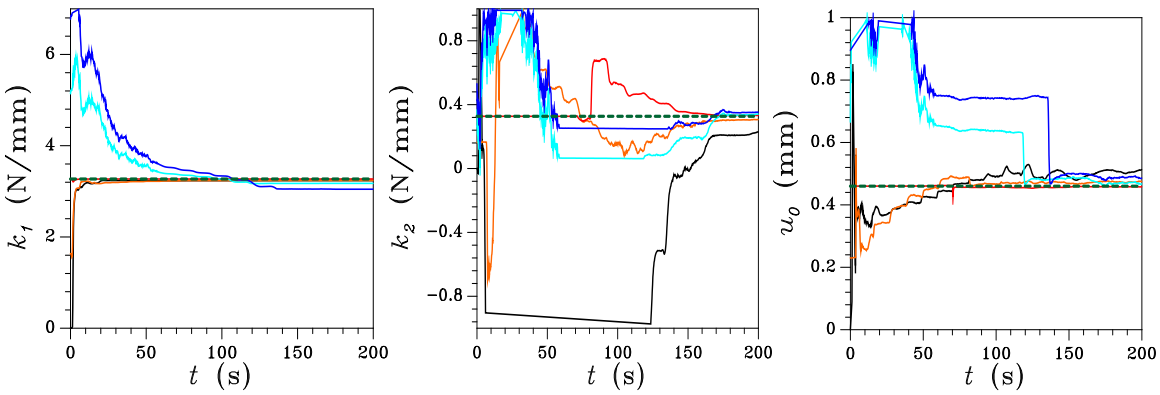

Figure 2-35: results of EK-PF for estimation of parameters of linear-hardening constitutive law

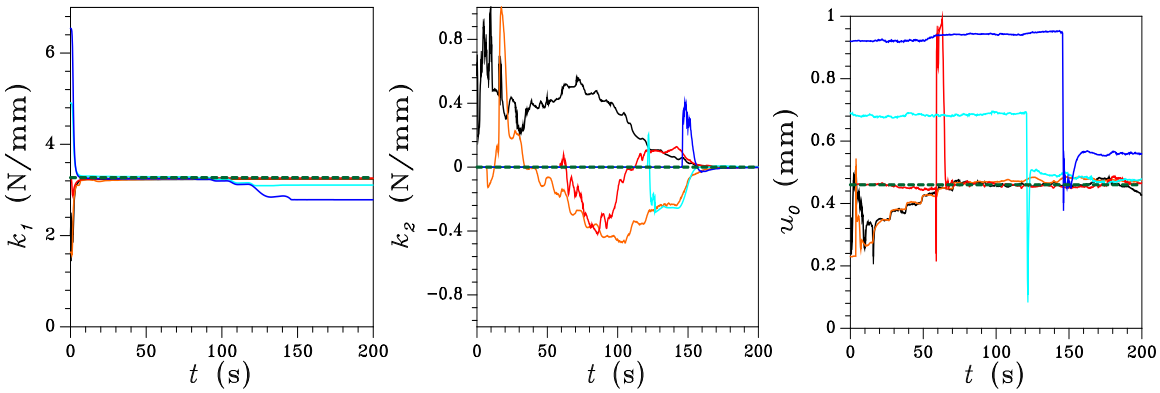

Figure 2-36: results of EK-PF for estimation of parameters of linear-plastic constitutive law

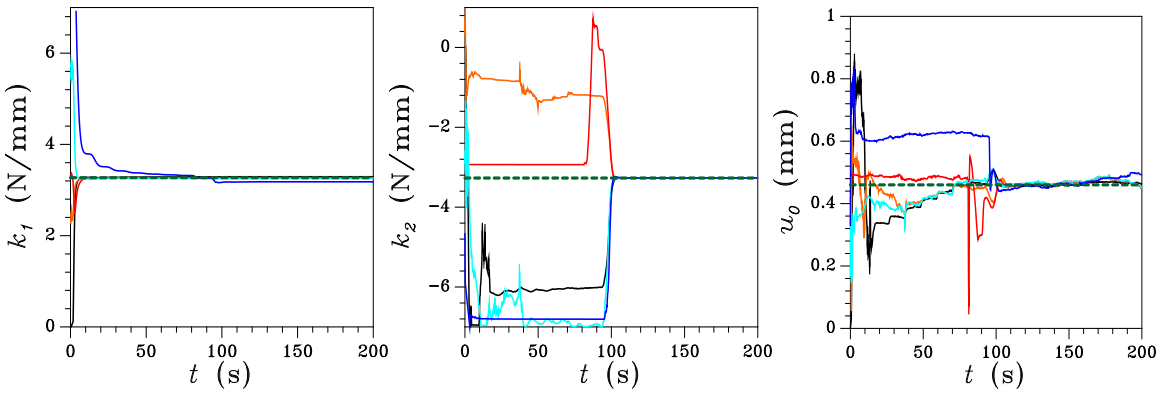

Figure 2-37: results of EK-PF for estimation of parameters of linear-softening constitutive law

To allow a clear understanding of the algorithm, let us look more closely at Figure 2-37. Filter results from the initialization at 50 % of the target values is chosen just as an example. Figures 2-38 and 2-39 show the state and parameter estimation obtained through the EK-PF. It is seen that an excellent convergence is achieved. Figure 2-40 supports the idea that, by updating each individual particle within cloud of samples via EKF, the ensemble has to approach the zones of high probability.

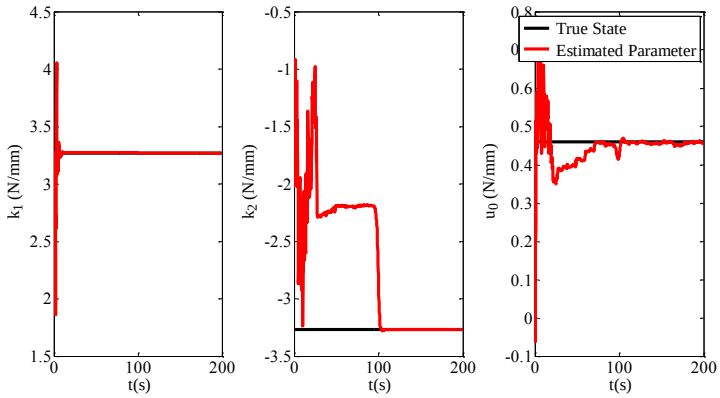

Figure 2-38: parameter estimation via EK-PF for a linear softening constitutive law

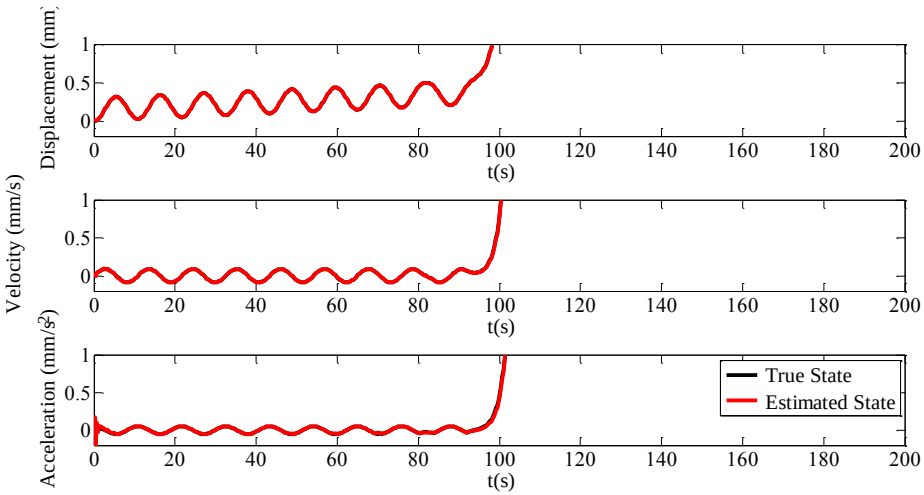

Figure 2-39: state estimation via EK-PF for a linear softening constitutive law

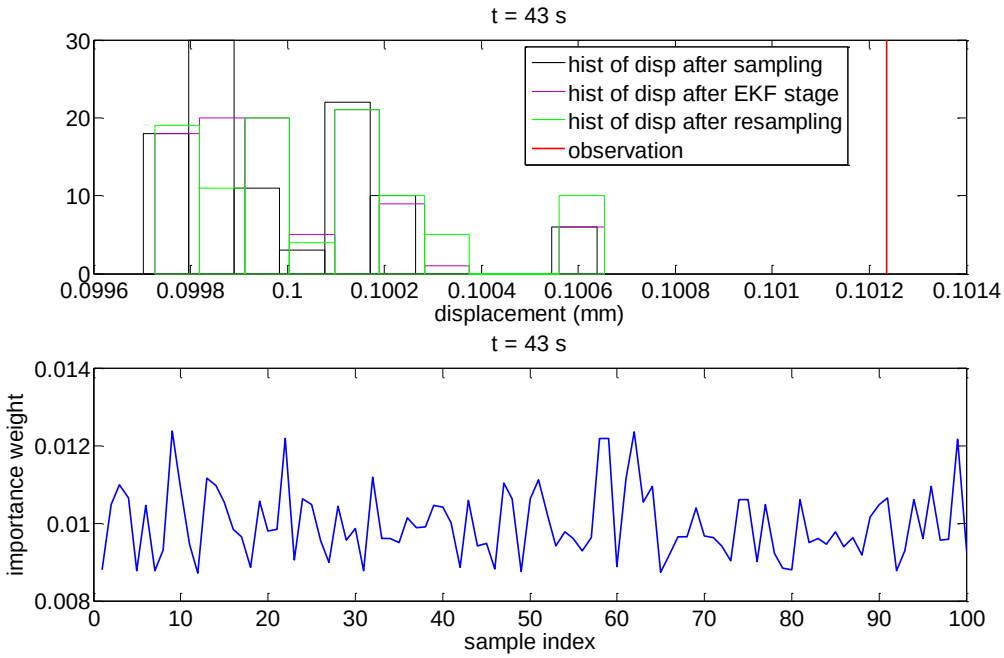

Figure 2-40: top: histograms of displacement of the system at sampling (black hist.), after EKF implemented on each sample (magenta hist.) and after resampling stage (green hist.), bottom: associated importance weight with each particle

As one can see in Figure 2-40, after the EKF stage is implemented the cloud of the samples drawn in the sampling stage, moves toward the red bar (observation vicinity). In the resampling stage, the particles with higher probabilities are duplicated, and the ones with lower probability

are eliminated; consequently, the cloud of the samples once again approaches the observation vicinity. Assessing other time instants always reveals the same results.

An extensive assessment of the performances of the Bayesian filters, when dealing with highly nonlinear dynamics of a SDOF system, has been presented. Though the studied mechanical system has only one degree-of-freedom, the extended state vector has three state components (displacement, velocity and acceleration) and 2 or 3 parameters (in case of a exponential softening constitutive law two parameters are to be calibrated, whereas in a bilinear one three parameters exist), consequently the extended state vector is multivariate even in present case. It was observed that EKF, SPKF and PF all fail to furnish satisfactory results concerning identification of the parameters of the system, whereas EK-PF provides quite good estimation of the states and parameters: for the exponential behavior of the spring the results are unbiased for a wide range of initializations; for the bilinear spring behavior EK-PF, in some cases it converges to unbiased solutions, and in some others it converges to values affected by small biases.

2.6.2 Multi degrees-of-freedom dynamic system

In this Section, dual estimation of state and parameters of a shear type building is studied, as seen in Figure 2-41. To start with the most simple case, we focus on the linear elastic response. By neglecting dissipating phenomena, the governing equations of motion thus read:

$$\boldsymbol{M}\ddot{\boldsymbol{u}} + \boldsymbol{K}\boldsymbol{u} = \boldsymbol{F}(t) \tag{2.54}$$

where $\boldsymbol{M}$ and $\boldsymbol{K}$ denote the stationary mass matrix and stiffness matrix respectively:

$$\boldsymbol{M} = \begin{bmatrix} m_1 & & & \\ & m_2 & & \\ & & \ddots & \\ & & & m_n \end{bmatrix} \tag{2.55}$$

$$\boldsymbol{K} = \begin{bmatrix} k_1 + k_2 & -k_2 & & & \\ -k_2 & k_2 + k_3 & & & \\ & & \ddots & & \\ & & & k_{n-1} + k_n & -k_n \\ & & & -k_n & k_n \end{bmatrix} \tag{2.56}$$

whereas $\boldsymbol{F}(t)$ is the external loading vector; in general, $\boldsymbol{F}(t)$ can be any kind of loading. However, here we assume that it is a harmonic force applied to the top floor:

$$\boldsymbol{F}(t) = \begin{bmatrix} 0 \\ \vdots \\ 0 \\ \varrho \ \sin \omega t \end{bmatrix} \tag{2.57}$$

where ϱ and ω are the amplitude and the frequency of the excitation, respectively. To numerically solve (2.54), the Newmark explicit time integrator has been used, see equations (2.40) to (2.44).

To write the equations in a discrete state-space form, we introduce an extended state $\boldsymbol{z}$ that, at each time instant t_k, includes $\boldsymbol{u}$, $\dot{\boldsymbol{u}}$ and $\ddot{\boldsymbol{u}}$ according to:

$$\boldsymbol{z}_k = \begin{bmatrix} \boldsymbol{u}_k \\ \dot{\boldsymbol{u}}_k \\ \ddot{\boldsymbol{u}}_k \end{bmatrix} \tag{2.58}$$

The state-space form of (2.54) then reads:

$$\boldsymbol{z}_k = \boldsymbol{A}_k \boldsymbol{z}_{k-1} + \boldsymbol{B}_k \tag{2.59}$$

where:

$$\boldsymbol{A}_k = \begin{bmatrix} \boldsymbol{I} - \beta\, \Delta t^2 \boldsymbol{M}^{-1}\boldsymbol{K} & \Delta t\, \boldsymbol{I} - \beta\, \Delta t^3 \boldsymbol{M}^{-1}\boldsymbol{K} & -\beta\left({}^1\!/_2 - \beta\right) \Delta t^4 \boldsymbol{M}^{-1}\boldsymbol{K} + \Delta t^2 \left({}^1\!/_2 - \beta\right) \boldsymbol{I} \\ -\gamma\, \Delta t\, \boldsymbol{M}^{-1}\boldsymbol{K} & \boldsymbol{I} - \gamma\, \Delta t^2 \boldsymbol{M}^{-1}\boldsymbol{K} & -\gamma\left({}^1\!/_2 - \beta\right)\Delta t^3 \boldsymbol{M}^{-1}\boldsymbol{K} + \Delta t (1-\gamma)\, \boldsymbol{I} \\ -\boldsymbol{M}^{-1}\boldsymbol{K} & -\Delta t\, \boldsymbol{M}^{-1}\boldsymbol{K} & -\Delta t^2 \left({}^1\!/_2 - \beta\right) \boldsymbol{M}^{-1}\boldsymbol{K} \end{bmatrix} \tag{2.60}$$

and :

$$\boldsymbol{B}_k = \begin{bmatrix} \beta\, \Delta t^2 \boldsymbol{M}^{-1}\, \boldsymbol{R}_k \\ \gamma\, \Delta t\, \boldsymbol{M}^{-1} \boldsymbol{R}_k \\ \boldsymbol{M}^{-1} \boldsymbol{R}_k \end{bmatrix} \tag{2.61}$$

In this study, it is assumed that displacements and accelerations of the floors can be measured, hence the observation equation reads:

$$\boldsymbol{y}_k = \boldsymbol{H}\boldsymbol{z}_k + \boldsymbol{w}_k \tag{2.62}$$

where: $\boldsymbol{H}$ denotes a Boolean matrix of appropriate dimension, which links the observation process to the state of the system; $\boldsymbol{w}_k$ denotes the associated measurement noise; β and γ are parameters of the Newmark integration algorithm. For the dual estimation, the model parameter vector results:

$$\boldsymbol{\vartheta} = \begin{bmatrix} k_1 \\ k_2 \\ \vdots \\ k_n \end{bmatrix} \tag{2.63}$$

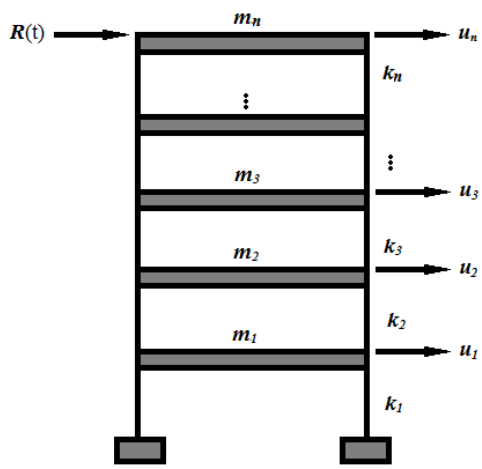

Figure 2-41: schematic view of a shear building

In the numerical analysis we deal with a multiple-story shear building, featuring the same stiffness and mass values at each floor. We start by considering the smallest possible number of floors (say two), and see how many parameters are calibrated unabiasedly. In this regard, we assume $m_i = 25$ kg and $k_i = 300$ kg/m $(i = 1{:}n)$. The outcomes of state estimation and

parameter calibration are a function of the quality and quantity of the information provided to the algorithms; by *quality* we intend the accuracy of measurement devices, accuracy of the model of the system and initialization guess; by *quantity* the number of degrees of freedom, whose evolution in time is measured, is intended.

This work focuses on the study of the effects of an increasing number of parameters in dual estimation of multi-dimensional mechanical systems. It has to be highlighted that the observable quantity is considered to be the displacement of the top floor only. Covariance of the measurement noise is assumed to be $2.7\ 10^{-6}\ \mathrm{m}^2$; the initial covariance of states (displacement, velocity and acceleration) is supposed to be very small ($10^{-10}\ m^2$), whereas diagonal entries of initial covariance of unknown parameters are assumed to be $10\frac{kg^2}{m^2}$. In all the analyses, the covariance of the fictitious noise for tuning the parameters is set to $10^{-3}\ \frac{kg^2}{m^2}$. Since states are always tracked unabiasedly, for the sake of brevity relevant results are not reported.

To ensure the algorithm has reached an unbiased estimate, it is a common practice to run analysis starting from different initializations; in case all converge to the same estimate, then it might be most likely an unbiased estimate. In this case we initialize the analyses by values 50% less and 50% more than target value. We begin our numerical assessment by study of a two DOF structure and report the results of parameter estimation in Figure 2-42: it is seen that two filters show the same performances. In EK-PF procedure 20 particles are deployed; by increasing the number of particles to 200, changes are visible in the plots of Figure 2-42. Hence number of the particles was fixed to 20.

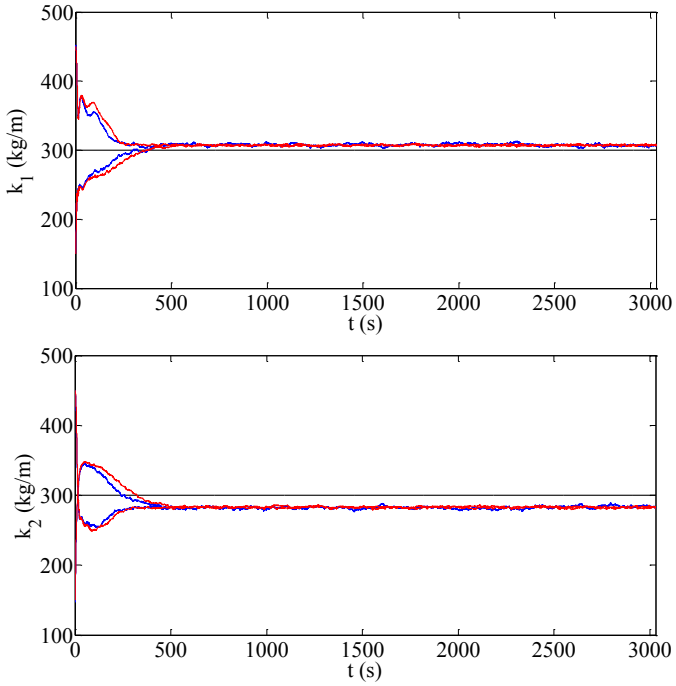

Figure 2-42: EKF (red line) and EK-PF (blue line) performances for calibration of a two-storey shear building stiffness's. the black line always represents the target value

Though by increasing the number of particles toward infinity, particle filter can furnish unbiased estimates (Cadini, Zio & Avram 2009), in practice such a number of particles may be intractable for current power of computational tools. By increasing the number of unknown parameters, it is seen that the bias in the estimates becomes more visible. In Figure 2-43 it is seen that again both EKF and EK-PF show the same performance, however the bias in the estimates is increased when compared to a 2-DOF system. Moving to a 3-DOF and 4-DOF system, Figure 2-44 and 2-44 reports the results when three and four inter-storey stiffnesses has to be estimated, respectively. Comparing with the case of a 2-storey shear building, again the bias in the estimate of the parameters increases.

By exploring the literature concerning online methods for the identification of structures, one will see that most of it is focused on shear building structures with less than four stories (e.g. see (Chatzi, Smyth & Masri 2010, Gao, Lu 2006, Koh, See & Balendra 1995, Xie, Feng 2011)). We avoid showing the results concerning estimation of more complicated structures, since they

confirm the same trend seen in this reported part of the analysis. As the dimension of the state vector (hence the number of the parameters) increases, estimation of the parameters become more and more difficult; in the jargon of dynamic programming, such a problem is termed *curse of dimensionality* (Bellman 1957). Powell (Powell 2007) illustrates this issue via an intuitive examples: if state space has i dimensions and if each state component can take j possible values then we might have i^j possible states, i.e. by a linear increase in dimension of state vector the dimension of the space of possibilities increases exponentially.

A possible remedy, for problems featuring high dimensionalities, is represented by searching for a possible subspace capturing the main variation in data; in forthcoming Chapters, first applicability of Proper Orthogonal Decomposition (POD) is shown in constructing reduced order models, and afterwards such a model will be embedded in filtering schemes.

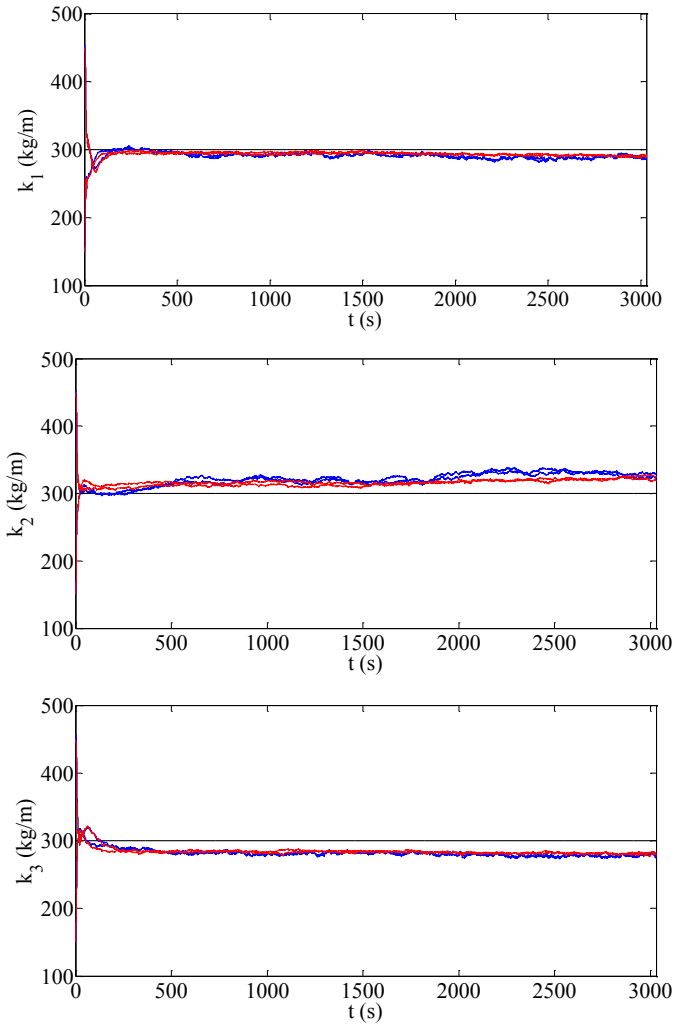

Figure 2-43: EKF (red line) and EK-PF (blue line) performances for calibration of a three-sotrey shear building stiffness's. the black line always represents the target value

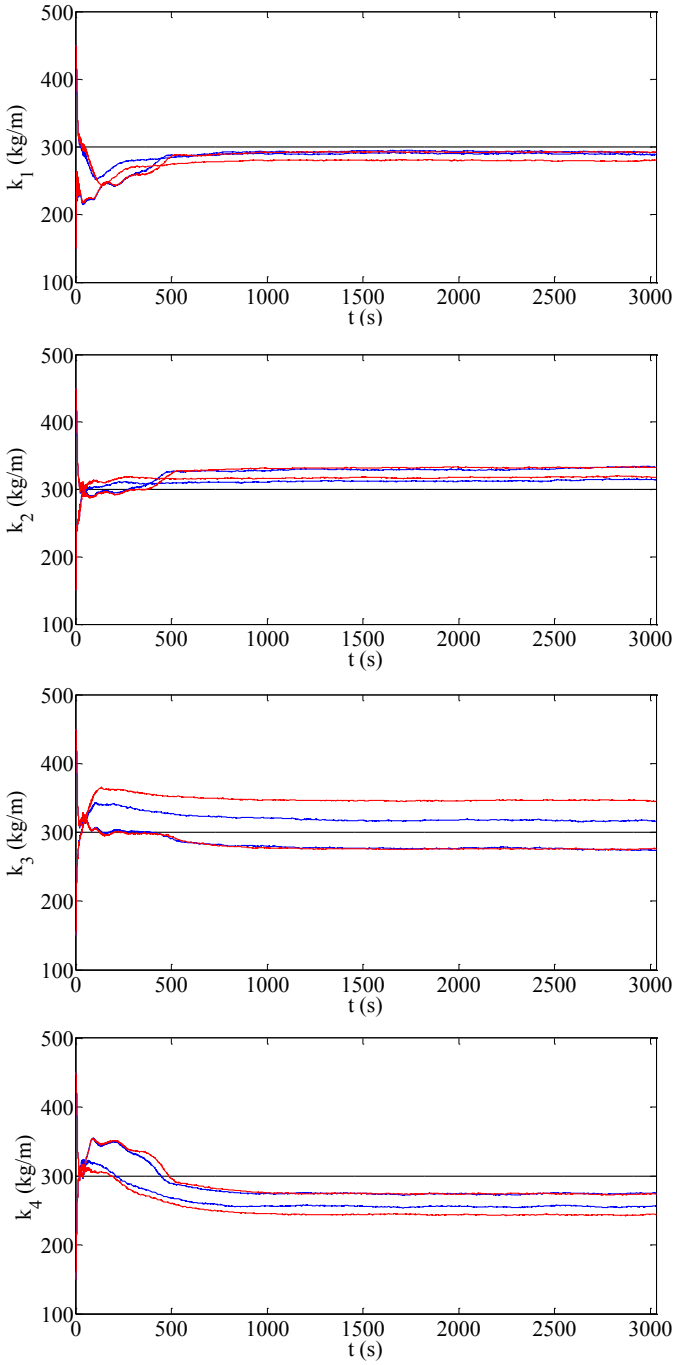

Figure 2-44: EKF (red line) and EK-PF (blue line) performances for calibration of a four-storey shear building stiffness's. the black line always represents the target value

2.7 Summary and conclusions

In this Chapter, recursive Bayesian inference of partially observed dynamical systems has been reviewed. As a tool for structural system identification, nonlinear Bayesian filters are applied to dual estimation problem of linear and nonlinear dynamical systems. Dealing with a SDOF structure, it has been shown that the hybrid EK-PF filter is able to furnish a good estimation of parameters of nonlinear constitutive models. Assessment of SDOF systems is followed by identification of multi storey buildings. In this regard, performances of the EK-PF and EKF algorithms are compared, and it has been concluded that they are almost the same, and by an increase in the number of storeys of the building the algorithms fail to provide an unbiased estimate of the parameters (stiffness of the storeys). Therefore, they are not reliable tools for monitoring state and parameters of multi storey systems.

To develop a robust algorithm for monitoring of health of the structures via recursive Bayesian inference, we would make recourse to model order reduction of the dynamic systems. To this end, next Chapter reviews important features of proper orthogonal decomposition and its application to model order reduction of dynamic systems.

Chapter 3: Model Order Reduction of dynamic systems via Proper Orthogonal Decomposition

3.1 Introduction

Dealing with a space discretized system, proper orthogonal decomposition (POD) automatically looks for a dependence structure between the degrees-of-freedom, which are normally assumed to be independent. This is achieved through a set of ordered, orthonormal bases, and through information concerning the relevant energy contents. POD has been developed independently by different scientists in different fields (see e.g.(Kosambi 1943, Karhunen 1947, Obukhov 1954)) and has been called with different names. When applied to finite dimensional systems, it is called principal component analysis (PCA) (Jolliffe 1986), its origins are found in the work of Pearson on plane and line fitting to point sets (Pearson 1901). When dealing with distributed parameter systems, it is named Karhunen–Loève decomposition (KLD); however, its discrete representation is also introduced (Fukunaga 1990). Another POD method is called singular value decomposition (SVD) (Mees, Rapp & Jennings 1978), novation of such method is attributed to Eckart and Young; where, they proposed extension of eigen value decomposition for general non square matrices (Klema, Laub 1980). For a detailed proof of equivalency of PCA, KLD and SVD readers may consult (Liang et al. 2002a).

Due to standard numerical tools developed for extracting proper orthogonal modes (POMs) of the systems, and due to its power in feature extraction and reduced modeling, POD is now extensively used in different engineering fields. For instance, it has been used for reduced order modeling of heat transfer phenomena (Samadiani, Joshi 2010), of computational fluid dynamics (Smith, Moehlis & Holmes 2005, Tadmor, Noack & Morzyński 2006), of micro electro

mechanical systems (Liang et al. 2002b) and other different fields of computational physics (Lucia, Beran & Silva 2004) and aeroelasticity (Thomas, Dowell & Hall 2003). The method of POD has gained popularity in the field of structural dynamics, where it is used for active sensing (Park et al. 2008) and active control of structures (Al-Dmour, Mohammad 2002), damage detection (De Boe, Golinval 2003, Galvanetto, Surace & Tassotti 2008, Shane, Jha 2011c), model updating (Lenaerts, Kerschen & Golinval 2003, Hemez, Doebling 2001), modal analysis (Han, Feeny 2003, Feeny 2002) and model reduction (Steindl, Troger 2001). For a review of pertinent literature readers are referred to (Kerschen et al. 2005). The work done in the literature suggests that POD is a strong tool for model order reduction of structural systems, however a specific study of speed-up, computational accuracy of the reduced model and robustness to the change in the source of excitation is missing. The work presented in this Chapter addresses those aforementioned issues.

In what follows, Section 3.2 reviews structural dynamics of systems that are studied in this Chapter, their associated set of governing differential equation and the numerical scheme used for time discretization. Section 3.3 reviews fundamentals of POD, and it is followed by section 3.4 which summarizes the fundamental works done in finding the links between POMs and eigen modes of linear structures. In Section 3.5 reduced model is constructed via Galerkin projection of the set of governing equations onto the reduced space spanned by POMs. Finally, Section 3.6 reports the results of the numerical assessment of efficiency of POD: speedup and accuracy of reduced models of Pirelli tower, as a case study, are investigated.

3.2 Structural dynamics and time integration

In this study, we exploit POD for reduced order modeling of dynamic systems. Such reduced model will be then embedded into a Bayesian filter in the forth-coming Chapters. In this section, we review the differential equations of the governing dynamics of structural systems studied herein; the numerical integration scheme used for time discretization of the aforementioned differential equations is briefly discussed.

Let the dynamic response of the structural system to the external loads be described by the following linear equations of motion:

$$\boldsymbol{M}\ddot{\boldsymbol{u}}(t) + \boldsymbol{D}\dot{\boldsymbol{u}}(t) + \boldsymbol{K}\boldsymbol{u}(t) = \boldsymbol{F}(t) \tag{3.1}$$

where: $\boldsymbol{M}$ is the mass matrix; $\boldsymbol{D}$ is the viscous damping matrix; $\boldsymbol{K}$ is the stiffness matrix; $\boldsymbol{F}$ is the time-dependent external force vector; $\ddot{\boldsymbol{u}}$, $\dot{\boldsymbol{u}}$ and $\boldsymbol{u}$ are the time-varying vectors of accelerations, velocities and displacements, respectively. For instance, in a shear model of a building (like the one adopted in Section 2.6) these vectors gather the lateral displacements, velocities and accelerations of the storeys.

Eq. (3.1) is usually arrived at once the structural system has been space discretized (e.g. through finite elements), or once assumptions concerning the behavior of the building (e.g. shear-type deformation) have taken into account. This preliminary stage of the analysis can affect the sparsity of matrices in Eq. (3.1), and can therefore have an impact on the speedup obtained through POD as well.

The solution of the vectorial differential equation (3.1) is here advanced in time by making use of the Newmark explicit integration scheme. For details the reader is referred to Section 2.6.

3.3 Fundamentals of Proper Orthogonal Decomposition for dynamic structural systems

The aim of reduced order modeling is to automatically find a solution to the following two conflicting requirements: create the smallest possible numerical model of the original dynamic system; preserve accuracy in the description of the system behavior. Standard techniques try to extract fundamental features from the dynamic model, so as the governing equations can be thereafter projected onto a reduced state space, or subspace.

POD, in its snapshot version (Sirovich 1987), is here adopted to build the model-specific optimal linear subspace on the basis of an ensemble of system observations. Let us consider the

displacement vector $\boldsymbol{u} \in \mathbb{R}^m$, $\mathbb{R}$ being the set of real numbers and m the dimension of vector $\boldsymbol{u}$; we assume that $\boldsymbol{u}$ effectively describes system evolution (i.e. it does not need to be supplemented by $\dot{\boldsymbol{u}}$ and $\ddot{\boldsymbol{u}}$ to define the full state space), and consider a set of arbitrary orthonormal bases $\{\boldsymbol{\varphi}_i\}$, $i = 1, \ldots, m$, spanning its vector space $\mathbb{R}^m$. Such bases satisfy $\boldsymbol{\varphi}_i^{\mathrm{T}} \boldsymbol{\varphi}_j = \delta_{ij}$ ($j = 1, \ldots, m$), where δ_{ij} is the Kronecker's delta (such that $\delta_{ij} = 1$ if $i = j$, otherwise $\delta_{ij} = 0$). The original vector $\boldsymbol{u}$ can then be written as a linear combination of the aforementioned bases, according to:

$$\boldsymbol{u} = \sum_{i=1}^{m} \boldsymbol{\varphi}_i \, y_i = \boldsymbol{\Phi} \boldsymbol{y} \tag{3.2}$$

where y_i are the combination coefficients, arranged in the column vector $\boldsymbol{y}$, and:

$$\boldsymbol{\Phi} = [\boldsymbol{\varphi}_1 \;\; \boldsymbol{\varphi}_2 \;\; \ldots \;\; \boldsymbol{\varphi}_m] \tag{3.3}$$

is the matrix gathering all the bases.

To ensure computational gain, we define a reduced representation of the state via:

$$\boldsymbol{u}_l = \sum_{i=1}^{l} \boldsymbol{\varphi}_i \, y_i = \boldsymbol{\Phi}_l \, \boldsymbol{\alpha} \tag{3.4}$$

where we enforce $l < m$ or, for large systems, even $l \ll m$. In (3.4), $\boldsymbol{\Phi}_l$ is the matrix gathering the first l columns of matrix $\boldsymbol{\Phi}$ (i.e. the first l bases), and $\boldsymbol{\alpha}$ collects the relevant first l components of vector $\boldsymbol{y}$. The goal of POD is to provide an ordered sequence of the bases $\boldsymbol{\varphi}_i$, so as to satisfy the following extreme value problem:

$$\min \|\boldsymbol{u} - \boldsymbol{u}_l\| \tag{3.5}$$

where $\|\blacksquare\|$ represents the L^2 norm of vector $\blacksquare$. Given l, Eq. (3.5) hence requires to find the optimal subspace spanned by the bases $\boldsymbol{\varphi}_1, \ldots, \boldsymbol{\varphi}_l$.

We now need to establish l on the basis of the required accuracy of the solution provided by the reduced order model, and to compute the bases gathered by $\boldsymbol{\Phi}_l$. Both problems can be attacked through the so-called snapshot version of POD. First, since we have to provide a subspace for the

state vector $\boldsymbol{u}$, the characteristic displacements $\boldsymbol{u}^{(k)} = \boldsymbol{u}(t_k)$ $(k = 1, \dots, n)$ at n time instants are computed and collected in an ensemble, or snapshot matrix $\boldsymbol{U}$, according to:

$$\boldsymbol{U} = \left[\boldsymbol{u}^{(1)} \ \boldsymbol{u}^{(2)} \dots \boldsymbol{u}^{(n)}\right] \tag{3.6}$$

Next PCA and SVD, two POD methods for extracting so-called POMs are briefly discussed.

3.3.1 Principal Component Analysis

To detect the main dependence structure in an ensemble of data, PCA looks for the subspace which is able to keep the maximum variability in the data. A very naïve justification of this procedures reads: in the state-space, the directions along which data vary are important, since the dynamics of the system is actually occurring along those directions, whereas the directions featuring no variations are redundant in the dynamic representation, and computational cost would be spent in calculating something that we already know if they were retained in the analysis. Consider the aforementioned vector $\boldsymbol{u} \in \mathbb{R}^m$; suppose $y_1, y_2, \dots, y_m \in \mathbb{R}$ are the first, second,… and m^{th} principal components respectively. Let the first principal component y_1 be a linear combination of each element of the original vector, i.e.:

$$y_1 = \sum_{i=1}^{m} \xi_{i1} u_i = \boldsymbol{\xi}_1^T \boldsymbol{u} \tag{3.7}$$

where: $\boldsymbol{\xi}_1 = \{\xi_{11}, \xi_{21}, \dots, \xi_{m1}\}^T$. The variance of y_1, assumed to be a random variable, is then:

$$S_{y_1}^2 = \boldsymbol{\xi}_1^T \ \boldsymbol{Z}_u \ \boldsymbol{\xi}_1 \tag{3.8}$$

where $\boldsymbol{Z}_u$ is the covariance of the variable $\boldsymbol{u}$, assumed to be random as well. To find the direction in which maximum variability of data is captured, we look for the direction in which the projection of the samples onto it yields maximum variance. The maximum of $S_{y_1}^2$ would not be achieved for a finite value of $\boldsymbol{\xi}_1$, so a constraint have to be imposed and reads:

$$\max_{\xi_1} \ (\boldsymbol{\xi}_1^T \boldsymbol{Z}_u \boldsymbol{\xi}_1), \quad s.t. \, (\boldsymbol{\xi}_1^T \boldsymbol{\xi}_1) = 1 \tag{3.9}$$

Introducing the Lagrangian multiplier λ_1, from (3.8) and (3.9) we get:

$$L(\boldsymbol{\xi}_1, \lambda_1) = \boldsymbol{\xi}_1^T \boldsymbol{Z}_u \boldsymbol{\xi}_1 + \lambda_1 (1 - \boldsymbol{\xi}_1^T \boldsymbol{\xi}_1) \tag{3.10}$$

where $L(\blacksquare)$ is Lagrangian operator. After differentiation, (3.10) gives:

$$\frac{\partial L(\xi_1, \lambda_1)}{\partial \xi_1} = 2(\boldsymbol{Z}_u - \lambda_1 \boldsymbol{I})\boldsymbol{\xi}_1 = 0 \;\; \Rightarrow \;\; \boldsymbol{Z}_u \boldsymbol{\xi}_1 = \lambda_1 \boldsymbol{\xi}_1 \tag{3.11}$$

where λ_1 and $\boldsymbol{\xi}_1$ are the eigenvalue and the corresponding eigenvector of the covariance matrix $\boldsymbol{Z}_u$, respectively.

Applying the same procedures, the objective function to be maximized in order to extract the principal components of a random variable writes:

$$\max_{\xi_i} \left(\sum_{i=1}^{m} \boldsymbol{\xi}_i^T \boldsymbol{Z_u} \boldsymbol{\xi}_i \right), \quad s.t. \left(\boldsymbol{\xi}_i^T \boldsymbol{\xi}_j \right) = \delta_{ij} \tag{3.12}$$

and the approximation error due to a representation by its first l principal components, $u \approx \sum_{i=1}^{l} y_i \boldsymbol{\xi}_i$, would be:

$$\varepsilon^2(l) = E(\|\boldsymbol{u} - \boldsymbol{u}(l)\|^2) = \sum_{i=l+1}^{m} E(y_i^2) = \sum_{i=l+1}^{m} S_{y_i}^2 \tag{3.13}$$

In order to compute the principal components, one has to handle the covariance matrix of the random vectorial variable. However, since in practical problems it is usually impossible to determine this covariance matrix, it is a common practice to use the correlation matrix as an acceptable approximation of it (Schilders 2008). To approximate the covariance matrix with the required accuracy, one needs an appropriately chosen ensemble of the samples; such a seed of samples is the so-called snapshot matrix, wherein each snapshot represents the state of the system at a specific time instant (see Figure 3-1).

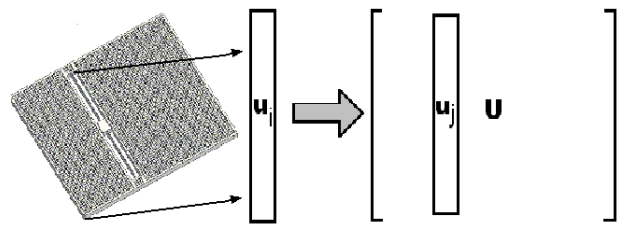

Figure 3-1: Building the matrix of snapshots.

The covariance of the data set, allocated in a snapshot matrix $\boldsymbol{U}$, is then calculated as (Schilders 2008):

$$\boldsymbol{Z}_u = \lim_{n\to\infty}(\widetilde{\boldsymbol{Z}}_u = \frac{1}{n}\boldsymbol{U}\boldsymbol{U}^T) \tag{3.14}$$

3.3.2 Singular Value Decomposition

Exploiting the singular value decomposition of the snapshot matrix $\boldsymbol{U}$ we get (Liang et al. 2002a):

$$\boldsymbol{U} = \boldsymbol{L}\,\boldsymbol{\Sigma}\,\boldsymbol{R}^{\mathrm{T}} \tag{3.15}$$

where: $\boldsymbol{L}$ is a $m \times m$ orthonormal matrix, whose columns are the left singular vectors of $\boldsymbol{U}$; $\boldsymbol{\Sigma}$ is a $m \times n$ pseudo-diagonal and semi-positive definite matrix, whose pivotal entries Σ_{ii} are the singular values of $\boldsymbol{U}$; $\boldsymbol{R}$ is a $n \times n$ orthonormal matrix, whose columns are the right singular vectors of $\boldsymbol{U}$.

The whole basis set $\boldsymbol{\Phi}$, i.e. the set of all the so-called POMs, is given by $\boldsymbol{L}$, i.e. by the left singular vectors of the snapshot matrix (Kerschen, Golinval 2002). If singular values Σ_{ii} are sorted decreasingly, and the columns of $\boldsymbol{L}$ and $\boldsymbol{R}$ are accordingly arranged, the decomposition (3.15) is such that the first l columns (with l given) of $\boldsymbol{\Phi} = \boldsymbol{L}$ represent the optimal basis subset that fulfills (3.5). Moreover, it is known (see, e.g. (Kerschen, Golinval 2002)) that the ith

singular value squared (i.e. Σ_{ii}^2) represents the maximum of the relevant oriented energy[1]; this means that the ith oriented energy is maximized, among all the possible unit vectors, by the basis $\boldsymbol{\varphi}_i$. Since we are looking for the most informative subspace, which should be able to furnish as much insight as possible into the dynamics of the original system and, therefore, into how energy fluxes take place inside it, we retain in the reduced order model the proper modes $\boldsymbol{\varphi}_i$ that feature the highest singular values. Additional proper modes, featuring less energy contents, would be redundant in the reduced order representation, and add computational costs with marginal enhancement in the accuracy.

Now, having established a way to sort bases $\boldsymbol{\varphi}_i$, and the link between the singular value Σ_{ii} and the energy content of the proper mode $\boldsymbol{\varphi}_i$, we need to set l. According to (Kerschen, Golinval 2002), we assign the required accuracy p of the reduced order solution, intended as a fraction of the total oriented energy of the full model, and select the dimension l of the subspace by fulfilling:

$$\frac{\sum_{i=1}^{l} {\Sigma_{ii}}^2}{\sum_{i=1}^{m} {\Sigma_{ii}}^2} \geq p \tag{3.16}$$

hence, on the basis of the ratio between the sum of the singular values of the kept modes and the sum of all the singular values.

[1] The oriented energy of a vector along a direction is given by the magnitude of the projection of the (m −dimensional) vector itself onto the mentioned direction, namely by the dot product of the two vectors. When we have to deal with a vector sequence like $\boldsymbol{U}$, the oriented energy of the sequence is given by the sum of the magnitudes of the projections of all the vectors $\boldsymbol{u}^{(k)}$ onto the same direction.

3.4 Physical interpretation of proper orthogonal modes

It is known that POD is a statistical technique that extracts POMs from the response of the system. However, a close relationship has been established between POMs and natural eigen-modes of a mechanical system (Feeny, Kappagantu 1998, Kerschen, Golinval 2002). The effort toward establishing a link between POMs and eigen-modes of the system intends in making POD a modal identification tool (Yadalam, Feeny 2011). To this end, theoretical and experimental work has been done to link POMs with eigen-modes of a linear (Feeny 2002) and nonlinear (Georgiou 2005) mechanical systems. In this Section, we do not discuss the details offered by existing literature and only mean to summarize interesting findings published therein.

Free vibrations of an undamped linear system, with mass matrix proportional with identity matrix (e.g. a shear building with equal masses at each storey) results in a set of POMs that asymptotically converge to eigen-modes of the system. POMs of a lightly damped similar system are a good approximation of eigen-modes of the system (Kerschen, Golinval 2002), however in case of forced harmonic vibration there is no guarantee that POMs converge to eigen-modes.

When the system resonates at a certain frequency, independently of mass matrix entries, the POMs coincides with the respective eigen-modes of that frequency (Kerschen et al. 2005). It has been shown that POMs coincide with eigen-modes for many noise driven oscillators (Preisendorfer 1979), moreover, North has established a general criteria for symmetry of POMs and eigen-modes of the mechanical systems excited by noise (North 1984).

3.5 Galerkin projection

Once POD has furnished the required subspace, the displacement vector can be approximated through $\mathbf{u}_l$. Since matrix $\boldsymbol{\Phi}_l$ is a function of the position vector only, and defines the shapes of POMs for the structure, while $\boldsymbol{\alpha}$ governs the evolution in time of the structural response, it follows that:

$$\ddot{\boldsymbol{u}} \approx \boldsymbol{\Phi}_l \ddot{\boldsymbol{\alpha}} \quad \dot{\boldsymbol{u}} \approx \boldsymbol{\Phi}_l \dot{\boldsymbol{\alpha}} \quad \boldsymbol{u} \approx \boldsymbol{\Phi}_l \boldsymbol{\alpha} \tag{3.17}$$

The equations of motion (3.1), allowing for (3.17), can now be approximately stated as:

$$\boldsymbol{M}\boldsymbol{\Phi}_l\ddot{\boldsymbol{\alpha}}(t) + \boldsymbol{D}\boldsymbol{\Phi}_l\dot{\boldsymbol{\alpha}}(t) + \boldsymbol{K}\boldsymbol{\Phi}_l\boldsymbol{\alpha}(t) \cong \boldsymbol{F}(t) \tag{3.18}$$

By defining the residual $\boldsymbol{r}$ of such approximation as:

$$\boldsymbol{r} = \boldsymbol{F}(t) - (\boldsymbol{M}\boldsymbol{\Phi}_l\ddot{\boldsymbol{\alpha}}(t) + \boldsymbol{D}\boldsymbol{\Phi}_l\dot{\boldsymbol{\alpha}}(t) + \boldsymbol{K}\boldsymbol{\Phi}_l\boldsymbol{\alpha}(t)) \tag{3.19}$$

within a Galerkin projection frame (Steindl, Troger 2001), we enforce it to be orthogonal to the subspace $\boldsymbol{\Phi}_l$ spanned by the solution, i.e.:

$$\boldsymbol{\Phi}_l^{\mathrm{T}}\boldsymbol{r} = \boldsymbol{0} \tag{3.20}$$

Hence, the equations of motion of the reduced order model turn out to be:

$$\boldsymbol{\Phi}_l^{\mathrm{T}}\boldsymbol{M}\boldsymbol{\Phi}_l\ddot{\boldsymbol{\alpha}}(t) + \boldsymbol{\Phi}_l^{\mathrm{T}}\boldsymbol{D}\boldsymbol{\Phi}_l\dot{\boldsymbol{\alpha}}(t) + \boldsymbol{\Phi}_l^{\mathrm{T}}\boldsymbol{K}\boldsymbol{\Phi}_l\boldsymbol{\alpha}(t) = \boldsymbol{\Phi}_l^{\mathrm{T}}\boldsymbol{F}(t) \tag{3.21}$$

or, equivalently:

$$\boldsymbol{M}_l\ddot{\boldsymbol{\alpha}}(t) + \boldsymbol{D}_l\dot{\boldsymbol{\alpha}}(t) + \boldsymbol{K}_l\boldsymbol{\alpha}(t) = \boldsymbol{F}_l(t) \tag{3.22}$$

Once the solution of (3.22) is obtained, the full state of the system can be computed by making use of (3.17).

Figure 3-2: The Pirelli Tower.

3.6 Results: Reduced-order modeling of a tall building excited by earthquakes

For linear systems, it would be beneficial if POMs $\boldsymbol{\varphi}_i$ depend only on physical and geometrical properties of the structure, with marginal effects of the kind of loading considered in the phase of construction of the snapshot matrix. Since different loading conditions may excite a different set of structural vibration modes, what claimed here above does not necessarily hold true. Though a thorough analysis of theoretical aspects of POD, when applied to structural systems, has been carried out in the literature, only a handful of work is available on some practical points including the load-dependency of POMs. Such issue may become crucial, especially when the structure is subject to seismic loadings, which are difficult to predict in nature.

The performance of POD has been already assessed in defining reduced models for multi-support structures subject to seismic excitation (Tubino, Carassale & Solari 2003); also, POD has been applied for efficient reduced modelling of high-rise buildings subject to earthquake loads (Gutiérrez, Zaldivar 2000, Aschheim, Black & Cuesta 2002). However, its efficiency for high fidelity reduced order modelling of multi-storey buildings trained by a certain seismic load and excited by another one, has not been done yet. In this section, we investigate whether a reduced order model, built by considering a specific input while constituting the snapshot matrix, can be

used to represent with a similar level of accuracy the dynamics of the full structure in case of different excitation, in terms e.g. of frequency content and, therefore, of excited vibration modes.

In the forthcoming numerical examples we will set $p > 0.99$ to ensure accuracy. As a case study, we investigate the capability of POD in speeding up the computations by considering the Pirelli Tower in Milan, see Figure 3-2. The building features 39 stories, and its total height is about 130 m. The plan dimensions of the standard floor are approximately 70×20 m. The structure is entirely made of CIP reinforced concrete. The structure is assumed to behave elastically, with lumped masses at each storey that basically undergo horizontal displacements. Such an assumption might be far from reality if the rigid diaphragm assumption does not hold true for vertical displacements of all the nodes at the same floor.

We start with a three-dimensional finite element discretization of the whole building featuring 6219 DOFs (Barbella, Perotti & Simoncini 2011). For the sake of simplicity we have neglected the damping effect; so, in a relative frame moving with the basement of the tower, the undamped equations of motion of the structure read:

$$\boldsymbol{M}\ddot{\boldsymbol{u}} + \boldsymbol{K}\boldsymbol{u} = -\,a(t)\boldsymbol{M}\boldsymbol{B} \tag{3.23}$$

where $a(t)$ denotes the earthquake-induced acceleration time history, whereas $\boldsymbol{B}$ is a Boolean matrix of appropriate dimension which defines the shacked DOFs. To simplify the problem, static condensation has been adopted to keep out the vertical displacements of the floors. By partitioning the nodal displacements $\boldsymbol{u}$ into horizontal $\boldsymbol{u}_h$ and vertical $\boldsymbol{u}_v$ components, we can write:

$$\begin{bmatrix} \boldsymbol{M}_h & \boldsymbol{0} \\ \boldsymbol{0} & \boldsymbol{M}_v \end{bmatrix} \begin{bmatrix} \ddot{\boldsymbol{u}}_h \\ \ddot{\boldsymbol{u}}_v \end{bmatrix} + \begin{bmatrix} \boldsymbol{K}_{hh} & \boldsymbol{K}_{hv} \\ \boldsymbol{K}_{vh} & \boldsymbol{K}_{vv} \end{bmatrix} \begin{bmatrix} \boldsymbol{u}_h \\ \boldsymbol{u}_v \end{bmatrix} = -\,a(t) \begin{bmatrix} \boldsymbol{M}_h\boldsymbol{B}_h \\ \boldsymbol{M}_v\boldsymbol{B}_v \end{bmatrix} \tag{3.24}$$

Keeping only the horizontal DOFs only in the equations of motion, to be thereafter managed by POD, we arrive at:

$$\boldsymbol{M}_h\ddot{\boldsymbol{u}}_h + [\boldsymbol{K}_{hh} - \boldsymbol{K}_{hv}\boldsymbol{K}_{vv}^{-1}\boldsymbol{K}_{vh}]\boldsymbol{u}_h = -\,a(t)\boldsymbol{M}_h\boldsymbol{B}_h \tag{3.25}$$

where now $\boldsymbol{u}_h \in \mathrm{R}^{39}$.

To obtain the reduced model, the building has been assumed to be shacked by the well-known El Centro earthquake, whose time *vs.* acceleration record, together with its relevant fast Fourier transform, is reported in Figure 3-3. To give an idea about the number of vibration modes that may be excited by such earthquake, the first natural eigen-frequencies of the structure (see also Table 3-1) are denoted by red vertical lines in Figure 3-3 (b). It can be deduced that only first five eigen-modes of structure can be effectively excited, as the power of the spectra of the accelerogram is intuitively seen to be small for the frequencies higher than the 6th natural frequency of the structure.

Table 3-1: First natural frequencies of the building.

vibration mode index	1	2	3	4	5	6	7	8	9	10	11	12	13
natural frequency (Hz)	0.26	1.09	2.61	4.71	7.07	8.79	9.56	9.92	11.38	13.36	14.64	18.30	22.14

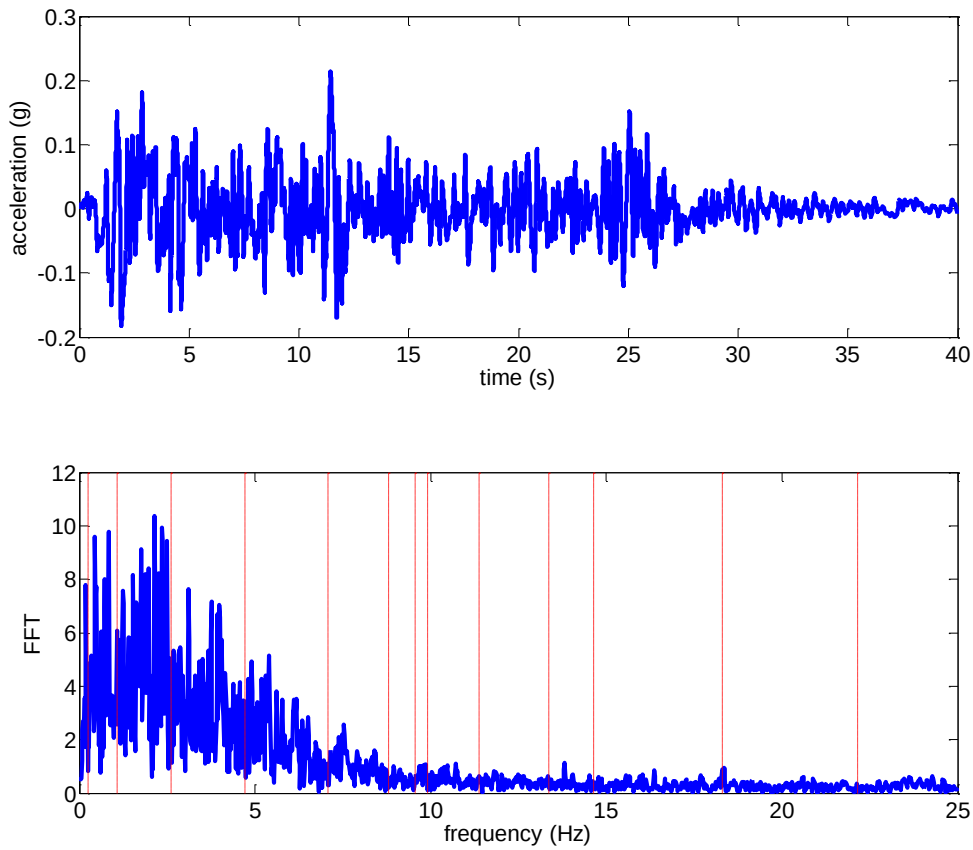

Figure 3-3: top: May 18–1940, El Centro accelerogram (east-west direction) and bottom: relevant FFT.

A comparison among the dynamics of the original 39-DOF system and the responses of reduced order models at varying accuracy index p (see Eq. (3.20)) has been performed. The link between p and the retained DOFs in the reduced systems is reported in Table 3-2. The result reported in Figures 3-4 and 3-5 compare the time histories of (lateral) displacements, velocities and accelerations of the 20th and 39th (roof) floors, respectively, with the target values which are available from the simulations. In these plots, the blue vertical line indicates the end of the time window within which the snapshots are collected; hence, only around $t = 4$ s all the reduced order analyses start departing from the full model response.

To have a more clear view of the time histories, a close up of the last 5 s of the time histories of 20th floor is presented in Figure 3-6. By making a comparison between time histories of displacements, velocities and accelerations, it can be seen that two POMs are enough for a

reduced model to accurately reproduce displacements of the full model; however, at least four POMs are necessary to feature the same level of accuracy for velocities and accelerations too. By investigating the FFTs of the aforementioned time histories (see Figures 3-7, 3-8 and 3-9), it is shown that in the FFT of the displacement time histories, only two first natural modes are effectively excited. Instead, in the velocity and acceleration time histories, looking at the FFTs it is seen that six and seven first natural frequencies are effectively excited. Such a trend suggests that a reduced model that retains a few POMs may feature a better accuracy in reconstruction of the displacements of the system, when compared with velocities and acceleration responses.

Table 3-2: Outcomes achieved through POD, in terms of accuracy p and speedup as functions of the number of DOFs retained in the reduced order model.

# DOFs	*p*	*speedup*
1	0.99	515
2	0.999	385
3	0.9999	276
4	0.99999	244

Moving to the speedup obtained by reducing the order of the full model, results here discussed have been obtained with a personal computer featuring and Intel Core 2 Duo CPU E8400, with 4 Gb of RAM, running Windows 7x64 as operating system and performing the simulations with MATLAB version 7.6.0.324. The speedup values reported in Table 2-1 testify the dramatic decrease of the computing time obtained through POD, and show how powerful this methodology can be to approach real-time computing.

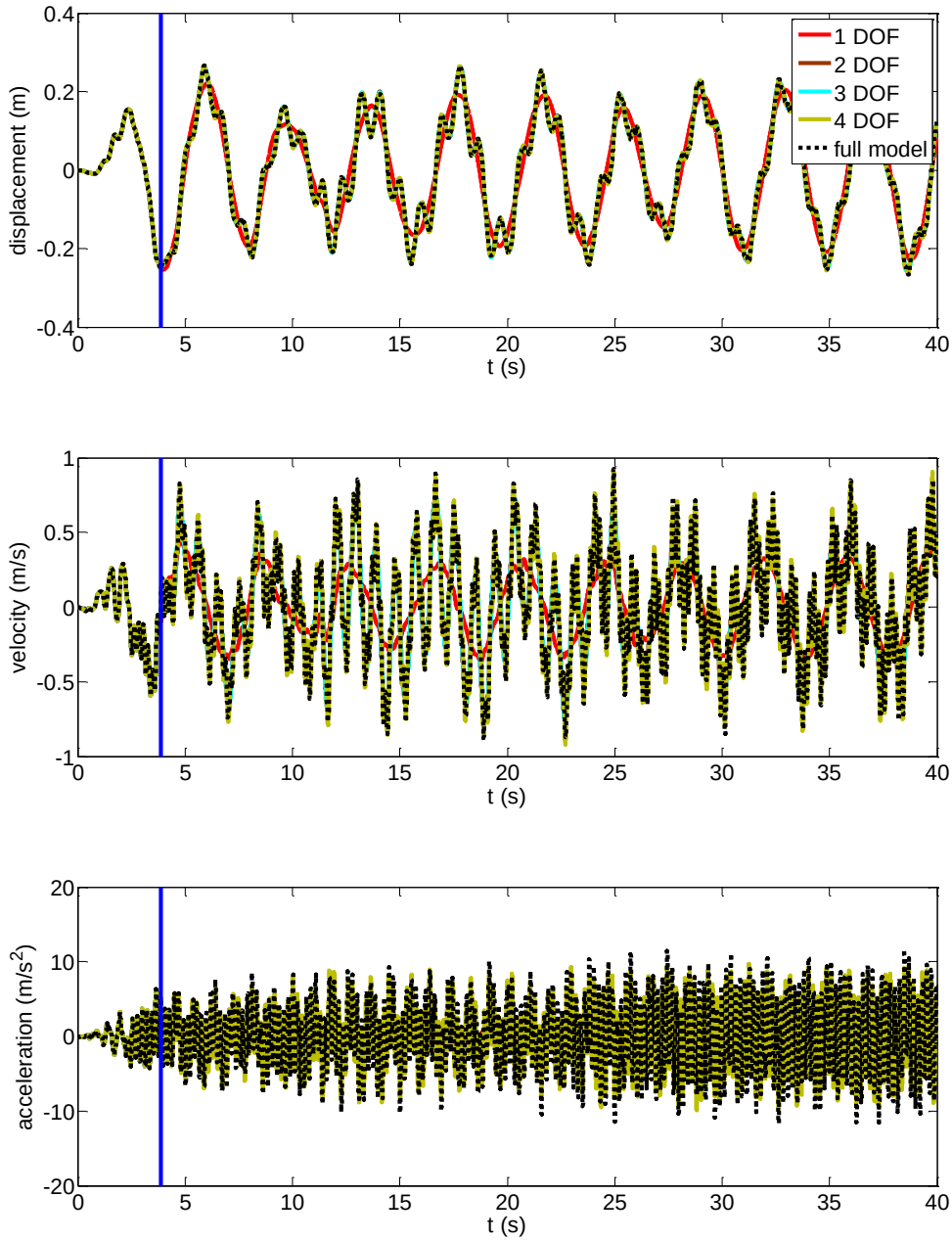

Figure 3-4: Time histories of the horizontal, displacement (top), velocity (middle) and acceleration (bottom) of the 20th floor, as induced by the El Centro earthquake.

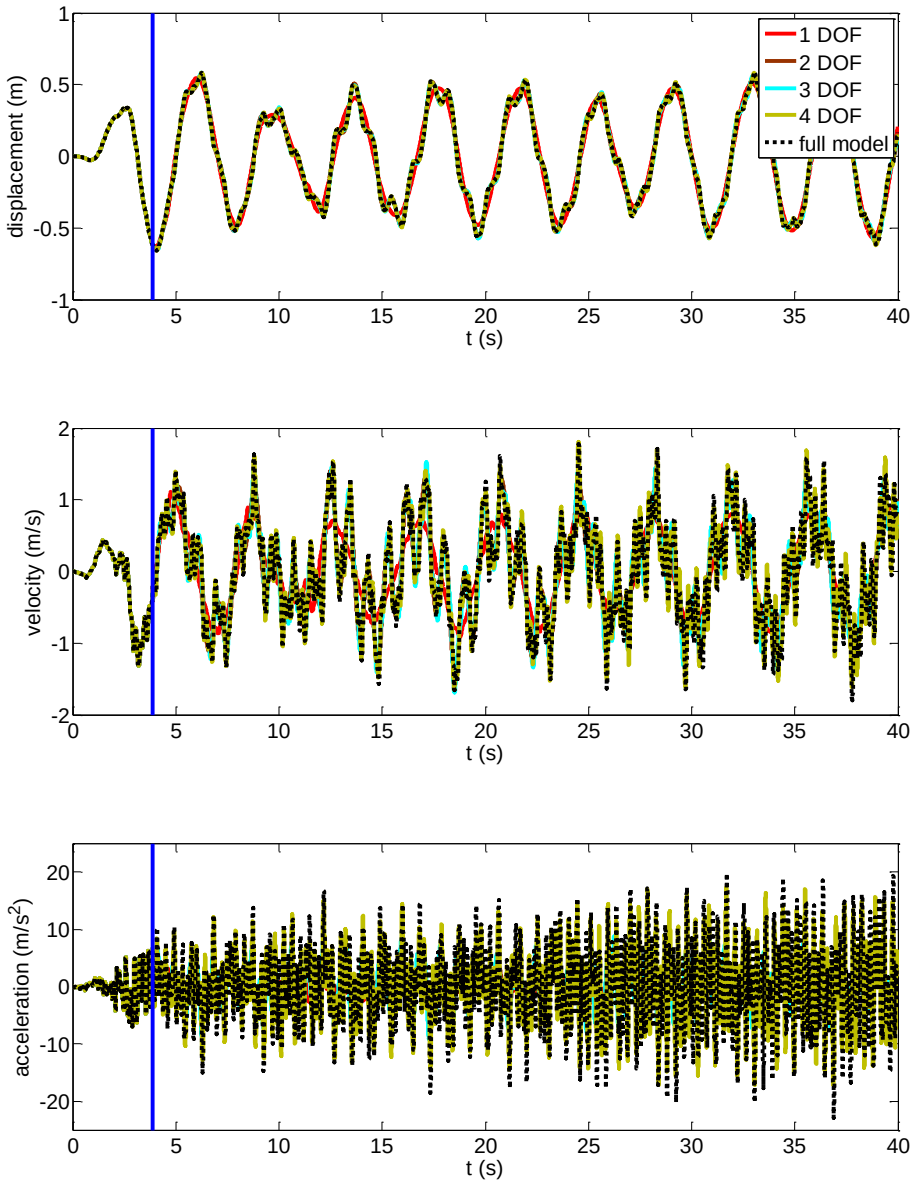

Figure 3-5: Time histories of the horizontal displacement (top), velocity (middle) and acceleration (bottom) of the 39th floor, as induced by the El Centro earthquake.

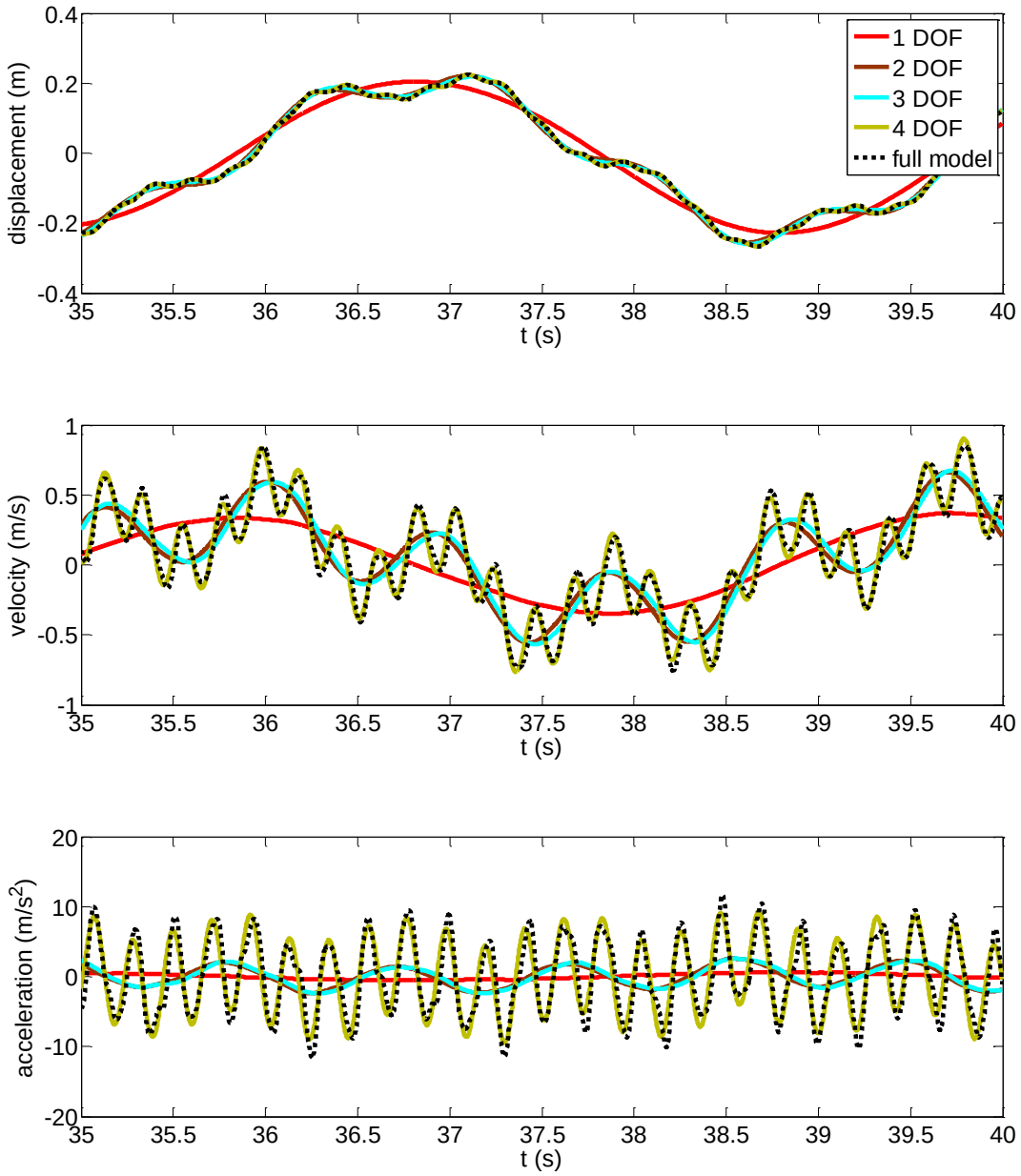

Figure 3-6: Close up of the time histories of the horizontal displacement (top), velocity (middle) and acceleration (bottom) of the 20th floor, as induced by the El Centro earthquake.

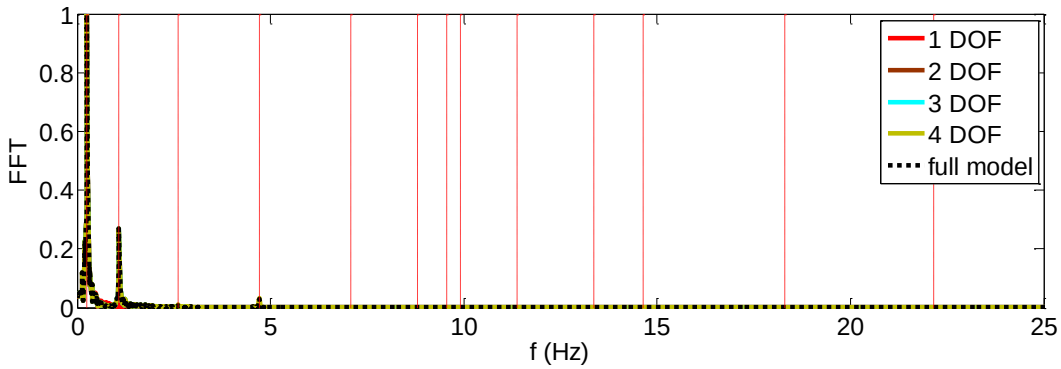

(a)

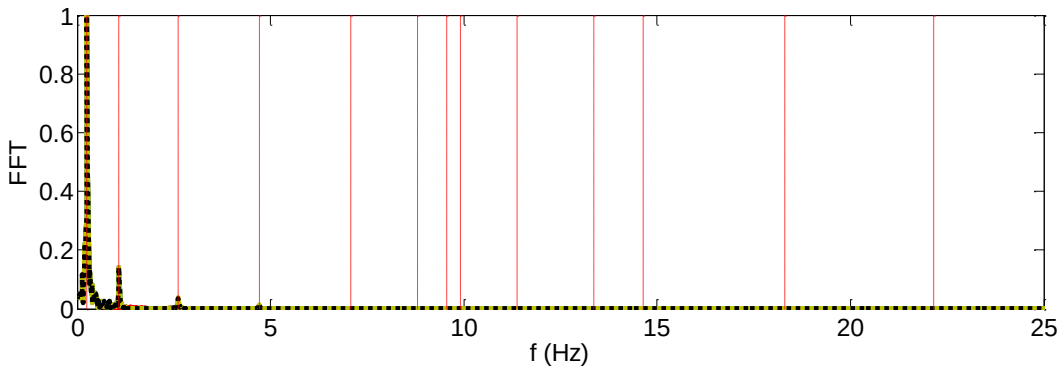

(b)

Figure 3-7: FFTs of the horizontal displacements of the storeys as induced by the El Centro earthquake at (a) 20th and (b) 39th floors

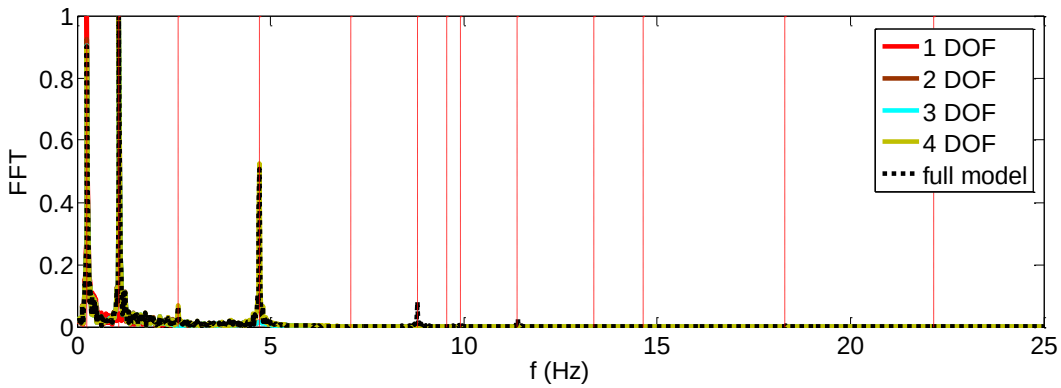

(a)

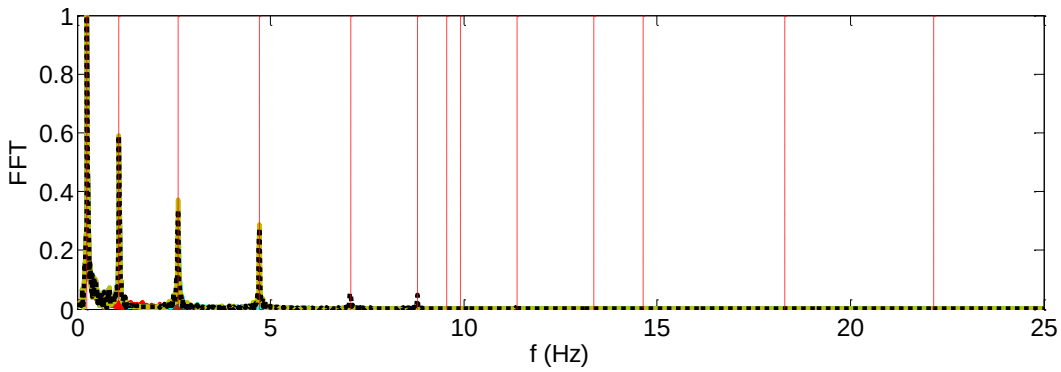

(b)

Figure 3-8: FFTs of the horizontal velocities of the storeys as induced by the El Centro earthquake at (a) 20th and (b) 39th floors

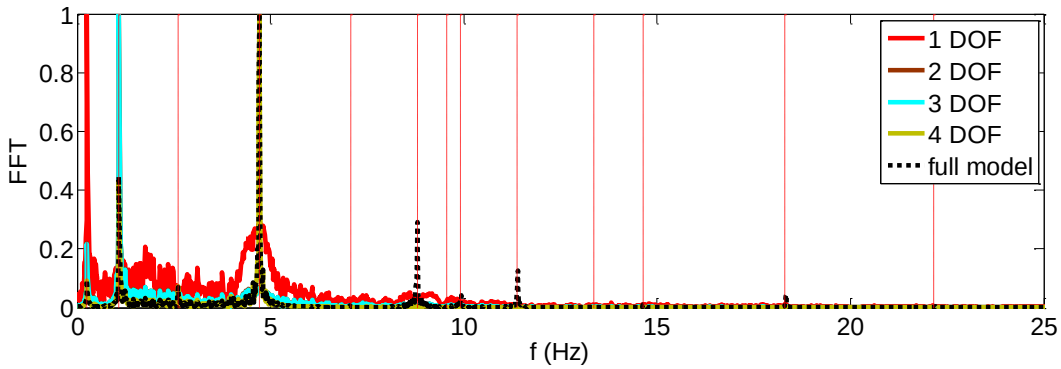

(a)

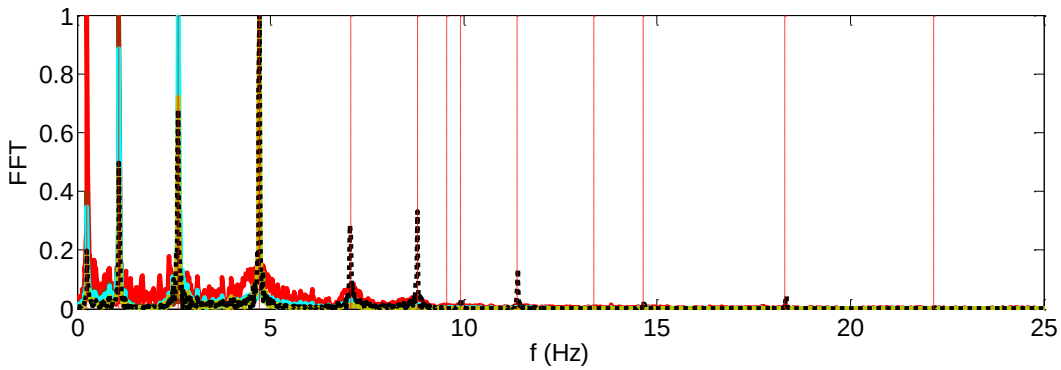

(b)

Figure 3-9: FFTs of the horizontal accelerations of the storeys as induced by the El Centro earthquake, (a) 20th (top), and (b) 39th floor

Previous figures have reported results concerning time histories of two representative storeys of the structure: 20th storey is the mid floor and 39th storey is the last floor (roof) of the building. To also test the efficiency of the reduced models in reconstructing snapshots of the system, and therefore assess the capacity of the methodology in tracking the dynamics of all the system DOFs, two time instants are selected for assessing the accuracy: Figures 3-10 (a) and (b) show snapshots taken in $t = 10$ s and $t = 30$ s of the analysis. At $t = 30$ s, the deformation of the structure is rather similar to a line with constant slope, that is the reduced model with two POMs can reconstruct the relevant snapshot, however more POMs are required to appropriately

approximate snapshot taken at $t = 10$ s, since the shape of the building is more complicated and higher modes are playing more significant role when compared to $t = 30$ s.

Another global feature of the reduced model which may be of interest for design practice is the envelope of the displacement, with is reported in Figure 3-11. It is seen that even the reduced model with a single POM has an acceptable performance in reconstructing the envelope, even though it underestimates the envelope itself. By increasing the flexibility of the reduced model through additional POMs, as the higher POMs are retained in the analysis, it is seen that the envelope of the reduced model almost matches that of full one.

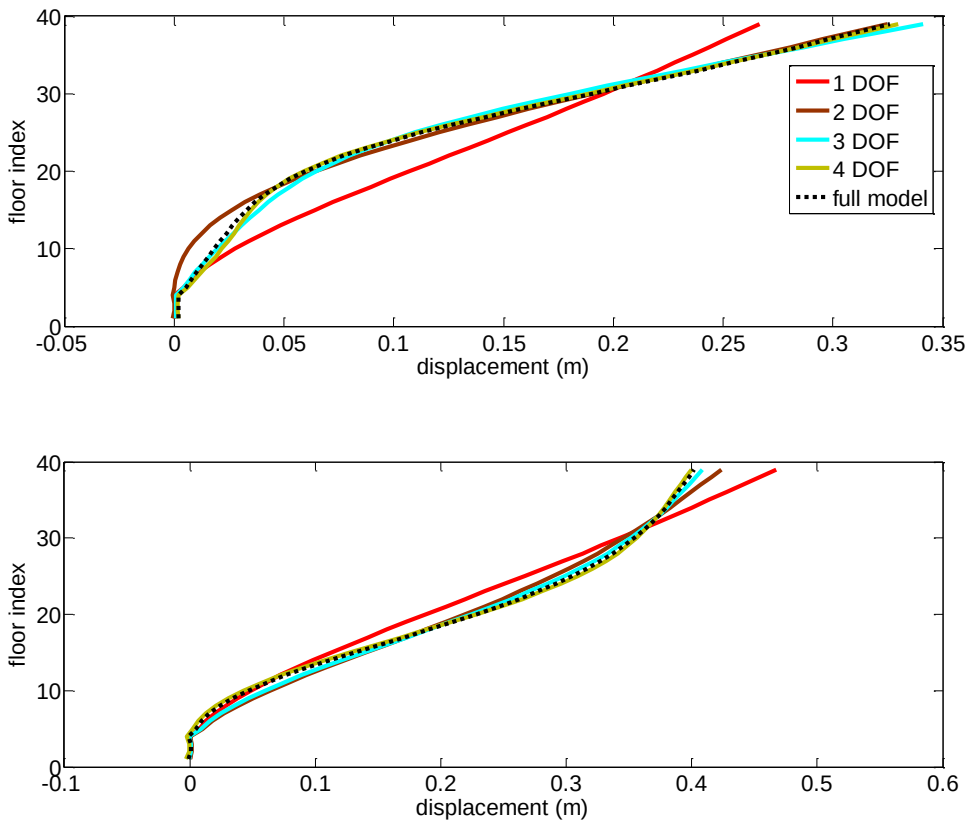

Figure 3-10: Snapshots of the horizontal storey displacements as induced by the El Centro earthquake. top: t=10 s and bottom: t=30 s

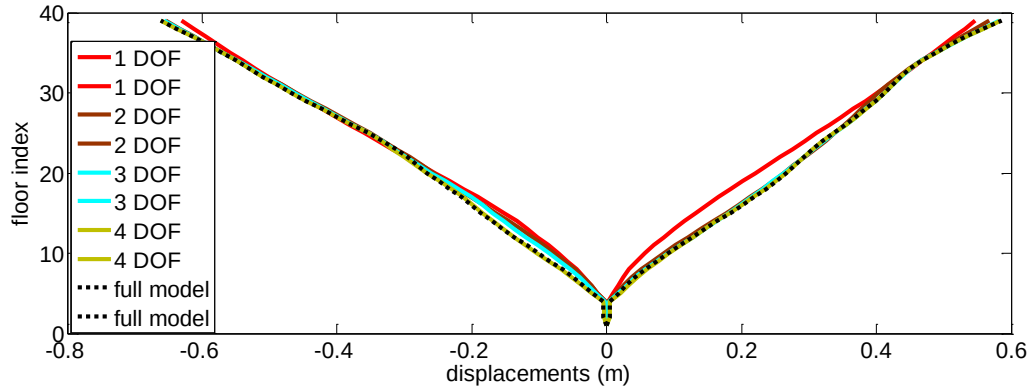

Figure 3-11: Envelope of horizontal storey displacements, as induced by the El Centro earthquake.

To assess the efficiency of the reduced models in retaining the energy of the system, we now compare the resulting time histories of kinetic and potential energies of the system (see Figure 3-12), respectively defined as: $E_k = \frac{1}{2}\dot{\boldsymbol{u}}^T\boldsymbol{M}\dot{\boldsymbol{u}}$ and $E_p = \frac{1}{2}\boldsymbol{u}^T\boldsymbol{M}\boldsymbol{u}$ for the full model; $E_{kl} = \frac{1}{2}\dot{\boldsymbol{\alpha}}^T\boldsymbol{M}_l\dot{\boldsymbol{\alpha}}$ and $E_{pl} = \frac{1}{2}\boldsymbol{\alpha}^T\boldsymbol{K}_l\boldsymbol{\alpha}$ for ROMs. The cumulative discrepancy of the energies of the reduced models from the target one is also considered (see Figure 3-13). It is seen that the energy time histories of the 4-DOF reduced model well match those of the full model. To have more insight into the ability of the models to preserve energy of the system, the cumulative discrepancies of kinetic and potential energies are reported as well. It is seen that as the number of the DOFs of the reduced model increases the slope of the relevant line decreases, it means the rate of accumulation of the discrepancy decreases. Besides, it is seen that the accumulation of the discrepancies features a line with an almost constant slope, it implies that, at different time intervals of the analysis, the amount of energy loss is the same. It means that the rate of energy loss is constant, hence accuracy of the reduced model in terms of energy preservation is constant over the interval of the analysis.

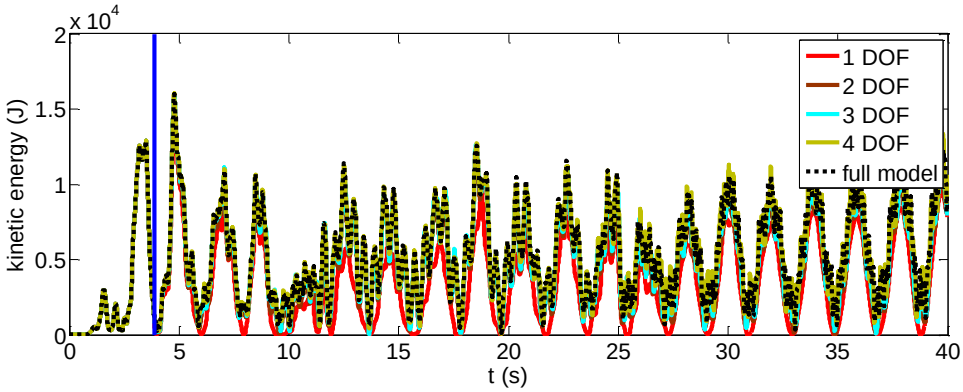

(a)

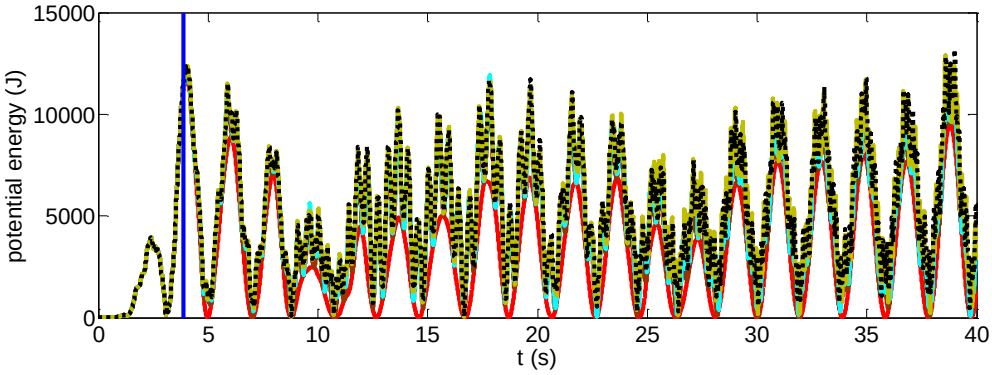

(b)

Figure 3-12: Time histories of (a) kinetic and (b) potential energies.

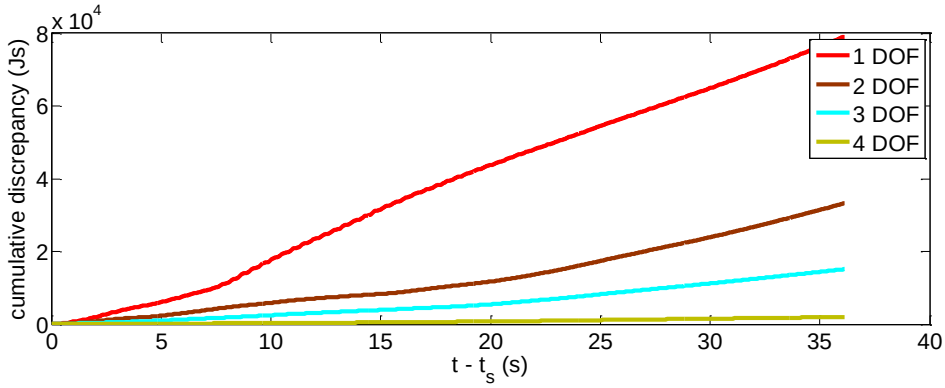

(a)

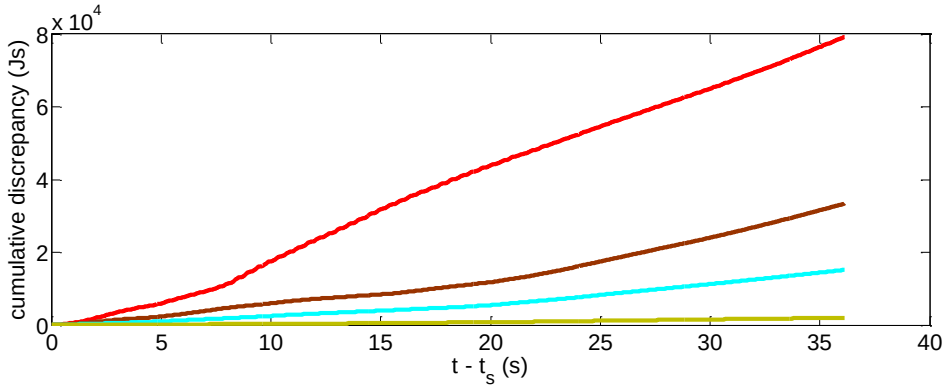

(b)

Figure 3-13: Time evolution of cumulative discrepancy between full model and reduced order model, in terms of (a) kinetic, (b) potential energies.

From this point on, we examine the accuracy of the reduced models that are built via snapshots resulting from excitation by the El Centro earthquake, when the building gets shacked by other seismic records. In this regard, as an instance we consider the May– 1976 Friuli earthquake; time history of its acceleration records along with the relevant FFT are shown in Figure 3-14. To have an idea concerning the number of natural frequencies that are covered by this seismic action,

again the red vertical lines (as indicator of the natural frequencies of the structure) are drawn in the figure to allow for understanding the number of eigen-modes that get excited by accelerogram of the relevant earthquakes. By an intuitive comparison of Figures 3-3 and 3-14, it is seen that a different amount of eigen-modes of the structure are excited by the two earthquake records.

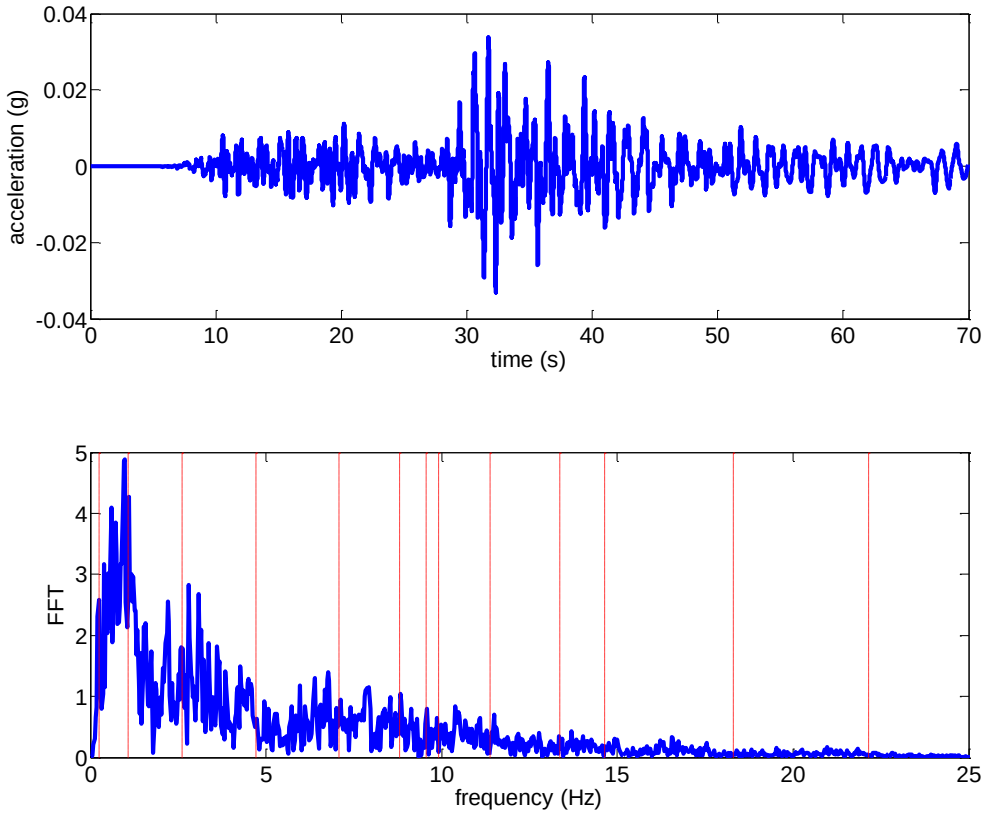

Figure 3-14: top: May 6–1976, Friuli earthquake and bottom: relevant FFT.

Let us now consider the time histories of displacement, velocity and acceleration of the 39th storey (see Figure 3-15). It is seen that, while a 2-DOF reduced model satisfactorily mimics the behavior of the full model in terms of displacement, a 4-DOF reduced model is required to match the full model in terms of velocity and acceleration time histories. The number of POMs required for reconstructing the whole state of the structure, when it gets shacked by Friuli

earthquake, is the same as if it got shacked by El Centro earthquake. This fact shows that a reduced model built by POD may be robust to change in the excitation source.

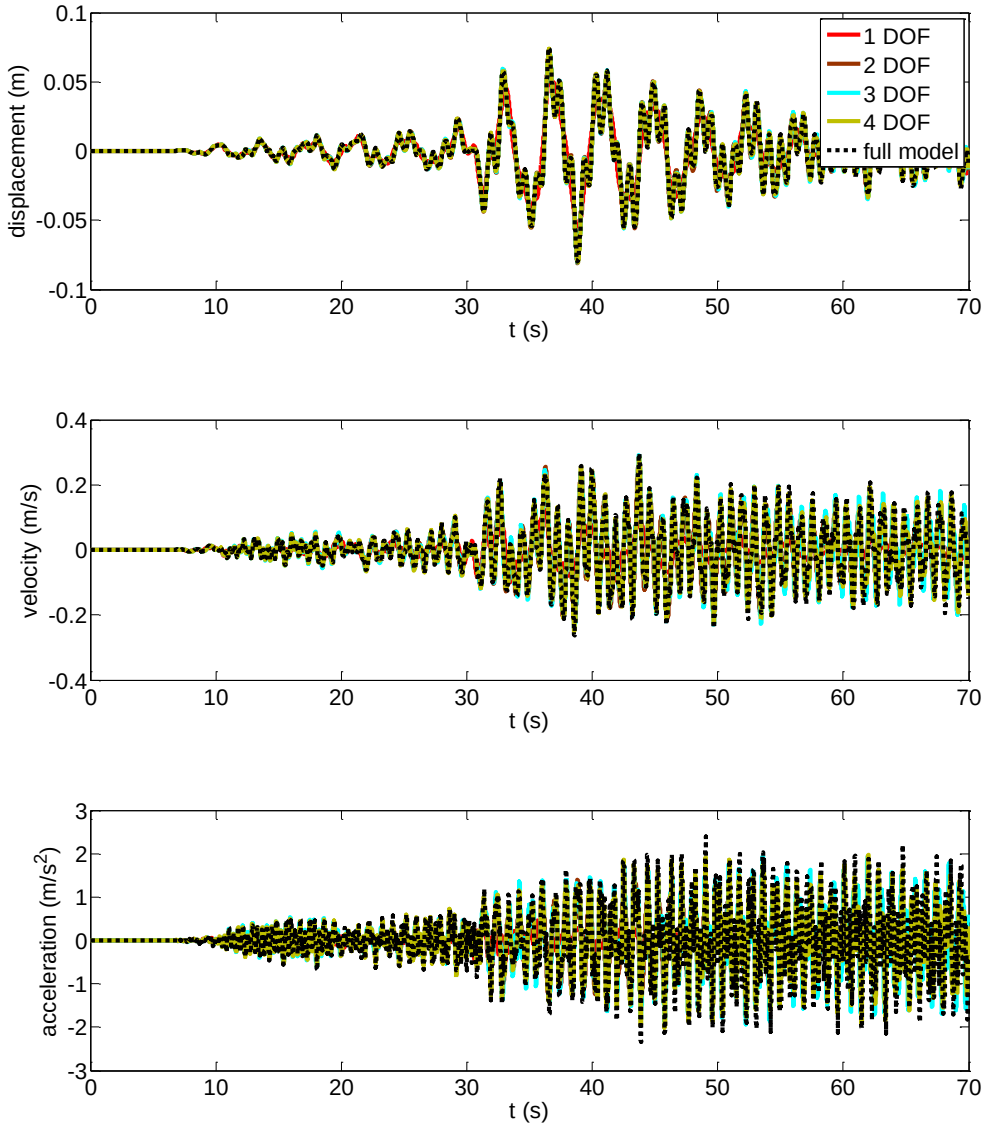

igure 3-15: Time histories of the horizontal floor displacement (top), velocity (middle) and acceleration (bottom) of the 39th floor, as induced by the Friuli earthquake.

By investigating the FFTs of the above reported time histories (see Figure 3-16 (a)), the trend seen in the time histories of the state reconstruction is corroborated: one can see there are several peaks in the displacement response of the structure, when shacked by Friuli record; similarly to

the FFTs of the structure when subjected to El Centro record, moving from displacement to velocity and acceleration FFTs, the number of peaks increases. Therefore, the number of POMs required to match the FFT of the response of the structure increases.

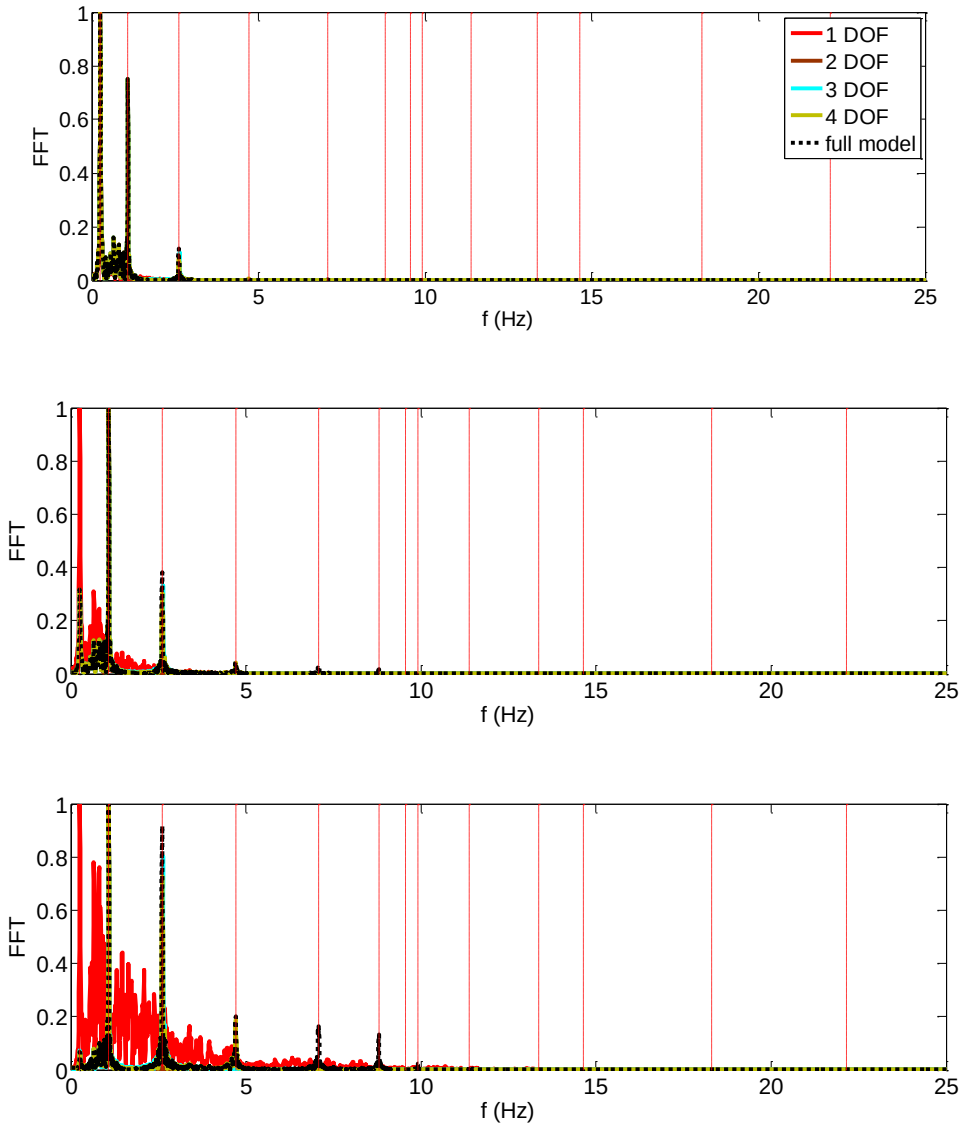

Figure 3-16: FFTs of the 39th floor, displacement (top), velocity (middle) and acceleration (bottom) as induced by the Friuli earthquake

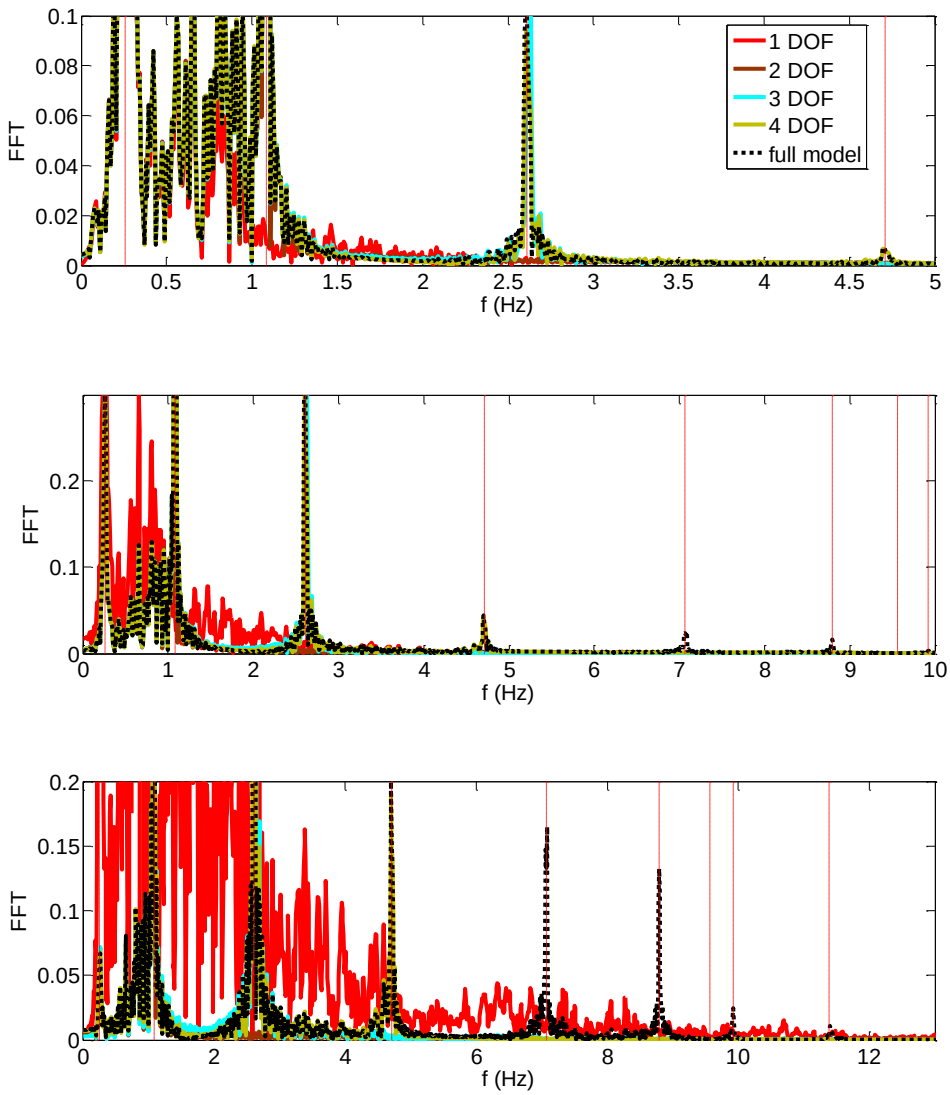

Figure 3-17: Close up of FFT of the horizontal displacement (a), velocity (b) and acceleration (c) of 39th floors, as induced by the Friuli earthquake.

In Figure 3-17 (top) it is seen that, out of the several spikes in FFT of the displacement, four are coincident with the system natural frequencies. A s DOF reduced model is able to match only first spike, however a two DOF reduced model matches the two of the spikes relevant to natural frequencies, the reduced models featuring three and four DOF models are match up to third and the fourth spikes coinciding with the third forth natural frequency of the system, respectively. Considering the velocities and accelerations the same trend is seen; however, in latter cases more

natural vibration modes are effectively excited. Hence, accuracy of a reduced model in reconstructing the acceleration responses of the system is not the same as the velocities and displacements.

The performance of the reduced models in approximating snapshots of the system are once again tested at $t = 10$ s and $t = 30$ s. Looking at Figure 3-18, it is seen that at $t = 10$ s the state of the system is like a line with constant slope; hence, all reduced models feature more or less similar accuracy; however, at $t = 30$ s the state of the structure is more complicated and at least four POMs are required to approximate the considered snapshot.

Concerning the envelope of the displacements (see Figure 3-19), it is seen that even a two DOF reduced model is matching the envelope featured by the full model. It is seen that, in the vicinity of the 25th floor, there is a break in the envelope of the structure, while in the envelope of floor displacements relevant to the El Centro earthquake such a break is not seen. This is due to the fact that, the range of frequency content of Friuli earthquake is wider than that of El Centro earthquake, see Figures 3-3(b) and 3-14(b), it results in excitation, and therefore contribution of higher natural modes in the response of the structure and as a consequence the shape of the structure may become more complicated.

To evaluate the accuracy of the reduced models concerning the energies, accumulated discrepancies has been considered; as before the time histories feature the same features of those related to El Centro record. Figure 3-20 shows the accumulated discrepancies of kinetic and potential energies for two scenarios: the continuous lines represent the case in which snapshots are related to the El Centro excitation, instead the dot lines stand for the case in which snapshots are related to Friuli record. It is worth recalling that in both cases the reduced and full model are shacked by Friuli record. It is seen that, despite the fact that the reduced models are constructed by different inputs in simulations, the accumulated discrepancies almost coincide. However, in this case the accumulated discrepancies appears to be bilinear: the graphs look like an straight line which changes its slope at $t = 30$ s. This is due to the fact that the amplitude of the

excitations increases at the vicinity of the $t = 30$ s, the increase in the energy of input excitation therefore changes the rate of accumulation of the discrepancies changes.

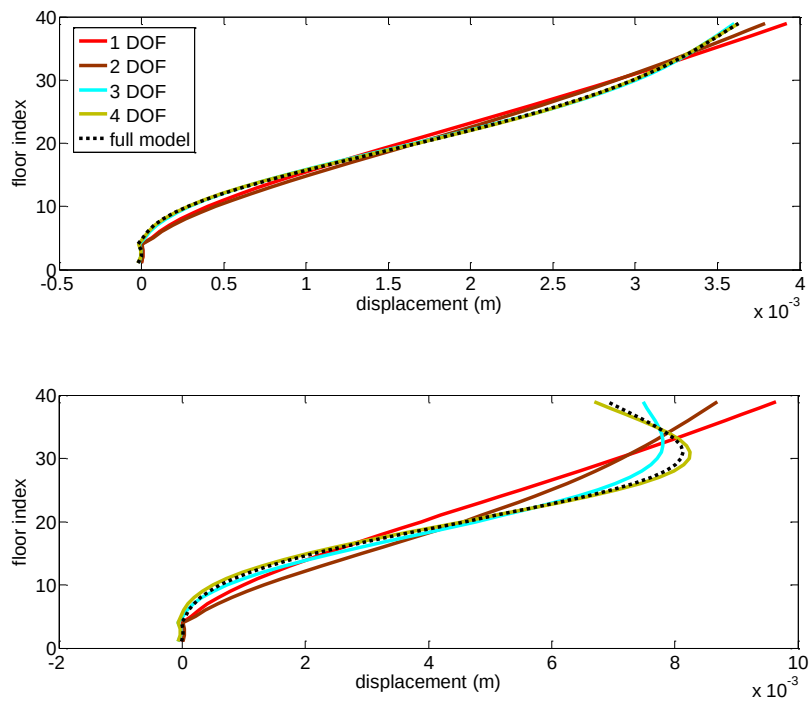

Figure 3-18: Snapshots of the horizontal storey displacements at (top) t=10 s, and (bottom) t=30 s, as induced by the Friuli earthquake.

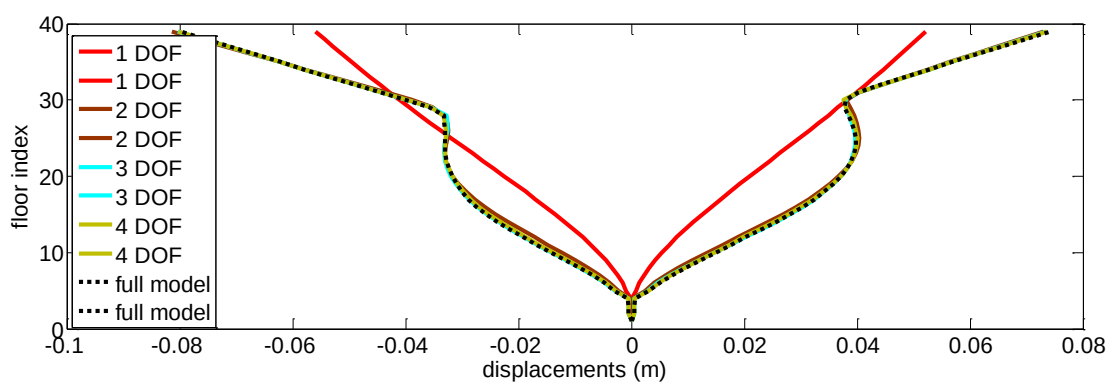

Figure 3-19: Envelope of horizontal storey displacements, as induced by the Friuli earthquake.

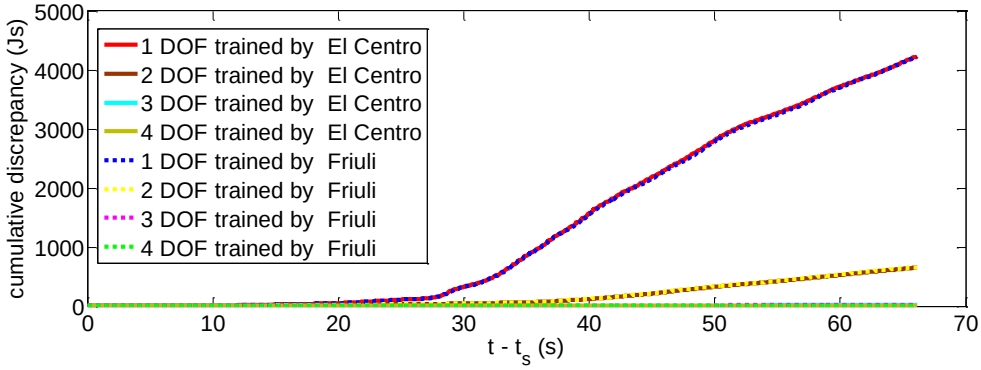

(a)

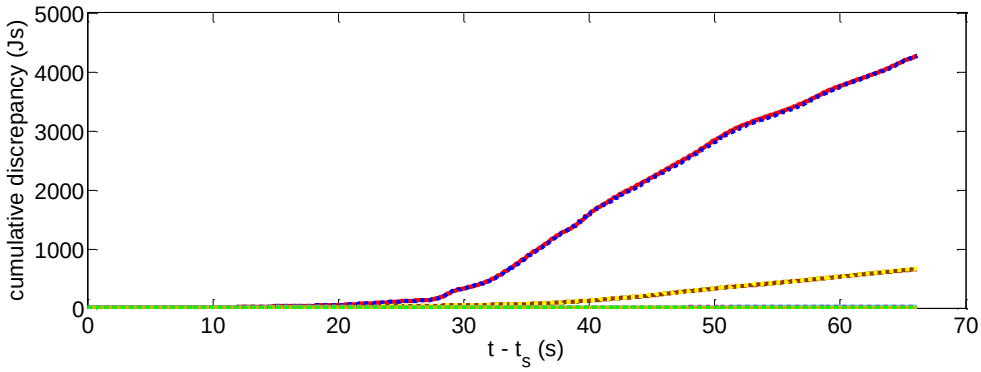

(b)

Figure 3-20: Time evolution of cumulative discrepancy between full model and reduced order model, in terms of (a) kinetic, and (b) potential energies. Comparison between outcomes of the reduced order model trained with the El Centro earthquake, and of the reduced o

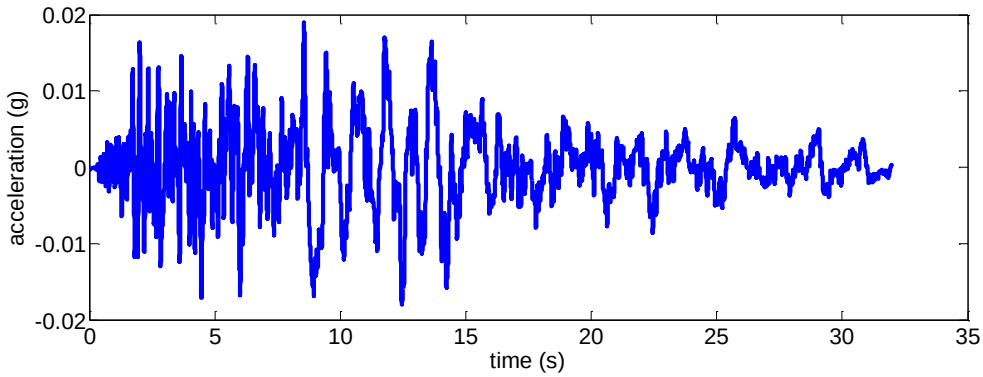

(a)

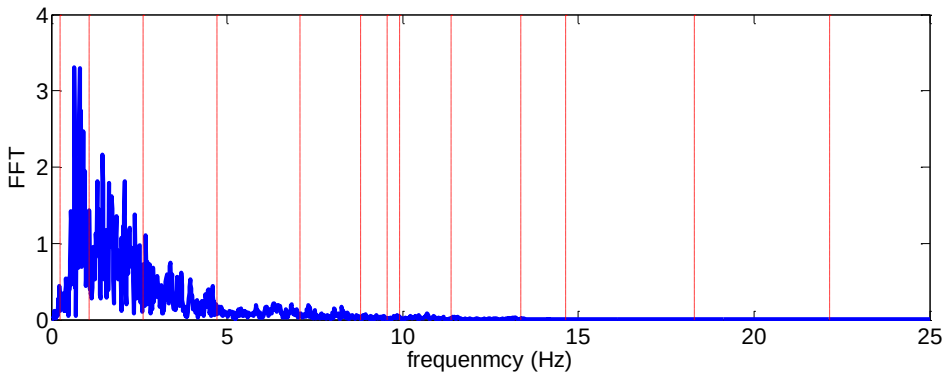

(b)

Figure 3-21: (a) January 17–1995, Kobe earthquake and (b) relevant FFT.

To conclude this section, we also assess the performance of the already built reduced models when excited by January 17–1995 Kobe acceleration record. In Figure 3-21 the acceleration time history and its relevant FFT is shown. Once more, one can see that the frequency content of this record is different from those of El Centro and Friuli. Figure 3-22 shows the time histories of displacement, velocity and acceleration of 39th storey. The situation is rather similar to the two previous cases: concerning displacements, reduced models retaining two or more DOFs almost coincide with the full model, whereas dealing with velocity and acceleration a four DOF model is necessary to fully capture the dynamics of the system.

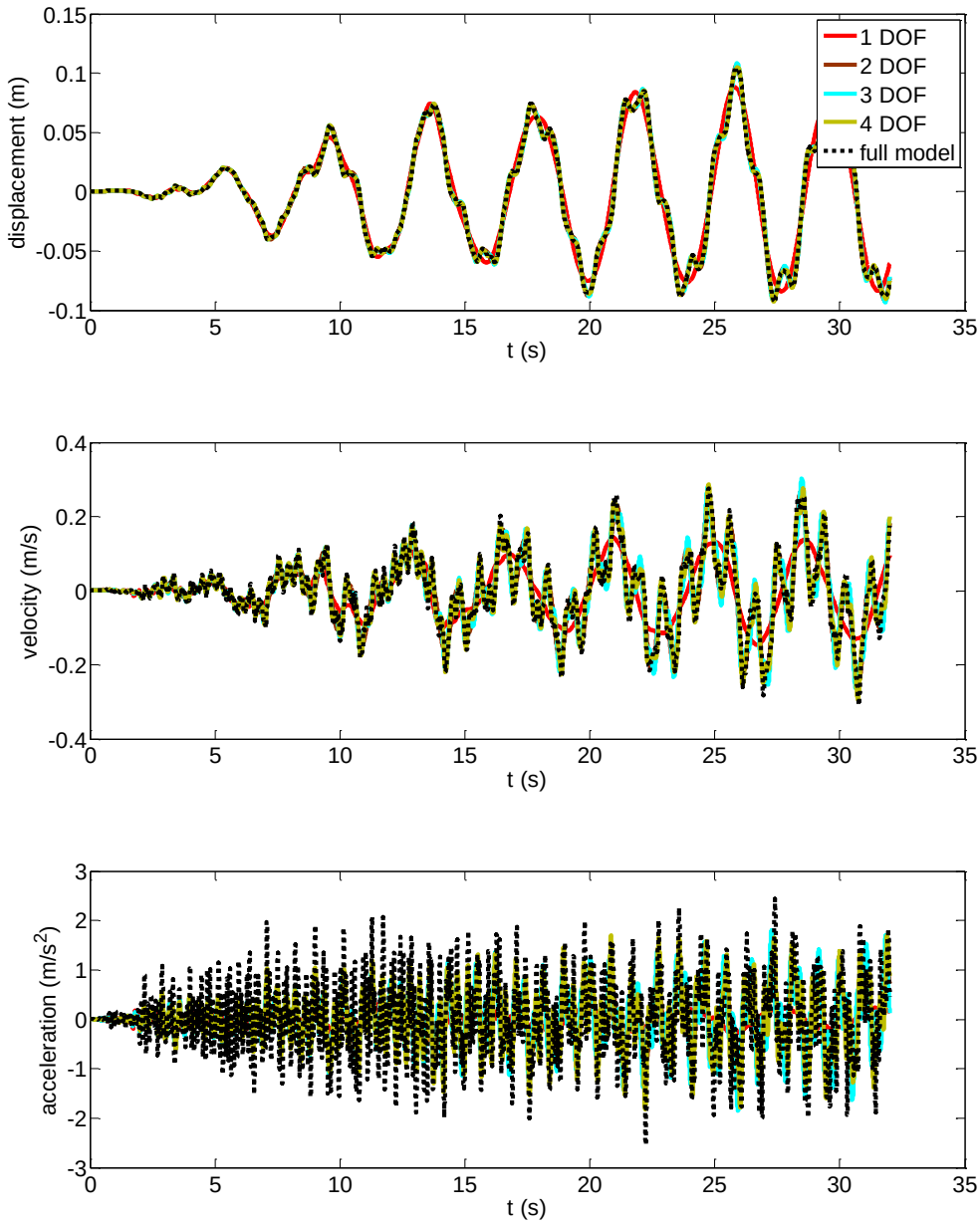

Figure 3-22: Time histories of the horizontal displacement (top), velocity (middle) and acceleration (bottom) of the 39th floor, as induced by the Kobe earthquake.

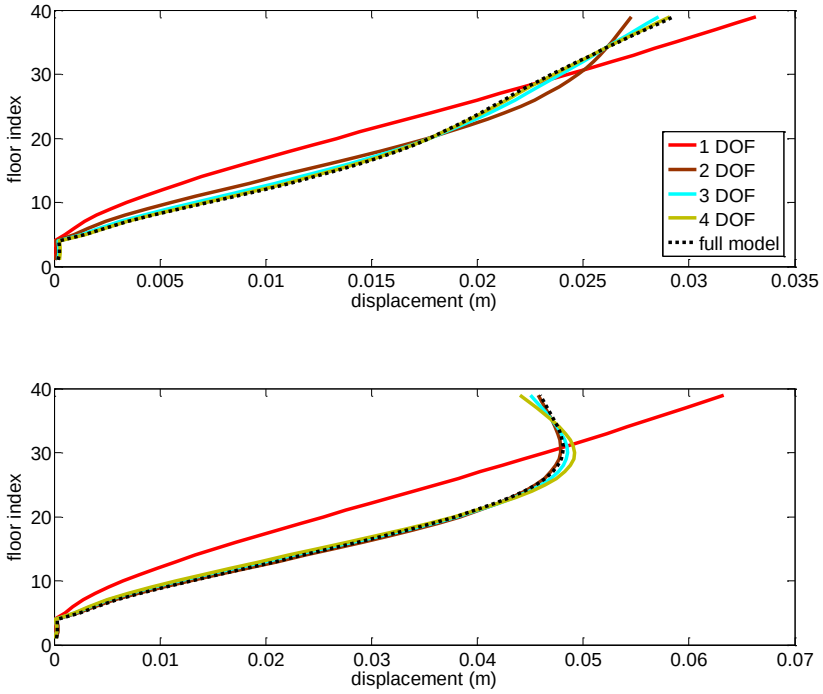

Figure 3-23: Snapshots of the horizontal storey displacements at (top) t = 10 s, and (bottom) t = 30 s, as induced by the Kobe earthquake.

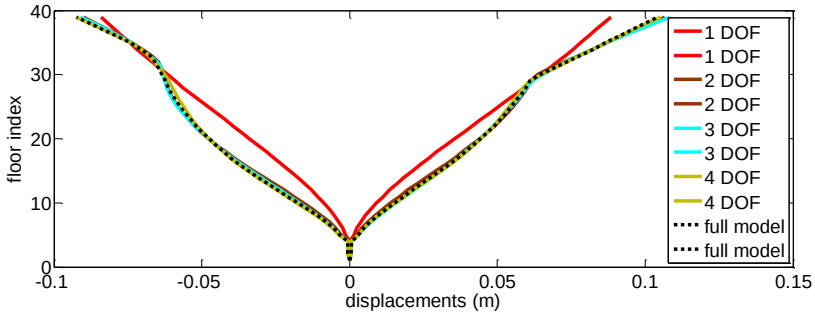

Figure 3-24: Envelope of horizontal storey displacements, as induced by the Kobe earthquake.

Considering snapshots and envelope of the displacements of the system (see Figures 3-24 and 3-25), a reduced model consisting of a single DOF is not able to feature the dynamics of the system likewise the case shacked by El Centro and Friuli earthquake. To assess the global efficiency of the reduced model when subject to Kobe record (see Figure 3-25), once more one can see that the ability to retain energy is independent of the training stage. The reduced models that have the

same number of DOFs, no matter snapshots are collected from simulation o El Centro or Kobe earthquake simulations, almost feature the same level of accuracy.

Through the results shown in this Section, it has been shown that prediction capabilities of POD-based reduced order models when dealing with different seismic excitations along with their high speed-up in computation makes them suitable candidates for models used in online and real-time structural health monitoring.

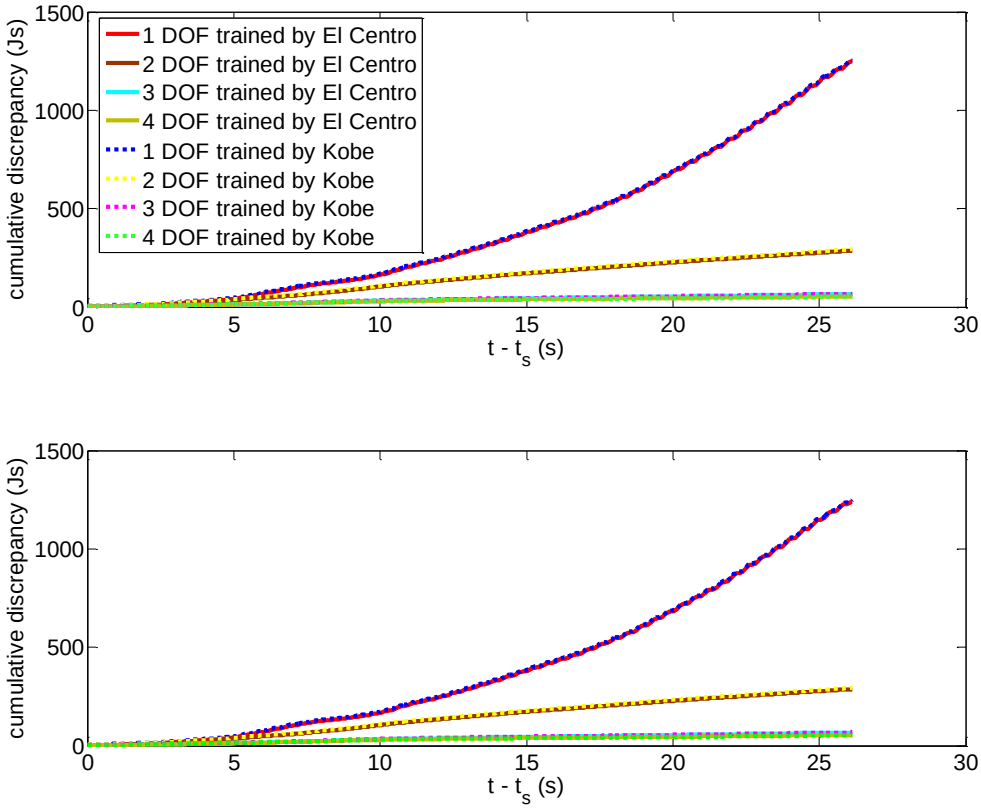

Figure 3-25: Time evolution of cumulative discrepancy between full model and reduced order model, in terms of (top) kinetic, and (bottom) potential energies. Comparison between outcomes of the reduced order model trained with the El Centro earthquake, and of the reduced o

3.7 Summary and conclusion

In this Chapter, we have investigated the capability and efficiency of POD in reducing the order of dynamic structural systems. In its SVD description, POD is expected to find the directions in which retain the maximum energy of the system, whereas its PCA explanation is based on the search for the directions which preserve maximum variability of the set of samples, which are gathered into the so-called matrix of snapshots. Handling snapshots collected in an initial time window, we have built the reduced model through a coupling of POD and Galerkin projection.

To assess the performance of the studied methodology, the Pirelli Tower in Milan has been assumed to get shacked by an earthquake. Concerning accuracy issues, time histories of the state of the system (storey displacements, velocities and accelerations), together with their associated Fourier transform, have been compared with their real values available through the simulations. The power of the order reduction method in preserving the energies of the system is tested via a comparison of their time histories with those of full model. It has been seen that energy time histories of a 4-DOF reduced model almost coincided with target values.

When dealing with accuracy versus sped-up, it has been shown that POD can decrease the number of DOFs from the original 39 (one at each storey) to just 1, guaranteeing an accuracy of 0.99 (1 being featured by the original model) according to what here explained, and leading to a speedup in the computations higher than 500. We have also shown that, to also match higher order frequency oscillations (accuracy of 0.99999), the retained degrees of freedom result to be increased to 4, still getting a speedup higher than 200.

It has been shown that the POD based reduced models are also robust to a change of loading; the models built by snapshots resulting from simulations of the full model subject to El Centro record feature the same level of accuracy when are shacked by Kobe and Friuli record.

In following Chapters, the reduced model built by POD will be incorporated into Bayesian filters to assess the capabilities of such an approach in state estimation of non-damaging and dual estimation of damaging structures, possibly detecting and locating the occurring damage.

Chapter 4: POD-Kalman observer for linear time invariant dynamic systems

4.1 Introduction

The ultimate objective of this thesis is to develop an online and real-time algorithm for the detection of damage in structural systems. To this end, in Chapter 2 we have first studied the possibility of exploiting Bayesian filters for fulfilling the objective of this study. However, it was shown that in the case of multi-storey buildings that, as the number of floors increases, the bias in the estimation of parameters and therefore, in damage detection increases as well.

Our proposal is then to use reduced order models in combination with Bayesian filters to monitor the state of the structure. In the previous Chapter, the efficiency of POD, in terms of speed-up and accuracy, has been investigated numerically. This Chapter deals with the numerical assessment of the efficiency of POD-based reduced order models in state estimation of linear time-invariant structural systems. It is known that the Kalman filter provides optimal estimates of the state of a linear state-space model affected by white Gaussian noises. However, in what follows we will show the uncertainties induced by POD are not white noises.

The analysis of the linear time-invariant model permits the analysis of the effect of uncertainties induced by POD on the optimal performance of the Kalman filter. In this regards, the reduced model of the system is incorporated into a Kalman filter; the speed-up and accuracy of state estimation is investigated, by assuming that a minimal number of observables is managed. It is known that POD models are not robust to a change in the parameters of the system; indeed, proper orthogonal modes (POMs) were anyhow used as indicators of the damage in different structures, like beams (Galvanetto, Violaris 2007a), trusses (Ruotolo, Surace 1999) and

composite materials (Shane, Jha 2011a). In case the system is subject to unpredictable change in the parameter, e.g. due to inception or growth of damage, the reduced model fails to be accurate. However, potential use of an approximated linear time invariant model in automatic control of the structural response (Gustafsson, Mäkilä 1996) motivates the search for high fidelity and computationally efficient reduced models. Estimation of the state of a system, even in an accurate fashion, does not explicitly contain information on the damage: in the next Chapter we will therefor address damage detection via Bayesian filtering and reduced order modelling. In the sequel, first the necessity of using observers in structural feedback control is discussed; then, statistical properties of the residual error process is assessed, to verify if they satisfy the requirements (whiteness and Gaussianity) of Kalman filter for providing optimal solution. Thence, Kalman-POD observer is briefly reviewed. The Chapter is finally concluded by illustrating the performance of Kalman-POD observer: the efficiency of the algorithms is assessed to ensure robustness to change in the seismic excitation source, as it was done in Chapter 3. The effect of correlated uncertainties in the performance of Kalman-POD observer is discussed. Computational gain obtained by the use of Kalman-POD observer, when compared to Kalman observer alone, is shown in terms of speed-up gained in calculations.

4.2 Structural feedback control and the Kalman observer

Feedback control intends in developing automated algorithms for harnessing response of the systems (Goodwin, Graebe & Salgado 2001). Early instances of control systems include clock regulating devices and mechanisms for keeping wind-mills pointed toward the wind. During industrial revolution, invention of machinery for transforming raw materials into goods, specifically steam engine, which includes transforming a large amount of energy to mechanical work, made engineers realize the need for organized control strategies of the power consumed by machinery in order to guarantee the safe operation of the facilities (Goodwin, Graebe & Salgado 2001). Nowadays control engineering has become an omnipresent element of industry. Though industrial instances of feedback control date back to the nineteenth century, its use in structural engineering field is quite recent. In last two decades, automatic control strategies are gaining popularity to further extend life cycle and performance of earthquake resistant structural systems;

for a review of the real applications of active structural control in Japan see (Ikeda 2009), were the use of active tuned mass dampers for vibration suppression of high rise buildings subject to lateral loads is discussed. For a list concerning the active control strategies used in other building types including bridges, tensegrity structures and trusses refer to (Korkmaz 2011). Control algorithm design is realized by merging many disciplines of science and technology, including but not limited to modelling (for capturing the underlying dynamics of the system), sensors (for measuring state of the system), actuators (for forcing the system to follow the desired trajectory), communications (for transmitting the data) and computing (for the task of computing action data based on measured observations) (Goodwin, Graebe & Salgado 2001). This Chapter of the thesis is aimed at developing computationally efficient reduced models for their possible use in control of seismically excited multi storey buildings.

We are not going to discuss control algorithms. However, to explain in further details how system control terms enter the state-space equations and to describe the need for the models in structural control, consider a linear time invariant system and its state-space equations:

$$\boldsymbol{z}_k = \boldsymbol{F}\,\boldsymbol{z}_{k-1} + \boldsymbol{G}\;\boldsymbol{e}_k + \;\boldsymbol{v}_k \tag{4.1}$$

$$\boldsymbol{y}_k = \boldsymbol{H}\,\boldsymbol{z}_k + \boldsymbol{w}_k \tag{4.2}$$

where: $\boldsymbol{z}_k$ represents the state of the system (e.g. displacement, velocity and acceleration of each storey in a structure) at time instant t_k; $\boldsymbol{e}_k$ is the control input, which is computed by using control algorithms in order to restrict the state of structure to a desired reference; $\boldsymbol{y}_k$ denotes the noisy system observations; $\boldsymbol{F}$ maps the state over time; $\boldsymbol{G}$ links the control feedback to the relevant degrees-of-freedom and $\boldsymbol{H}$ links the observation and state; $\boldsymbol{v}_k$ and $\boldsymbol{w}_k$ are evolution and observation uncertainties. The idea in the state space approach to feedback control, is to synthesize a full state feedback through:

$$\boldsymbol{e}_k = \boldsymbol{K}\;\boldsymbol{z}_k \tag{4.3}$$

where $\boldsymbol{K}$, the gain matrix, is computed to satisfy the objective of the closed loop system; in a civil structure such an objective would be, e.g. the suppression of vibrations induced by external

loads (e.g. loads or seismic excitations). The problem is that, in most practical cases the state vector is not fully known: it may require too many sensors, or it may be due to technical reasons (for instance, displacements of a multi-storey structure are difficult to monitor).

The process of reconstructing the whole state of a system, based on a physical model and observation signals, is called observer design (Preumont 2011). It is known that, dealing with linear state-space models, provided that the distribution of the uncertainties is Gaussian and there is no correlation in uncertainty time series, Kalman Filter furnishes the optimal observer of the system (Preumont 2011). This Chapter of the thesis deals with the reduction of the computational cost of a Kalman observer of the linear time invariant dynamic systems, by making use of a surrogate POD-based reduced model of the system to be incorporated into the Kalman filter algorithm. The efficiency of POD for model reduction of models studied in current Chapter, in terms of speed-up and accuracy, has been ascertained in Chapter 3, where it has been shown that POD can be a reasonable candidate to reduce the computational costs of structural analysis.

4.2 Statistical assessment of residual errors induced by POD

We start by recalling from Chapter 3 the set of ordinary differential equation that governs the dynamics of a structural system:

$$\boldsymbol{M}\ddot{\boldsymbol{u}} + \boldsymbol{K}\boldsymbol{u} = \boldsymbol{R}(t) \tag{4.4}$$

where: $\boldsymbol{M}$ and $\boldsymbol{K}$ are the stationary mass and stiffness matrices, respectively; $\boldsymbol{R}(t)$ is the external load vector; $\ddot{\boldsymbol{u}}$ and $\boldsymbol{u}$ are the storey acceleration and displacement vectors, respectively.

By making use of a Newmark time-integration algorithm, (4.4) is discretized in the time domain, through definition of the vector $\boldsymbol{z}_k = [\boldsymbol{u}_k \quad \dot{\boldsymbol{u}}_k \quad \ddot{\boldsymbol{u}}_k]^T$ at time t_k. The discrete state space form of (4.4) reads:

$$\boldsymbol{z}_k = \boldsymbol{A}\,\boldsymbol{z}_{k-1} + \boldsymbol{B}_k + \boldsymbol{v}_k \tag{4.5}$$

$$\boldsymbol{y}_k = \boldsymbol{H}\,\boldsymbol{z}_k + \boldsymbol{w}_k \tag{4.6}$$

where:

$$\boldsymbol{A} = \begin{bmatrix} \boldsymbol{I} - \beta\,\Delta t^2 \boldsymbol{M}^{-1}\boldsymbol{K} & \Delta t\,\boldsymbol{I} - \beta\,\Delta t^3 \boldsymbol{M}^{-1}\boldsymbol{K} & -\beta\left({}^1\!/_2 - \beta\right)\Delta t^4 \boldsymbol{M}^{-1}\boldsymbol{K} + \Delta t^2\left({}^1\!/_2 - \beta\right)\boldsymbol{I} \\ -\gamma\,\Delta t\,\boldsymbol{M}^{-1}\boldsymbol{K} & \boldsymbol{I} - \gamma\,\Delta t^2 \boldsymbol{M}^{-1}\boldsymbol{K} & -\gamma\left({}^1\!/_2 - \beta\right)\Delta t^3 \boldsymbol{M}^{-1}\boldsymbol{K} + \Delta t(1-\gamma)\,\boldsymbol{I} \\ -\boldsymbol{M}^{-1}\boldsymbol{K} & -\Delta t \boldsymbol{M}^{-1}\boldsymbol{K} & -\Delta t^2\left({}^1\!/_2 - \beta\right)\boldsymbol{M}^{-1}\boldsymbol{K} \end{bmatrix} \tag{4.7}$$

and:

$$\boldsymbol{B}_k = \begin{bmatrix} \beta\,\Delta t^2 \boldsymbol{M}^{-1}\,\boldsymbol{R}_k \\ \gamma\,\Delta t\,\boldsymbol{M}^{-1}\boldsymbol{R}_k \\ \boldsymbol{M}^{-1}\boldsymbol{R}_k \end{bmatrix} \tag{4.8}$$

$\boldsymbol{v}_k$ and $\boldsymbol{w}_k$ are evolution and measurement noises, assuming the full model to be deterministic, former one is not considered to enter the evolution of state of the system, while latter is assumed to be a stationary zero mean white Gaussian noise featuring time invariant covariance matrix of $\boldsymbol{W}$.

With the same notation of Chapter 3, the reduced order model of the system can now be written as:

$$\boldsymbol{M}_l \ddot{\boldsymbol{\alpha}}(t) + \boldsymbol{K}_l \boldsymbol{\alpha}(t) = \boldsymbol{R}_l(t) \tag{4.9}$$

where: $\boldsymbol{\alpha}$ is the coordinate of the reduced model and governs the evolution in time of the structural response along the POMs. Once the solution of (4.9) is obtained, the full state of the system can be computed by making use of (4.9):

$$\ddot{\boldsymbol{u}} \approx \boldsymbol{\Phi}_l \ddot{\boldsymbol{\alpha}} \quad \dot{\boldsymbol{u}} \approx \boldsymbol{\Phi}_l \dot{\boldsymbol{\alpha}} \quad \boldsymbol{u} \approx \boldsymbol{\Phi}_l \boldsymbol{\alpha} \tag{4.10}$$

or equivalently:

$$\begin{Bmatrix} \boldsymbol{u} \\ \dot{\boldsymbol{u}} \\ \ddot{\boldsymbol{u}} \end{Bmatrix} \approx \begin{bmatrix} \boldsymbol{\Phi}_l & \boldsymbol{0} & \boldsymbol{0} \\ \boldsymbol{0} & \boldsymbol{\Phi}_l & \boldsymbol{0} \\ \boldsymbol{0} & \boldsymbol{0} & \boldsymbol{\Phi}_l \end{bmatrix} \begin{Bmatrix} \boldsymbol{\alpha} \\ \dot{\boldsymbol{\alpha}} \\ \ddot{\boldsymbol{\alpha}} \end{Bmatrix} = \boldsymbol{L} \begin{Bmatrix} \boldsymbol{\alpha} \\ \dot{\boldsymbol{\alpha}} \\ \ddot{\boldsymbol{\alpha}} \end{Bmatrix} \tag{4.11}$$

Hence, the reduced state space model of the system can be obtained by coupling the time evolution of the coordinates of the reduced model and the observation equation. By definition of the vector $\boldsymbol{z}_{r,k} = [\boldsymbol{\alpha}_k \quad \dot{\boldsymbol{\alpha}}_k \quad \ddot{\boldsymbol{\alpha}}_k]^T$, the state space equation reads:

i.e.:

$$\boldsymbol{z}_{r,k} = \boldsymbol{A}_r \boldsymbol{z}_{r,k-1} + \boldsymbol{B}_{r,k} + \boldsymbol{v}_k \tag{4.12}$$

$$\boldsymbol{y}_k = \boldsymbol{H}\ \boldsymbol{L}\ \boldsymbol{z}_{r,k} + \boldsymbol{w}_k \tag{4.13}$$

where:

$$\boldsymbol{A}_r = \begin{bmatrix} \boldsymbol{I} - \beta\,\Delta t^2 \boldsymbol{M}_l^{-1}\boldsymbol{K}_l & \Delta t\,\boldsymbol{I} - \beta\,\Delta t^3 \boldsymbol{M}_l^{-1}\boldsymbol{K}_l & -\beta\left({}^1\!/_2 - \beta\right)\Delta t^4 \boldsymbol{M}_l^{-1}\boldsymbol{K}_l + \Delta t^2\left({}^1\!/_2 - \beta\right)\boldsymbol{I} \\ -\gamma\,\Delta t\,\boldsymbol{M}_l^{-1}\boldsymbol{K}_l & \boldsymbol{I} - \gamma\,\Delta t^2 \boldsymbol{M}_l^{-1}\boldsymbol{K}_l & -\gamma\left({}^1\!/_2 - \beta\right)\Delta t^3 \boldsymbol{M}_l^{-1}\boldsymbol{K}_l + \Delta t(1-\gamma)\,\boldsymbol{I} \\ -\boldsymbol{M}_l^{-1}\boldsymbol{K}_l & -\Delta t \boldsymbol{M}_l^{-1}\boldsymbol{K}_l & -\Delta t^2\left({}^1\!/_2 - \beta\right)\boldsymbol{M}_l^{-1}\boldsymbol{K}_l \end{bmatrix} \tag{4.14}$$

and:

$$\boldsymbol{B}_{r,k} = \begin{bmatrix} \beta\,\Delta t^2 \boldsymbol{M}_l^{-1}\,\boldsymbol{R}_{l,k} \\ \gamma\,\Delta t\,\boldsymbol{M}_l^{-1}\boldsymbol{R}_{l,k} \\ \boldsymbol{M}_l^{-1}\boldsymbol{R}_{l,k} \end{bmatrix} \tag{4.15}$$

Since it is assumed that the original model is deterministic, $\boldsymbol{v}_k$ is solely attributed to inaccuracy of the reduced model; $\boldsymbol{w}_k$ instead is representative of measurement errors and model reduction inaccuracies together. In case $\boldsymbol{v}_k$ and $\boldsymbol{w}_k$ are white Gaussian noises, the Kalman filter can furnish optimal estimates of the state of the reduced model; on the contrary, if the distributions of the uncertainties are not Gaussian, uncorrelated or a combination thereof, the performance of Kalman filter is not a priori known to be satisfactory.

In this section, Bartlett white noise test (Bartlett 1978) is profited to verify the null hypothesis of whiteness of the errors induced by the reduced order modelling. In this regard, Bartlett test compares the empirical cumulative normalized periodogram of the given signal with the cumulative distribution of a uniform random variable. The periodogram of an arbitrary random

signal (e.g. $s_k, k = 1,2, \dots, N$), as a mean for spectral analysis, is defined as (Stoica, Moses 1997):

$$I(\omega) = \frac{1}{N} \left| \sum_{k=1}^{N} s_k \, e^{-i\omega_k} \right| \tag{4.16}$$

while, the cumulative periodogram is computed:

$$J(\omega_k) = \frac{\sum_{i=1}^{k} I(\omega_i)}{\sum_{j=1}^{N} I(\omega_j)} \tag{4.17}$$

To perform the comparison, and measure the possible deviation from the whiteness assumption, the Kolmogorov-Smirnov statistics is adopted by Bartlett test (Reschenhofer 1989). In case the associated Kolmogorov-Smirnov statistics of the test exceeds the critical values, for a given confidence interval, the null hypothesis of whiteness would be rejected. For each sample size, and for some confidence levels, the critical values of Kolmogorov-Smirnov statistics are tabulated and reported in references (Miller 1956, Kececioglu 2002). The highest confidence interval, for which the test statistics are reported in (Kececioglu 2002), are related to a probability equal to 99 %; therefore, to accept or reject the hypothesis by maximum probability, in this Chapter we compare test statistics to the value associated with probability of 99%. The critical values of the test statistics also depend on the sample size, which in our case is the length of the error signal. These critical values are estimated trough Monte Carlo simulations (Lilliefors 1967): if the sample size (N) is higher than 35, the critical value of the test statistics is curve fitted and is represented by $\frac{1.63}{\sqrt{N}}$ (Kececioglu 2002). It is reported that the Bartlett test is not a suitable method to test whiteness of observation signals with small sample sets (Reschenhofer 1989). However, dealing with time series of error signal, there is practically no limitation in increasing the number of the samples, and samples size issues are not affecting test results. The results of the test are reported graphically, where empirical cumulative normalized periodogram of the given signal and the cumulative distribution of a uniform random variable (a straight line, passing from the origin and with a slope equal to the inverse of the Nyquist frequency), accompanied by two lines representing the confidence interval, are plotted in the same graph.

Assuming that the true dynamics of the system is known and obtained by analysis of the full model, the errors induced by the model order reduction are here defined as the difference between the true dynamics of the system and the dynamics furnished by the reduced model. The error is considered in terms of difference between the physical coordinates (i.e. $\boldsymbol{u}$, $\dot{\boldsymbol{u}}$, $\ddot{\boldsymbol{u}}$) and the POD temporal coordinates (i.e. $\boldsymbol{\alpha}$, $\dot{\boldsymbol{\alpha}}$, $\ddot{\boldsymbol{\alpha}}$). At time instant t_k, the error signals can therefore be written:

$$\boldsymbol{o}_k = \ddot{\boldsymbol{u}}_k - \boldsymbol{\Phi}_l \ddot{\boldsymbol{\alpha}}_k \quad \boldsymbol{p}_k = \dot{\boldsymbol{u}}_k - \boldsymbol{\Phi}_l \dot{\boldsymbol{\alpha}}_k \quad \boldsymbol{q}_k = \boldsymbol{u}_k - \boldsymbol{\Phi}_l \boldsymbol{\alpha}_k \tag{4.18}$$

while the errors concerning POD coordinates are:

$$\boldsymbol{\rho}_k = \boldsymbol{\Phi}_l^T \ddot{\boldsymbol{u}}_k - \ddot{\boldsymbol{\alpha}}_k \quad \boldsymbol{\sigma}_k = \boldsymbol{\Phi}_l^T \dot{\boldsymbol{u}}_k - \dot{\boldsymbol{\alpha}}_k \quad \boldsymbol{\tau}_k = \boldsymbol{\Phi}_l^T \boldsymbol{u}_k - \boldsymbol{\alpha}_k \tag{4.19}$$

It is seen in (4.18) and (4.19) that the error signals relevant to velocity and acceleration are not assumed as temporal derivatives of displacement error signal. This fact is due to the uncertainties induced by the model order reduction.

In the next section, it is shown that the errors in the reconstructing the state of the full model affects the observation equation of the reduced state space model. Instead the error in the reconstructing the state of the reduced model enters affects the evolution equation of the reduced model.

4.3 Formulation of Kalman-POD observer for linear time invariant systems

The bulk of Chapter 2 has been dedicated to Bayesian filters for the estimation of states and parameters of mechanical systems, of which only a part of the state is observed. However, to keep this Chapter self-contained, key points of recursive Bayesian estimation of mechanical systems are reviewed. The outline of all the Bayesian filters can be drawn in the two stages of prediction and update: in the prediction stage, a model of the system is used to predict the dynamics of the whole state vector, whereas in the update stage, as observations from a part of the state, or as measurable quantities that are correlated with the state become available, the whole state vector is updated. For instance, in a multi storey building it is expensive or even

practically impossible to measure displacements of the storeys directly, while accelerations are easy to measure. In such cases, provided that a model of the structure is available and the model is linear, if uncertainties in the model and in the measurements are uncorrelated Gaussian noises the Kalman filter is the optimal tool for estimating the state of the system.

In practice, it may happen that the high dimension of the model of the structure prevent the filter to fulfill its task in real-time. In such a case, exploiting a reduced model would be beneficial for reducing the computational cost of the Kalman filter. In this chapter, reduced models that are built by POD are used to speed-up the calculations.

The idea of speeding up the calculations required by Kalman filters via reduced order modelling has been already exploited in meteorology, to predict the near surface winds over the tropical Pacific ocean (Wikle, Cressie 1999). A set of empirical functions was adopted to reduce the computational burden of the reconstruction of the wind velocity field, via data available from a few observation points. Malmberg and co-workers (Malmberg, Holst & Holst 2005) adopted subspace realized by PCA for attacking the same problem; they assumed that the weather condition can be thought of as a linear combination of some dominant modes (the weather condition is modeled by a linear time invariant state-space model), the modes being supposed to be invariant; however, the contribution of each mode may vary over time, and the Kalman filter was used for estimating the contribution of each one. Though the concept of reduced state-space Kalman filter is gaining popularity in meteorology (He, Sarma & Durlofsky 2011, Tian, Xie & Sun 2011), its possible application in structural engineering field has not been considered yet. In this section, we deal with the use of Kalman filter to estimate the POD coordinates of Eq. (4-12). At each time instant, after the reduced states are estimated, the whole state vector is reconstructed. For details concerning the synergy of POD and Kalman filter, see Table 4-1.

Provided that the reduced model of the structure is already available, it is seen that the algorithm is simply the application of a Kalman filter to estimate the current state of a linear time-invariant system. In such a system, a linear combination of POMs can represent the dynamics of the system. The POMs are constant over time and do not change; however, the contribution of each

mode in the construction of the response of the structure is changing over time. The Kalman filter, based on the observation made from a part of state vector (e.g. accelerations of some storeys) quantifies the contribution of each POM in the estimation of the state of the system.

Table 4-1: POD-Kalman observer

- Initialization at time t_0: $$\hat{\boldsymbol{z}}_{r,0} = \boldsymbol{\Phi}_l^T \mathbb{E}[\boldsymbol{z}_0]$$ $$\boldsymbol{P}_{r,0} = \boldsymbol{\Phi}_l^T \, \mathbb{E}[(\boldsymbol{z}_0 - \hat{\boldsymbol{z}}_0)(\boldsymbol{z}_0 - \hat{\boldsymbol{z}}_0)^{\mathrm{T}}]\boldsymbol{\Phi}_l$$
- At time t_k, for $k = 1, \dots, N_t$: • Prediction stage: 2. Evolution of state and prediction of covariance $$\boldsymbol{z}_{r,k}^- = \boldsymbol{A}_{r,k}\, \boldsymbol{z}_{r,k-1} + \boldsymbol{B}_{r,k}$$ $$\boldsymbol{P}_{r,k}^- = \boldsymbol{A}_{r,k}\boldsymbol{P}_{r,k-1}\boldsymbol{A}_{r,k}^T + \boldsymbol{V}$$ • Update stage: 3. Calculation of Kalman gain: $$\boldsymbol{G}_k = \boldsymbol{P}_{r,k}^- \boldsymbol{L}^{\mathrm{T}} \boldsymbol{H}_{r,k}^{\mathrm{T}} \left(\boldsymbol{H}_{r,k} \boldsymbol{L}\, \boldsymbol{P}_{r,k}^- \, \boldsymbol{L}^{\mathrm{T}} \boldsymbol{H}_{r,k}^{\mathrm{T}} \; + \boldsymbol{W}\right)^{-1}$$ 4. Improve predictions using latest observation: $$\hat{\boldsymbol{z}}_{r,k} = \boldsymbol{z}_{r,k}^- + \boldsymbol{G}_k\left(\boldsymbol{y}_k - \boldsymbol{H}_{r,k}\, \boldsymbol{L}\, \boldsymbol{z}_{r,k}^-\right)$$ $$\boldsymbol{P}_{r,k} = \boldsymbol{P}_{r,k}^- - \boldsymbol{G}_k \boldsymbol{H}_{r,k} \boldsymbol{L}\, \boldsymbol{P}_{r,k}^-$$ • Reconstruction stage: $$\hat{\boldsymbol{z}}_k = \boldsymbol{L}\, \hat{\boldsymbol{z}}_{r,k}$$

4.4 Numerical assessment of POD-Kalman observer for seismic analysis of linear time invariant systems

As a case study, in Chapter 3 we investigated the capability of POD in speeding up the computations required to model the dynamics of the Pirelli Tower in Milan; in this Section, whiteness of the uncertainties in the reduced models built in Chapter 3 is first assessed, so as to verify the satisfaction of requirements of the Kalman filer for optimal performance. Then, robustness of the Kalman-POD approach to changes in the seismic excitation source is investigated. The Section finally ends with the numerical assessment of speed-up and accuracy of the Kalman-POD algorithm.

As for the error of reduced models for reconstructing the displacement history of the roof floor, Figure 4-1 shows the relevant error for reduced models with various number of retained POMs. The errors are related to the analysis of the building when acceleration time history of El Centro earthquake is used to shake the structure. It is seen that, by increasing the number of POMs, the amplitude of the error signal drastically decreases. However, from the time evolution of the error signals relevant to reduced models featuring different number of POMs, it seems that there is a strong correlation in them, as the signals look like a sinusoid with a time varying amplitude. This is corroborated by the cumulative periodograms of the error signals shown in Figure 4-2. By increasing the number of POMs retained in the reduced models from one to eight, despite the decrease in the error amplitudes, the hypothesis of the whiteness can still be rejected, as all three periodograms relevant to the reduced model exceed the 99% confidence interval (indicated by two parallel black lines in the closeup presented in Figure 4-2). By looking at the cumulative periodograms it can be seen that, as the number of POMs of the reduced model increases, the main jumps move to higher frequency zones.

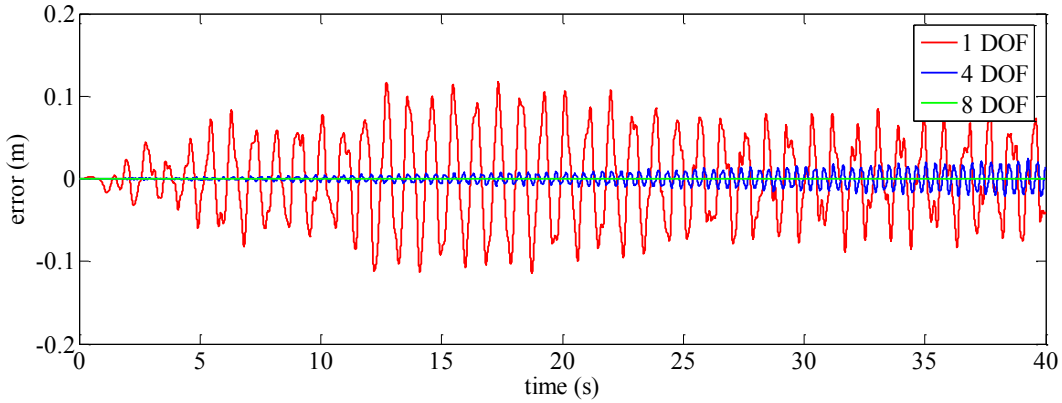

Figure 4-1: Errors in the displacement time histories furnished by reduced order models

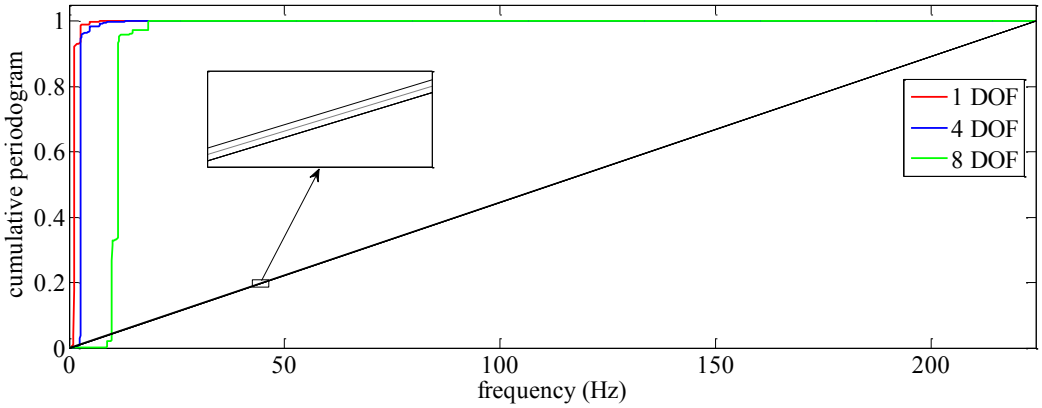

Figure 4-2: Cumulative periodograms of error signals

To investigate this issue in further details, we look at the periodograms of the error signals shown in Figure 4-3. For ease of comparison, the first few natural frequencies of the structure are indicated by vertical dashed lines (see Table 3-1). It is seen that the main peak in the error of the 1-DOF reduced model is coincident in second natural frequency of the structure. By increasing the number of DOFs of the reduced models, according to the decrease in the error amplitude already shown in Figure 4-3, the power of the harmonic components embedded in the signal attenuates severely, to the extent that it is not possible to distinguish the corresponding peaks in Figure 4-3.

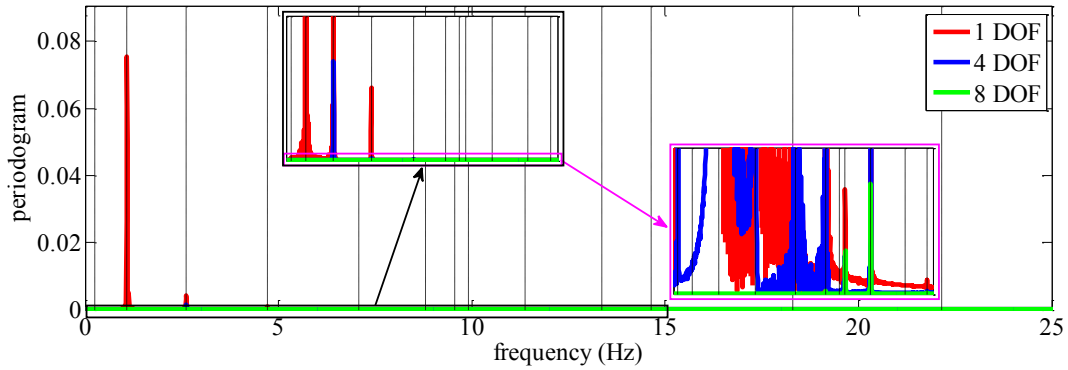

Figure 4-3: Periodograms of the error signals

Close-ups in Figure 4-3 allow to compare the spectral power of the error of three reduced models in a clearer fashion: it is seen that the main periodicity of the error signal of the 4-DOF reduced model coincides with third natural frequency of the system; the close up also shows that, in frequency content of the error signal of the 8-DOF reduced model, the first peak is coincident in the 8th natural frequency of the system. The trend in Figure 4-1 suggests that as the number of DOFs of the reduced model increases, the amplitude of the error signal decreases; consequently, the spectral power of the error signal decreases as well. Also, as the number of DOFs retained in the reduced model increases, the dominant frequency contents coincide with higher natural frequencies of the system. This trend suggests that the subspace spanned by POMs has a degree of similarity with the subspace spanned by the eigenmodes of the system: frequency content of the error induced by neglected POMs is coincident in the higher order eigen-frequencies of the structure.

In what precedes it was observed that the uncertainties in the errors of reduced order models are correlated, and not white noises; hence, optimal performance of the Kalman observer is not guaranteed. However, it was also shown that, by an increase in the number of POMs retained in the reduced model, the spectral density of the correlation in the errors diminishes rapidly.

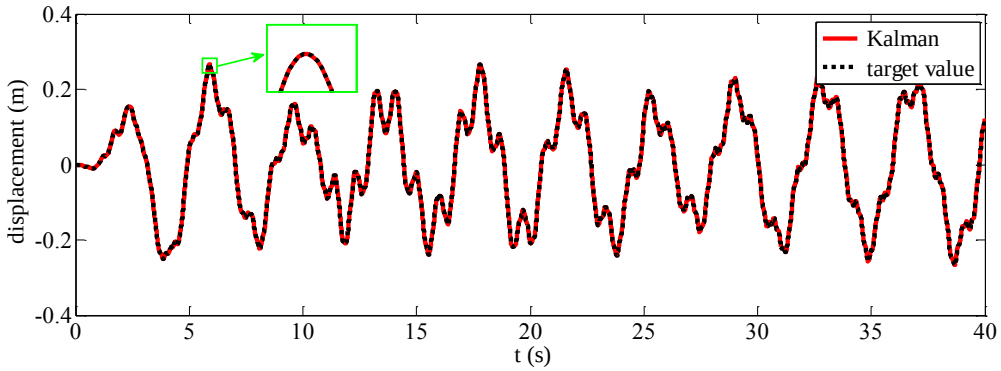

(a)

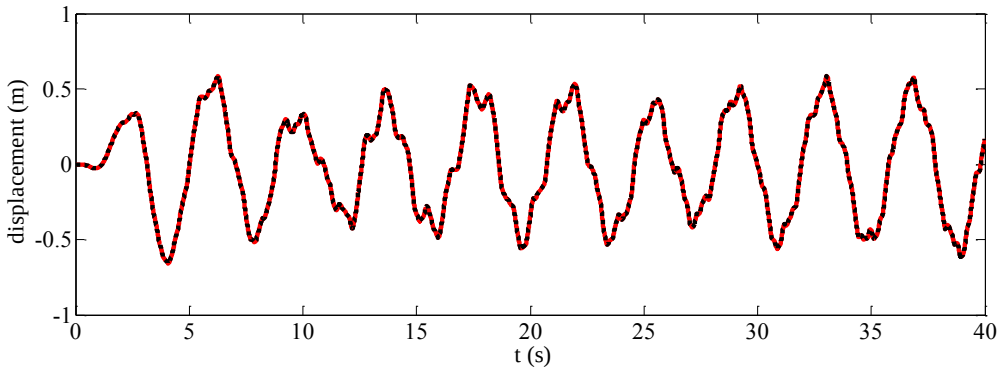

(b)

Figure 4-4: Time histories of the horizontal displacements of 20th floor (a) and 39th floor (b) as induced by the El Centro earthquake, performance of the Kalman filter.

In what follows, the performance of the Kalman observer, if applied to the estimation of the whole state vector on the basis of observations of the acceleration time history of the 39th storey (roof floor) is assessed. Choosing other storeys for observation, or adding more data yields the similar results: it is known that state of a linear state space model with white Gaussian noises is optimality estimated through the Kalman observer. In Figures 4-4 to 4-6, displacement, velocity and acceleration time histories of the 20th (mid floor) and 39th (roof) floors are shown as representative outcomes for the performance of the filter.

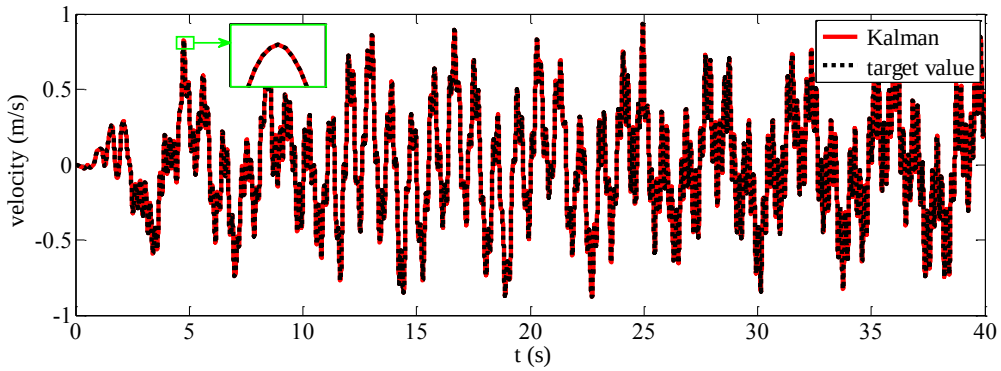

(a)

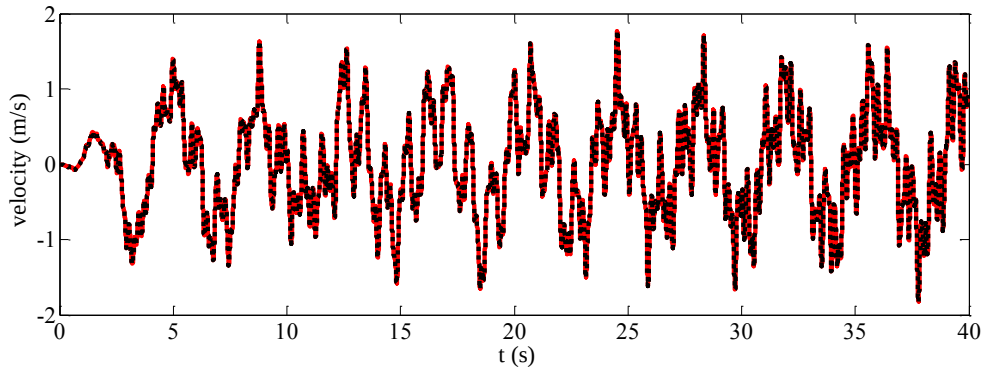

(b)

Figure 4-5: Time histories of the horizontal velocities of 20th floor (a) and 39th floor (b) as induced by the El Centro earthquake, performance of the Kalman filter.

In the analysis for numerical assessment of performance of the Kalman filter, the evolution equation is assumed to be deterministic, and the noise in the observations is supposed to be a white stationary Gaussian process. As expected from optimality of the Kalman observer for dealing with aforementioned problems, it is seen that the estimates furnished by the Kalman filter almost coincide with the target values. This fact is seen through the close-ups in each time history graph.

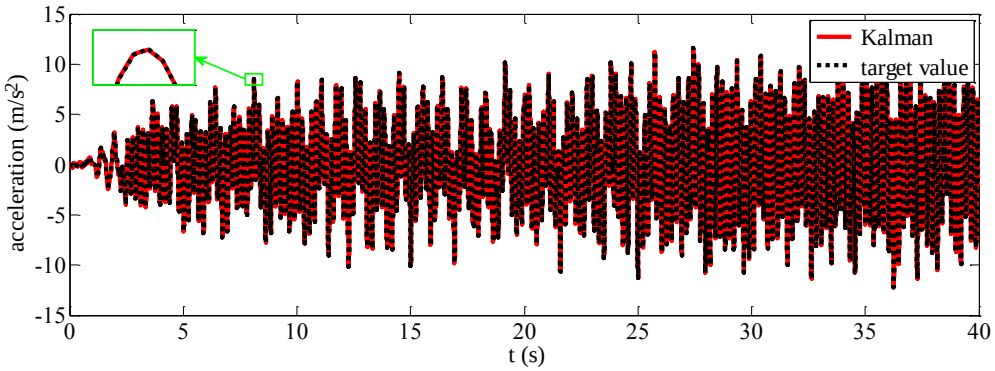

(a)

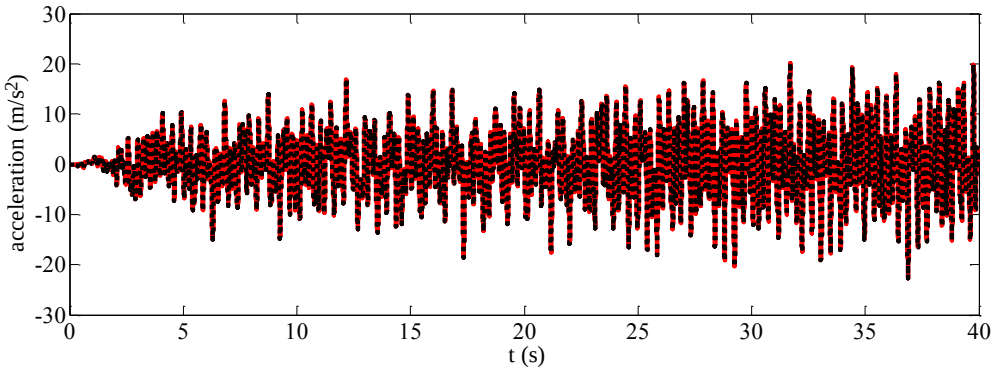

(b)

Figure 4-6: Time histories of the horizontal accelerations of 20th floor (a) and 39th floor (b) as induced by the El Centro earthquake, performance of the Kalman filter.

In the remainder of this Section, the performance of Kalman-POD algorithm for estimating the state of the Pirelli tower is assessed. As it has been shown, the uncertainties in the state-space model are not white; consequently, the performance of the Kalman observer is not a priori known. In this Chapter, we make use of the POD-based reduced models, for the details the readers are referred to see Chapter 3. The reduced model is used by snapshots taken from the simulation of the response of the full model to El Centro accelerogram excitation. Figures 4-7 to 4-9 show time histories of the estimations of displacements, velocities and accelerations of 20th and 39th floor via Kalman-POD algorithm, when the building is shacked by Friuli acceleration

record. It is seen that by keeping only 3 POMs in the reduced model, the time histories estimated by POD-Kalman match those of the full model. To have insights on the improvement in the quality of the estimates by Kalman-POD when it is compared to POD, Table 4-3 and Table 4-4 report residual mean squared error (RMSE) of the 20th and 39th floors, respectively.

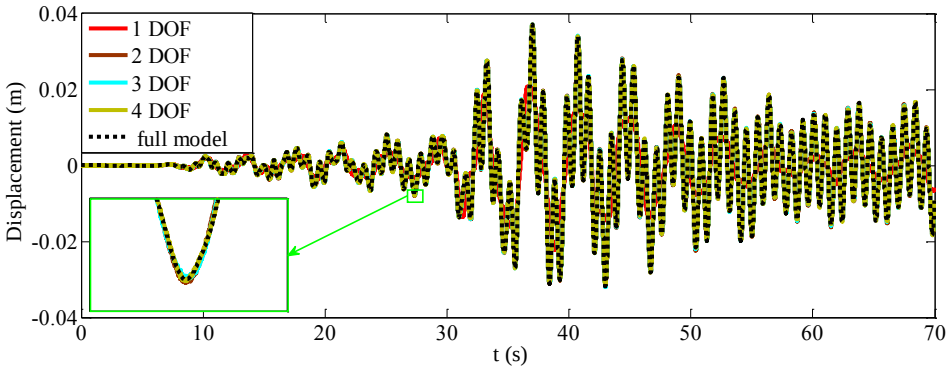

(a)

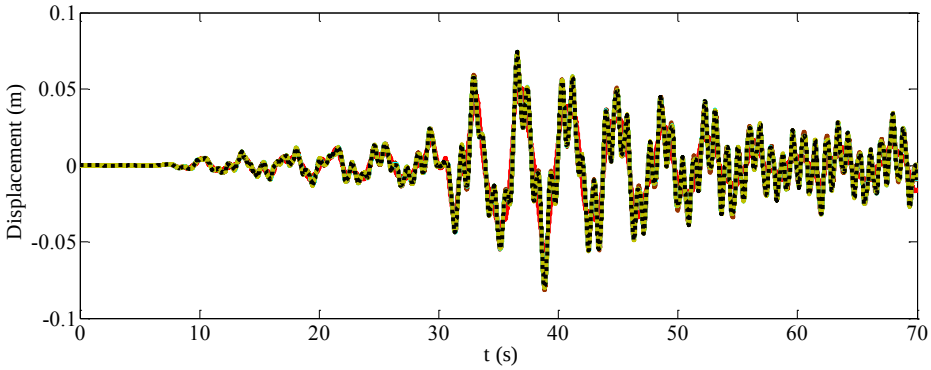

(b)

Figure 4-7: Time histories of the horizontal displacements of 20th floor (a) and 39th floor (b) as induced by the Friuli earthquake, performance of the POD-Kalman.

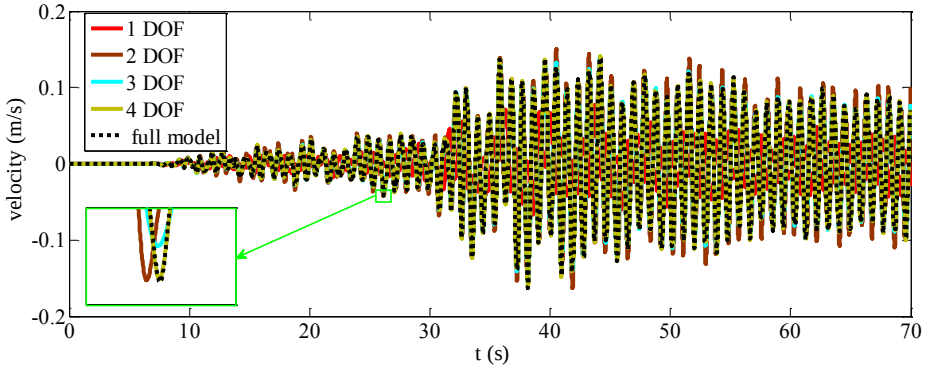

(a)

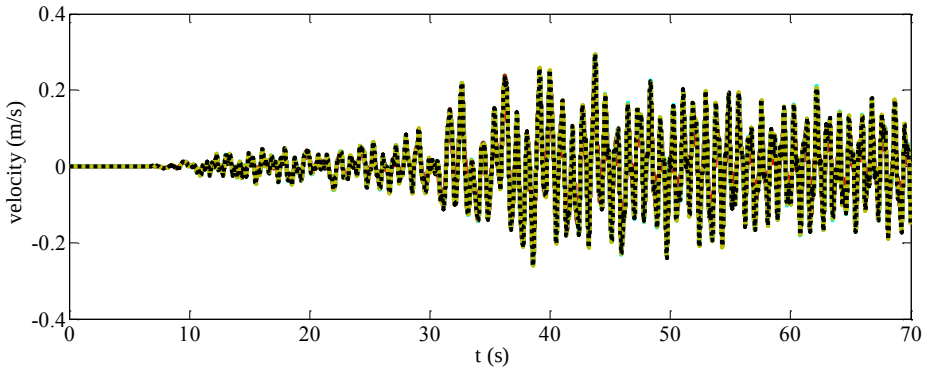

(b)

Figure 4-8: Time histories of the horizontal displacements of 20th floor (a) and 39th floor (b) as induced by the Friuli earthquake, performance of the Kalman-POD.

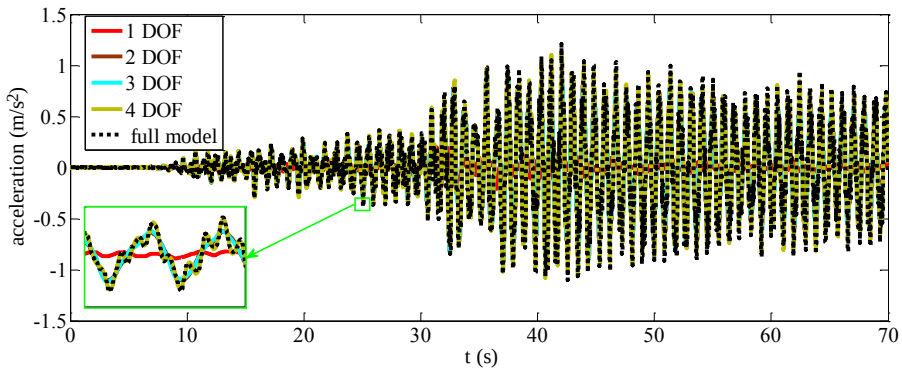

(a)

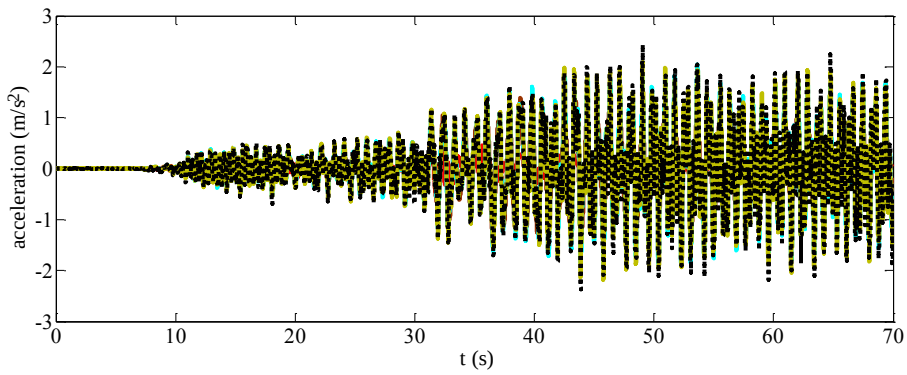

(b)

Figure 4-9: Time histories of the horizontal accelerations of 20th floor (a) and 39th floor (b) as induced by the Friuli earthquake, performance of the POD-Kalman.

In Table 4-3 it is seen that, as the number of DOFs in the reduced model increases, the RMSE error of reconstruction of displacements, velocities and accelerations realized by POD rapidly decreases. When using reduced models with 1 and 2 POMs, the RMSEs of POD solely are less than those of Kalman-POD. However, moving to reduced models with 3 and 4 POMs Kalman-POD is able to improve the quality of the estimate with respect to what the use of POD alone offers. This phenomenon is mainly due to the high spectral power of the correlation structure embedded in the error signal: it has been shown that by increasing the POMs retained in the reduced model the spectral power of the noise correlations decrease rapidly.

Moving to the 39th floor, whose acceleration is measured, it is seen that RMSE of accelerations estimated by POD-Kalman is several orders of magnitude lower than the RMSE of the estimates

provided by POD alone, see Table 4-4. Concerning RMSE of displacements and velocities, it is seen that estimates of POD-Kalman always are smaller than estimates of POD. Unlike the 20th storey RMSEs, which the estimates of the Kalman-POD observer in some cases featured higher error when compared with POD alone, in this case RMSE of Kalman-POD always is lower than POD. This is due to the fact that the response of the system is measured at 39th floor. The trend suggests that, as the number of POMs in the reduced model increases, the estimates of POD-Kalman outperform POD only.

Concerning the speedup obtained by reducing the order of the full model, similarly to Chapter 3, results here discussed have been obtained with a personal computer featuring and Intel Core 2 Duo CPU E8400, with 4 Gb of RAM, running Windows 7x64 as operating system and performing the simulations with MATLAB version 7.6.0.324. The speedup values reported in Table 4-2 confirms the efficiency of Kalman-POD in reducing the computational costs related to the Kalman filter algorithm. It is seen that, using POD-based models incorporated in a Kalman observer can render the calculations hundreds of times faster.

Table 4-2: speed-up obtained by Kalman-POD and POD

# DOFs	*p*	speed-up (Kalman-POD)	speed-up (POD)
1	0.99	309	515
2	0.999	279	385
3	0.9999	225	276
4	0.99999	187	244

Table 4-3: RMSE of time histories of displacemens, velocities and accelerations of 20th floor, comparison between POD and Kalman-POD approaches

# DOFs	*RMSE of POD*			*RMSE of POD-Kalman*		
	disp.	vel.	acc.	disp.	vel.	acc.
1	5.9×10^{-5}	2.7×10^{-3}	1.4×10^{-1}	9.6×10^{-5}	4.4×10^{-3}	3.3×10^{-1}
2	1.0×10^{-6}	1.0×10^{-4}	1.2×10^{-2}	7.0×10^{-7}	1.9×10^{-4}	1.7×10^{-1}
3	2.0×10^{-8}	1.5×10^{-5}	1.4×10^{-2}	1.7×10^{-8}	1.1×10^{-5}	1.1×10^{-2}
4	5.0×10^{-9}	2.0×10^{-6}	2.7×10^{-3}	1.3×10^{-9}	1.3×10^{-6}	1.8×10^{-3}

Table 4-4: RMSE of time histories of displacemens, velocities and accelerations of 39th floor, comparison between POD and Kalman-POD approaches

# DOFs	*RMSE of POD*			*RMSE of POD-Kalman*		
	disp.	vel.	acc.	disp.	vel.	acc.
1	1.1×10^{-4}	5.7×10^{-3}	4.6×10^{-1}	2.6×10^{-5}	1.3×10^{-3}	1.2×10^{-5}
2	5.0×10^{-6}	1.0×10^{-3}	3.1×10^{-1}	1.9×10^{-6}	1.6×10^{-4}	1.8×10^{-6}
3	3.9×10^{-6}	9.0×10^{-4}	2.4×10^{-1}	1.7×10^{-8}	4.0×10^{-6}	1.1×10^{-6}
4	8.7×10^{-7}	2.4×10^{-4}	7.8×10^{-2}	6.8×10^{-9}	1.3×10^{-6}	9.8×10^{-7}

4.5 Summary and conclusion

In this section, the problem of monitoring the whole state of a structure via a numerical model and observations relevant to some points of interest is addressed. It has been shown that, dealing with a linear model of the Pirelli tower, when the building is shacked by the El Centro earthquake record, the Kalman filter can provide almost perfect results by using only acceleration time history of the last floor, as the observation signal.

The reduced models built via POD are then introduced into the Kalman filter to reduce the computational cost of the filter. It has been shown that the reduced models incorporated into the Kalman filter dramatically reduce the computing time, leading to speed-up of 300 for a POD model featuring 1 POM, which is able to accurately reconstruct the displacement time history of the structure. Moreover, it has been shown that the coupling of POD and Kalman filter can improve the estimations provided by POD alone.

This chapter has been limited to linear time invariant systems, the bulk of next Chapter will be instead dealing with the time-varying systems, when there is no a priori information concerning the variation of parameters.

Chapter 5: Dual estimation and reduced order modeling of damaging structures

5.1 introduction

Detection of changes in the mechanical properties of a structural members can be assumed as a method for health monitoring. In many cases, the damage in the structure can be considered as a reduction of the stiffness (Yang, Lin 2005); it may be due to failure of a member to sustain further action, or it can be due to degradation in its material properties. That is, detection of damage in a structure can be posed as a system identification problem. Dealing with a linear structure, offline identification of system matrices can be done via several robust algorithms; as for output only techniques, data driven stochastic subspace identification (SSI) algorithm is the de facto standard stochastic system identification method (Van Overschee, De Moor 1996); subspace identification algorithm is instead widely applied for the identification of deterministic input-output systems (Loh et al. 2011). The aforementioned methodologies include singular value decomposition (SVD) and QR decomposition techniques (Moaveni et al. 2011). Extension of such methodologies to online system identification is usually realized via setting a fixed length moving time window; as new observations become available, a new subspace identification is realized. Computational costs associated with SVD and QR prevent real-time application of such methods. To reduce the computational burden of SVD and QR operations, several methods were proposed, based on updating SVD and QR decomposed matrices, making them suitable for near real-time applications (Loh et al. 2011). In this research, damage detection has been approached via dual estimation of state and stiffness parameters by making use of recursive Bayesian filters, in an online fashion. We have shown in Chapter 2 that, as the number of DOFs of the space model of the structure increases, biases often affect the estimates furnished

by the filters. To cope with this problem, we resort to dual estimation of state and parameters of a reduced model of the structure.

However, unlike the identification of the full model of the system, estimating components of the reduced stiffness does not provide explicit information concerning the intensity and location of the damage. It is known that proper orthogonal modes of the structures contain information concerning location and intensity of the damage (Ruotolo, Surace 1999, Vanlanduit et al. 2005, Galvanetto, Violaris 2007b, Shane, Jha 2011b); this feature of POMs can potentially resolve shortcomings of parameter estimation of a reduced model as indicator of damage location and severity. To this end, we propose an algorithm for dual estimation of state and parameters of a reduced model, accompanied by an online estimation of the POMs of the structure. The proposed procedure makes use of proper orthogonal decomposition for model order reduction, and then exploits Bayesian filters for dual estimation of the full state and reduced parameters of the system. At each recursion, Kalman filter is adopted to update the subspace spanned by the POMs retained in the reduced model. This approach can effectively detect, locate and identify the severity of the damage in shear building type structures. The efficiency of the methodology is testified through pseudo experimental data, obtained with direct analyses.

The remainder of this Chapter is organized as follows. In Section 5.2 the state space formulation of shear buildings is reviewed, it is followed by Section 5.3 that highlights key features of the reduced order state space model of the system. In Section 5.4 the peculiarities of dual estimation and reduced order modelling of a damaging structure are presented and discussed, and our proposal for attacking the problem is defined. In Section 5.5, efficiency of our proposed approach is numerically testified.

5.2 State space formulation of shear building-type structural systems

Aiming to develop an algorithm for multi-storey buildings, in this study we investigate shear buildings, i.e. models obtained by lumped mass assumption for each story, see Figure 5-1.

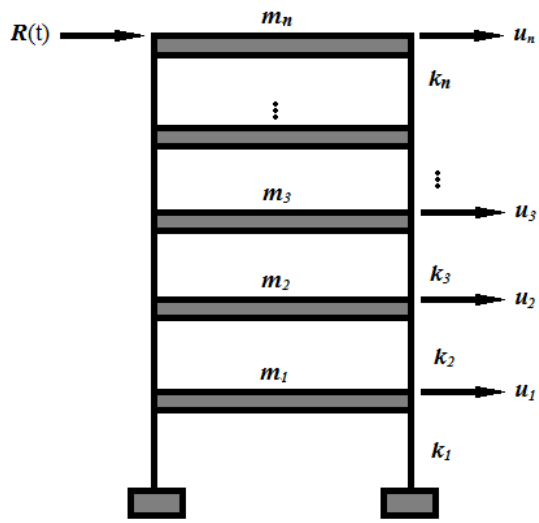

Figure 5-1: schematic view of a shear building

Representing storey displacements, velocities and accelerations by $\boldsymbol{u}$, $\dot{\boldsymbol{u}}$ and $\ddot{\boldsymbol{u}}$ respectively, the governing equation of motion of the building reads:

$$\boldsymbol{M}\ddot{\boldsymbol{u}} + \boldsymbol{D}\dot{\boldsymbol{u}} + \boldsymbol{K}(t)\boldsymbol{u} = \boldsymbol{R}(t) \tag{5.1}$$

where $\boldsymbol{M}$ is the stationary mass matrix, $\boldsymbol{D}$ denotes time invariant damping matrix and $\boldsymbol{K}(t)$ stands for time varying stiffness matrix, whose variation in time is due to possible damage phenomena and is usually unpredictable; $\boldsymbol{R}(t)$ is the loading vector:

$$\boldsymbol{M} = \begin{bmatrix} m_1 & & & \\ & m_2 & & \\ & & \ddots & \\ & & & m_n \end{bmatrix} \tag{5.2}$$

$$\boldsymbol{K}(t) = \begin{bmatrix} k_1(t) + k_2(t) & -k_2(t) & & \\ -k_2(t) & k_2(t) + k_3(t) & & \\ & & \ddots & \\ & & k_{n-1}(t) + k_n(t) & -k_n(t) \\ & & -k_n(t) & k_n(t) \end{bmatrix} \tag{5.3}$$

In general, $\boldsymbol{R}(t)$ can be any kind of loading; however, here we assume that it is a harmonic force applied to the top floor:

$$\boldsymbol{R}(t) = \begin{bmatrix} 0 \\ \vdots \\ 0 \\ a \ \sin \omega t \end{bmatrix} \tag{5.4}$$

where a and ω are the amplitude and frequency of excitation, respectively. For the sake of simplicity, in this study we neglect damping effects.

To numerically solve the set of ordinary differential equations, Newmark explicit integrator is used. To write the equations in the discrete state-space form we introduce an extended state, $\boldsymbol{z}$, that at each time instant t_k includes $\boldsymbol{u}$, $\dot{\boldsymbol{u}}$ and $\ddot{\boldsymbol{u}}$ according to:

$$\boldsymbol{z}_k = \begin{bmatrix} \boldsymbol{u}_k \\ \dot{\boldsymbol{u}}_k \\ \ddot{\boldsymbol{u}}_k \end{bmatrix} \tag{5.5}$$

State-space form of Eq. (5.1) then writes:

$$\boldsymbol{z}_k = \boldsymbol{A}_k \, \boldsymbol{z}_{k-1} + \boldsymbol{B}_k \tag{5.6}$$

where:

$$\boldsymbol{A}_k = \begin{bmatrix} \boldsymbol{I} - \beta \, \Delta t^2 \boldsymbol{K}_k \, \boldsymbol{M}^{-1} & \Delta t \, \boldsymbol{I} - \beta \, \Delta t^2 \boldsymbol{M}^{-1}(\boldsymbol{D} + \Delta t \, \boldsymbol{K}_k) & -\beta \, \Delta t^2 \boldsymbol{M}^{-1}\left(\Delta t^2 \left(1/2 - \beta\right) \boldsymbol{K}_k + \Delta t (1 - \gamma) \, \boldsymbol{D}\right) + \Delta t^2 \left(1/2 - \beta\right) \boldsymbol{I} \\ -\gamma \, \Delta t \, \boldsymbol{K}_k \boldsymbol{M}^{-1} & \boldsymbol{I} - \gamma \, \Delta t \boldsymbol{M}^{-1}(\boldsymbol{D} + \Delta t \, \boldsymbol{K}_k) & -\gamma \, \Delta t \boldsymbol{M}^{-1}\left(\Delta t^2 \left(1/2 - \beta\right) \boldsymbol{K}_k + \Delta t (1 - \gamma) \, \boldsymbol{D}\right) + \Delta t (1 - \gamma) \, \boldsymbol{I} \\ -\boldsymbol{K}_k \boldsymbol{M}^{-1} & -\boldsymbol{M}^{-1}(\boldsymbol{D} + \Delta t \, \boldsymbol{K}_k) & -\boldsymbol{M}^{-1}\left(\Delta t^2 \left(1/2 - \beta\right) \boldsymbol{K}_k + \Delta t (1 - \gamma) \, \boldsymbol{D}\right) \end{bmatrix} \tag{5.7}$$

and :

$$\boldsymbol{B}_k = \begin{bmatrix} \beta \, \Delta t^2 \boldsymbol{M}^{-1} \, \boldsymbol{R}_k \\ \gamma \, \Delta t \, \boldsymbol{M}^{-1} \boldsymbol{R}_k \\ \boldsymbol{M}^{-1} \boldsymbol{R}_k \end{bmatrix} \tag{5.8}$$

β and γ are parameters of the Newmark algorithm, for details see Section 2.6.

Concerning the observation process, it is assumed that a part of state vector is directly observable; hence, observation equation reads:

$$\boldsymbol{y}_k = \boldsymbol{H}\boldsymbol{z}_k + \boldsymbol{w}_k \tag{5.9}$$

where $\boldsymbol{H}$ denotes a Boolean matrix of appropriate dimension which links the states of the system to observation process, and $\boldsymbol{w}_k$ denotes associated measurement noise.

5.3 Reduced order modelling of structural systems

A detailed study of the use of POD for model order reduction of structural system has been presented in Chapter 3. However, to keep this Chapter self-contained, in this Section we review key features of the procedure. Let us assume that the displacement field $\boldsymbol{u} \in \mathbb{R}^m$of the system can be written in a separable form, according to:

$$\boldsymbol{u}(\boldsymbol{x}, t) = \sum_{i=1}^{m} \boldsymbol{\varphi}_i(x)\alpha_i(t) \tag{5.10}$$

where $\boldsymbol{\varphi}_i(x)$ are a set of orthonormal vectors that satisfy proper orthogonal decomposition (POD) requirements and, α_i are temporal functions. Dealing with structural problems with high dimensional state vectors, the main variation in the data is usually occurring in a rather small subspace; consequently, it is often possible to approximate the state of the system by keeping just a few, say l proper orthogonal modes, with $l \ll m$:

$$\begin{aligned} \boldsymbol{u}(\boldsymbol{x}, t) \approx & \sum_{i=1}^{m} \boldsymbol{\varphi}_i(x)\alpha_i(t) \\ & = \boldsymbol{\Phi}_l\, \boldsymbol{\alpha} \end{aligned} \tag{5.11}$$

where $\boldsymbol{\Phi}_l$ denotes the matrix containing the retained l POMs of the system.

Substituting (5.11) into (5.1), and applying Galerkin projection yield the reduced dynamic model of the system:

$$\boldsymbol{M}_l\ddot{\boldsymbol{\alpha}} + \boldsymbol{D}_l\dot{\boldsymbol{\alpha}} + \boldsymbol{K}_l\boldsymbol{\alpha} = \boldsymbol{R}_l(t) \tag{5.12}$$

where:

$$\boldsymbol{M}_l = \boldsymbol{\Phi}_l{}^T\boldsymbol{M}\boldsymbol{\Phi}_l, \quad \boldsymbol{D}_l = \boldsymbol{\Phi}_l{}^T\boldsymbol{D}\boldsymbol{\Phi}_l, \quad \boldsymbol{K}_l = \boldsymbol{\Phi}_l{}^T\boldsymbol{K}\boldsymbol{\Phi}_l, \quad \boldsymbol{R}_l(t) = \boldsymbol{\Phi}_l{}^T\boldsymbol{R}(t) \tag{5.13}$$

The reduced dynamic model in state-space form then reads:

$$\boldsymbol{z}_{r,k} = \boldsymbol{A}_k\boldsymbol{z}_{r,k} + \boldsymbol{B}_k + \boldsymbol{v}_k^z \tag{5.14}$$

$$\boldsymbol{y}_k = \boldsymbol{H}\,\boldsymbol{C}\,\boldsymbol{z}_{r,k} + \boldsymbol{w}_k \tag{5.15}$$

where the reduced order state includes the temporal coefficient, its first and second time derivatives:

$$\boldsymbol{z}_{r,k} = \begin{bmatrix} \boldsymbol{\alpha}_k \\ \dot{\boldsymbol{\alpha}}_k \\ \ddot{\boldsymbol{\alpha}}_k \end{bmatrix} \tag{5.16}$$

In (5.14):

$$\boldsymbol{A}_k = \begin{bmatrix} \boldsymbol{I} - \beta\,\Delta t^2\boldsymbol{M}_l{}^{-1}\boldsymbol{K}_{l,k} & \Delta t\boldsymbol{I} - \beta\,\Delta t^2\boldsymbol{M}_l{}^{-1}(\boldsymbol{D}_l + \Delta t\,\boldsymbol{K}_{l,k}) & -\beta\,\Delta t^2\boldsymbol{M}_l{}^{-1}(\Delta t^2({}^1/_2 - \beta)\boldsymbol{K}_{l,k} + \Delta t(1-\gamma)\,\boldsymbol{D}_l) + \Delta t^2({}^1/_2 - \beta)\,\boldsymbol{I} \\ -\gamma\,\Delta t\,\boldsymbol{M}_l{}^{-1}\boldsymbol{K}_{l,k} & \boldsymbol{I} - \gamma\,\Delta t\boldsymbol{M}_l{}^{-1}(\boldsymbol{D}_l + \Delta t\,\boldsymbol{K}_{l,k}) & -\gamma\,\Delta t\boldsymbol{M}_l{}^{-1}(\Delta t^2({}^1/_2 - \beta)\boldsymbol{K}_{l,k} + \Delta t(1-\gamma)\,\boldsymbol{D}_l) + \Delta t(1-\gamma)\,\boldsymbol{I} \\ -\boldsymbol{M}_l{}^{-1}\boldsymbol{K}_{l,k} & -\boldsymbol{M}_l{}^{-1}(\boldsymbol{D}_l + \Delta t\,\boldsymbol{K}_{l,k}) & -\boldsymbol{M}_l{}^{-1}(\Delta t^2({}^1/_2 - \beta)\boldsymbol{K}_{l,k} + \Delta t(1-\gamma)\,\boldsymbol{D}_l) \end{bmatrix} \tag{5.17}$$

$$\boldsymbol{B}_{l,k} = \begin{bmatrix} \beta\,\Delta t^2\boldsymbol{M}_l{}^{-1}\,\boldsymbol{R}_{l,k} \\ \gamma\,\Delta t\,\boldsymbol{M}_l{}^{-1}\boldsymbol{R}_{l,k} \\ \boldsymbol{M}_l{}^{-1}\boldsymbol{R}_{l,k} \end{bmatrix} \tag{5.18}$$

and, in (5.15):

$$\boldsymbol{C} = \begin{bmatrix} \boldsymbol{\Phi}_l & & \\ & \boldsymbol{\Phi}_l & \\ & & \boldsymbol{\Phi}_l \end{bmatrix} \tag{5.19}$$

Throughout the paper, whenever two indexes are used to denote a variable, the first subscript (r) refers to a property associated to reduced order model, while the second subscript refers to the time instant at which variable is considered.

In (5.14) and (5.15), $\boldsymbol{v}_k^z$ and $\boldsymbol{w}_k$ are the process and measurement noises, respectively. The former uncertainty stems from the loss of accuracy due to the reduced modeling, and needs to be further assessed, to determine its probability distribution and verify the correlation structure in it. In Chapter 4, we have tested the whiteness of the residual error signal of POD-based reduced model of Pirelli tower; it has been shown that, by an increase in the number of POMs retained in the analysis, a reduction occurs in the amplitude of the noise signal and its spectral power. As a consequence, the effect of the non-white uncertainty in the Kalman-POD observer becomes negligible. Hence, in this Chapter we assume that the noises satisfy the requirements of the family of recursive Bayesian inference algorithms.

To attack the dual estimation problem, we now augment the parameters of the reduced model into the state vector, to comply with the state space form. We then introduce the augmented state vector $\boldsymbol{x}_{r,k}$, that at any time t_k encompasses both states and parameters of the system $\boldsymbol{x}_{r,k} = [\,\boldsymbol{z}_{r,k} \quad \boldsymbol{\vartheta}_{r,k}]^T$. In Section 2.2, it is shown that dual estimation of states and parameters of a linear system leads to a nonlinear state-space model. The new state space equation writes:

$$\boldsymbol{x}_{r,k} = \boldsymbol{f}_{r,k}\left(\boldsymbol{x}_{r,k-1}\right) + \boldsymbol{v}_k \tag{5.20}$$

$$\boldsymbol{y}_k = \boldsymbol{H}\,\boldsymbol{L}\,\boldsymbol{x}_{r,k} + \boldsymbol{w}_k \tag{5.21}$$

$$\boldsymbol{L} = \begin{bmatrix} \boldsymbol{C} & \boldsymbol{0} \end{bmatrix} \tag{5.22}$$

where: $\boldsymbol{0}$ in $\boldsymbol{L}$ is a null matrix of appropriate dimension to annihilate the effects in the observation mapping of parameters in the augmented state vector; $\boldsymbol{f}_{r,k}(.)$ maps the state of the system in time and $\boldsymbol{H}$ denotes the correlation between states and observables of the system; $\boldsymbol{L}$ links the reduced states of the system to the full state; whereas $\boldsymbol{v}_k$ and $\boldsymbol{w}_k$ stand for the zero mean white Gaussian processes with associated covariance matrices $\boldsymbol{V}$ and $\boldsymbol{W}$. Likewise previous

Chapters, $\boldsymbol{\vartheta}_{r,k}$ includes the parameters of the reduced state space model that should be estimated, namely the components of the reduced stiffness matrix $\boldsymbol{K}_{l,k}$.

5.4 Dual estimation of reduced states and parameters of a damaging structure

Dual estimation problem for a non-damaging (elastic) structure can be pursued via the estimation of reduced state and parameters, since there wouldn't be changes in the subspace of the problem. On the contrary, subspace of a damaging structure varies in time: for instance, a change in a story stiffness can lead to a change in the POMs. As a consequence, dual estimation of the reduced state and parameters of a damaging structure not only includes tracking of the reduced state and estimation of the reduced parameters of the system, but also needs online update of the relevant subspace of the structure.

In this Section, we introduce a novel approach for simultaneous state and parameter estimation, accompanied by an online subspace update in order to obtain an estimate of the full state. In this regard, we adopt recursive Bayesian filters: the extended Kalman filter (EKF) and the extended Kalman particle filter (EK-PF). They have been discussed in Chapter 2, and used for dual estimation. A Kalman filter is instead used to update the subspace furnished by POD. Likewise all recursive Bayesian inference algorithms, the iterations start by an initial guess; then, within each time interval $[t_{k-1}\ \ t_k]$, provided that at t_{k-1} estimations of state, parameters and subspace of the system are available, the state $\boldsymbol{z}_{r,k}$ and parameters in $\boldsymbol{K}_{l,k}$ are simultaneously estimated. Let us consider the following state space model:

$$\boldsymbol{x}_{r,k} = \boldsymbol{f}_{r,k}\left(\boldsymbol{x}_{r,k-1}\right) + \boldsymbol{v}_k \tag{5.23}$$

$$\boldsymbol{y}_k = \boldsymbol{H}\ \boldsymbol{L}_k\ \boldsymbol{x}_{r,k} + \boldsymbol{w}_k \tag{5.24}$$

where:

$$\boldsymbol{L}_k = \begin{bmatrix} \boldsymbol{\Phi}_{l,k} & & & \\ & \boldsymbol{\Phi}_{l,k} & & \\ & & \boldsymbol{\Phi}_{l,k} & \\ & & & \mathbf{0} \end{bmatrix} \tag{5.25}$$

Along with Eqs. (5.23) and (5.24), an additional equation should be introduced in order to permit time variation and update of $\boldsymbol{\Phi}_l$, similar to the trick used for dual estimation of states and parameters. The following equation is introduced to allow the subspace to vary over time, and use the data in observation in order to adapt to the possible changes:

$$\boldsymbol{\Phi}_{l,k} = \boldsymbol{\Phi}_{l,k-1} + \boldsymbol{\upsilon} \tag{5.26}$$

where $\boldsymbol{\upsilon}$ denotes a fictitious zero mean, white Gaussian noise with associated covariance $\boldsymbol{\Upsilon}$, that needs to be obviously tuned to obtain unbiased estimates of the subspace vectors.

To recursively update the subspace, Eqs. (5.26) and (5.24) are assumed as the state-space model for subspace evolution. The former equation governs the evolution of the subspace, and the latter one links the observation to the subspace. In Eqs. (5.26) and (5.24), it is assumed that $\boldsymbol{x}_{r,k}$ remains independent of $\boldsymbol{\Phi}_{l,k}$. The observation equation (5.24), when used for subspace update can be rewritten as:

$$\boldsymbol{y}_k = \boldsymbol{H}_{ss}\boldsymbol{\Phi}_{l,k} + \boldsymbol{w}_k \tag{5.27}$$

where $\boldsymbol{H}_{ss}$ is a stationary matrix which links the observation process to the subspace spanned by the POMs, and can be computed by manipulating Eq. (5.26). Eq. (5.27) establishes a linear relationship between the observation $\boldsymbol{y}_k$ and the subspace $\boldsymbol{\Phi}_{l,k}$, whose linearity allows us to use the Kalman filter (the optimal estimator for linear state-space models) for the estimation of the subspace.

In Tables 5.1 and 5.2, an algorithmic description of the procedure is reported; the EKF and the EK-PF are used for dual estimation. In the Table 5-1, $\nabla_x \boldsymbol{f}_{r,k}(\boldsymbol{x})|_{\boldsymbol{x}=\hat{\boldsymbol{x}}_{k-1}}$denotes Jacobian of $\boldsymbol{f}_{r,k}(\blacksquare)$, at $\boldsymbol{x}_r = \boldsymbol{x}_{r,k}^-$.

Table 5-1: EKF-KF algorithm for dual estimation of the reduced model and subspace update

- Initialization at time t_0:

$$\hat{\boldsymbol{x}}_{r,0} = \boldsymbol{L}_0^{\mathrm{T}}\,\mathbb{E}[\boldsymbol{x}_0] \qquad \boldsymbol{P}_{r,0} = \boldsymbol{L}_0^{\mathrm{T}}\,\mathbb{E}[(\boldsymbol{x}_0 - \hat{\boldsymbol{x}}_0)(\boldsymbol{x}_0 - \hat{\boldsymbol{x}}_0)^{\mathrm{T}}]\boldsymbol{L}_0$$
$$\hat{\boldsymbol{\Phi}}_{l,0} = \mathbb{E}\left[\boldsymbol{\Phi}_{l,0}\right] \qquad \boldsymbol{P}_{ss,0} = \mathbb{E}\left[\left(\boldsymbol{\Phi}_{l,0} - \hat{\boldsymbol{\Phi}}_{l,0}\right)\left(\boldsymbol{\Phi}_{l,0} - \hat{\boldsymbol{\Phi}}_{l,0}\right)^{\mathrm{T}}\right]$$

- At time t_k, for $k = 1, \dots, N_t$:
  - Prediction stage:
    1. Computing process model Jacobian:
    $$\boldsymbol{F}_{r,k} = \nabla_x \boldsymbol{f}_{r,k}(\boldsymbol{x})|_{\boldsymbol{x} = \hat{\boldsymbol{x}}_{k-1}}$$
    2. Evolution of state and prediction of covariance:
    $$\boldsymbol{x}_{r,k}^{-} = \boldsymbol{f}_{r,k}\left(\boldsymbol{x}_{r,k-1}\right)$$
    $$\boldsymbol{P}_{r,k}^{-} = \boldsymbol{F}_{r,k}\boldsymbol{P}_{r,k-1}^{-}\boldsymbol{F}_{r,k}^{T} + \boldsymbol{V}$$
  - Update stage:
    1. Use $\boldsymbol{\Phi}_{l,k-1}$ to estimated $\boldsymbol{L}_k$ and Kalman gain:
    $$\boldsymbol{G}_k = \boldsymbol{P}_{r,k}^{-}\boldsymbol{L}_k^{\mathrm{T}}\boldsymbol{H}^{\mathrm{T}}\left(\boldsymbol{H}\boldsymbol{L}_k\boldsymbol{P}_{r,k}^{-}\boldsymbol{L}_k^{\mathrm{T}}\,\boldsymbol{H}^{\mathrm{T}} + \boldsymbol{W}\right)^{-1}$$
    2. Update state and covariance:
    $$\boldsymbol{x}_{r,k} = \boldsymbol{x}_{r,k}^{-} + \boldsymbol{G}_k\left(\boldsymbol{y}_k - \boldsymbol{H}\boldsymbol{L}_k\boldsymbol{x}_{r,k}^{-}\right)$$
    $$\boldsymbol{P}_{r,k} = \boldsymbol{P}_{r,k}^{-} - \boldsymbol{G}_k\boldsymbol{H}\boldsymbol{L}_k\boldsymbol{P}_{r,k}^{-}$$
    3. Predict subspace and its associated covariance:
    $$\boldsymbol{\Phi}_{l,k}^{-} = \boldsymbol{\Phi}_{l,k-1}$$
    $$\boldsymbol{P}_{ss,k}^{-} = \boldsymbol{P}_{ss,k-1} + \Upsilon$$
    4. Calculate Kalman gain for updating subspace:
    $$\boldsymbol{G}_{ss,k} = \boldsymbol{P}_{ss,k}^{-}\boldsymbol{H}_{ss}^{\mathrm{T}}\left(\boldsymbol{H}_{ss}\boldsymbol{P}_{ss,k}^{-}\boldsymbol{H}_{ss}^{\mathrm{T}} + \boldsymbol{W}\right)^{-1}$$
    5. Update subspace and its associated covariance:
    $$\boldsymbol{\Phi}_{l,k} = \boldsymbol{\Phi}_{l,k}^{-} + \boldsymbol{G}_{ss,k}\left(\boldsymbol{y}_k - \boldsymbol{H}_{ss}\boldsymbol{\Phi}_{l,k}^{-}\right)$$
    $$\boldsymbol{P}_{ss,k} = \boldsymbol{P}_{ss,k}^{-} - \boldsymbol{G}_{ss,k}\boldsymbol{H}_{ss}\boldsymbol{P}_{ss,k}^{-}$$

As seen in Table 5.1, the algorithm has two main stages of prediction and update. In the prediction stage, the evolution equations are used to map in time the reduced state $\boldsymbol{x}_{r,k-1}$ along with its covariance. In the update stage, first the reduced state and parameters and their associated covariances are corrected by incorporating the information contained in the latest observation (steps #1 and #2), then the Kalman filter is exploited to update the subspace $\boldsymbol{\Phi}_l$. Step #3 in the prediction stage of dual estimation algorithm, is indeed the predictor stage of the Kalman filter to update the subspace. In step #4, Kalman gain is computed and is used in step #5 to update the estimate of the subspace by taking the latest observation into account.

Concerning the use of EK-PF for dual estimation, according to previous Chapter 2, combined with the Kalman filter for subspace update, similar to the procedure used by EKF-KF algorithm, the reader is referred to Table 5-2. In the Table 5-2, $\boldsymbol{F}_{r,k}^{(i)}$ is:

$$\nabla_x \boldsymbol{f}_{r,k}(\boldsymbol{x})|_{\boldsymbol{x}=\hat{\boldsymbol{x}}_{k-1}} \tag{5.28}$$

where it denotes Jacobian of the reduced evolution $\boldsymbol{f}_{r,k}(\boldsymbol{x}_r)$ at $\boldsymbol{x}_r = \boldsymbol{x}_{r,k}^{(i)-}$.

Table 5-2: EK-PF-KF algorithm for dual estimation of the reduced model and subspace update

- Initialization at time t_0:

$$\hat{\boldsymbol{x}}_{r,0} = \boldsymbol{L}_0^{\mathrm{T}}\mathbb{E}[\boldsymbol{x}_0] \qquad \boldsymbol{P}_{r,0} = \boldsymbol{L}_0^{\mathrm{T}}\,\mathbb{E}[(\boldsymbol{x}_0 - \hat{\boldsymbol{x}}_0)(\boldsymbol{x}_0 - \hat{\boldsymbol{x}}_0)^{\mathrm{T}}]\boldsymbol{L}_0$$
$$\hat{\boldsymbol{\Phi}}_{l,0} = \mathbb{E}\left[\boldsymbol{\Phi}_{l,0}\right] \qquad \boldsymbol{P}_{ss,0} = \mathbb{E}\left[\left(\boldsymbol{\Phi}_{l,0} - \hat{\boldsymbol{\Phi}}_{l,0}\right)\left(\boldsymbol{\Phi}_{l,0} - \hat{\boldsymbol{\Phi}}_{l,0}\right)^{\mathrm{T}}\right]$$
$$\boldsymbol{x}_{r,0}^{(i)} = \hat{\boldsymbol{x}}_0 \qquad \omega_0^{(i)} = p\left(\boldsymbol{y}_0|\boldsymbol{x}_{r,0}\right), \qquad i = 1, \dots, N_{\mathrm{P}}$$

- At time t_k, for $k = 1, \dots, N_t$:

- Prediction stage:

  1. Draw particles:
  $$\boldsymbol{x}_{r,k}^{(i)-} \sim p\left(\boldsymbol{x}_{r,k}|\boldsymbol{x}_{r,k-1}^{(i)}\right) \qquad i = 1, \dots, N_{\mathrm{P}}$$
  2. Push the particles toward the region of high probability through an EKF:

$$\boldsymbol{P}_{r,k}^{(i)-} = \boldsymbol{F}_{r,k}^{(i)} \boldsymbol{P}_{r,k-1}^{(i)} \boldsymbol{F}_{r,k}^{(i)\,T} + \boldsymbol{V}$$

$$\boldsymbol{G}_k^{(i)} = \boldsymbol{P}_{r,k}^{(i)-} \boldsymbol{L}_{k-1}^{\mathrm{T}} \boldsymbol{H}_k^{\mathrm{T}} \left(\boldsymbol{H} \boldsymbol{L}_{k-1} \boldsymbol{P}_{r,k}^{(i)-} \boldsymbol{L}_{k-1}^{\mathrm{T}} \boldsymbol{H}^{\mathrm{T}} + \boldsymbol{W} \right)^{-1}$$

$$\boldsymbol{x}_{r,k}^{(i)} = \boldsymbol{x}_{r,k}^{(i)-} + \boldsymbol{G}_k^{(i)} \left(\boldsymbol{y}_k - \boldsymbol{H} \boldsymbol{L}_{k-1} \boldsymbol{x}_{r,k}^{(i)-} \right) \qquad i = 1, \dots, N_{\mathrm{P}}$$

$$\boldsymbol{P}_{r,k}^{(i)} = \boldsymbol{P}_{r,k}^{(i)-} - \boldsymbol{G}_k^{(i)} \boldsymbol{H} \boldsymbol{L}_{k-1} \boldsymbol{P}_{r,k}^{(i)-}$$

- Update stage:

1. Evolve weights:

$$\omega_k^{(i)} = \omega_{k-1}^{(i)}\, p\left(\boldsymbol{y}_k | \boldsymbol{x}_{r,k}^{(i)} \right) \qquad i = 1, \dots, N_{\mathrm{P}}$$

2. Resampling, see Table 2-5.
3. Compute expected value or other required statistics:

$$\widehat{\boldsymbol{x}}_{r,k} = \sum_{i=1}^{N_{\mathrm{P}}} \omega_k^{(i)}\, \boldsymbol{x}_{r,k}^{(i)}$$

4. Predict subspace and its associated covariance:

$$\boldsymbol{\Phi}_{l,k}^{-} = \boldsymbol{\Phi}_{l,k-1}$$
$$\boldsymbol{P}_{ss,k}^{-} = \boldsymbol{P}_{ss,k-1} + \Upsilon$$

5. Calculate Kalman gain for updating subspace:

$$\boldsymbol{G}_{ss,k} = \boldsymbol{P}_{ss,k}^{-} \boldsymbol{H}_{ss}^{\mathrm{T}} \left(\boldsymbol{H}_{ss} \boldsymbol{P}_{ss,k}^{-} \boldsymbol{H}_{ss}^{\mathrm{T}} + \boldsymbol{W} \right)^{-1}$$

6. Update subspace and its associated covariance:

$$\boldsymbol{\Phi}_{l,k} = \boldsymbol{\Phi}_{l,k}^{-} + \boldsymbol{G}_{ss,k} \left(\boldsymbol{y}_k - \boldsymbol{H}_{ss} \boldsymbol{\Phi}_{l,k}^{-} \right)$$
$$\boldsymbol{P}_{ss,k} = \boldsymbol{P}_{ss,k}^{-} - \boldsymbol{G}_{ss,k} \boldsymbol{H}_{ss} \boldsymbol{P}_{ss,k}^{-}$$

5.5 Numerical results: damage detection in a ten storey shear building

This section deals with the numerical assessment of the proposed algorithm for detecting damage in a 10-storey shear building. To deal with the damage scenarios, it is not straight forward to use

the model of Pirelli tower, due to the fact that a static condensation has been carried out to derive matrices of lumped mass system of the Pirelli towers. For the sake of simplicity, in the numerical example it is assumed that all the floors have equal mass and inter-storey stiffness, i.e. $m_i = 20$ Kg and $k_i = 300$ kg/m where $i = 1,2,..,10$, and the damping effect is neglected. It the analysis, the external load shaking the structure, is a sinusoidal load applied to the last floor (roof) of the building, varying according to:

$$R(t) = a_m \sin 2\pi\omega t \tag{5.29}$$

where $a_m = 10$ N and $\omega = 0.01$ Hz.

Consider a case in which a stiffness reduction equal to 50% has occurred at the 5th floor. The POMs of the structure, before and after damage occurrence, are computed and presented in the Figure 5-2. To compute these POMs of the healthy and damaged cases, two direct analyses have been carried out to assemble the so-called snapshot matrices. Looking at Figure 5-2, it can be seen that the ten POMs of the structure are affected by the stiffness reduction at the 5th floor. The effect of the damage in the first POM is quite visible, the usefulness of such sensitivity to damage, even in the first POM, helps tracking the evolution of damage in a single DOF reduced model.

Figure 5-3 compares the first POM of the structure when the 5th floor of the structure suffers a damage of varying intensity; the close-up in the graph allows to compare the shape of the POM in the vicinity of the damage location. Obviously, the intensity of damage leads to an increase in the deviation of the POM relevant to the damaged state with respect to the healthy state of the structure. To highlight the sensitivity of the 1st POM to damage location, in Figure 5-4 the first POM of the damaged state is compared with healthy state of it, when damage occurs at different floors. The imposed level of the damage in all the cases is equal to a 50% reduction of the stiffness of the relevant floor.

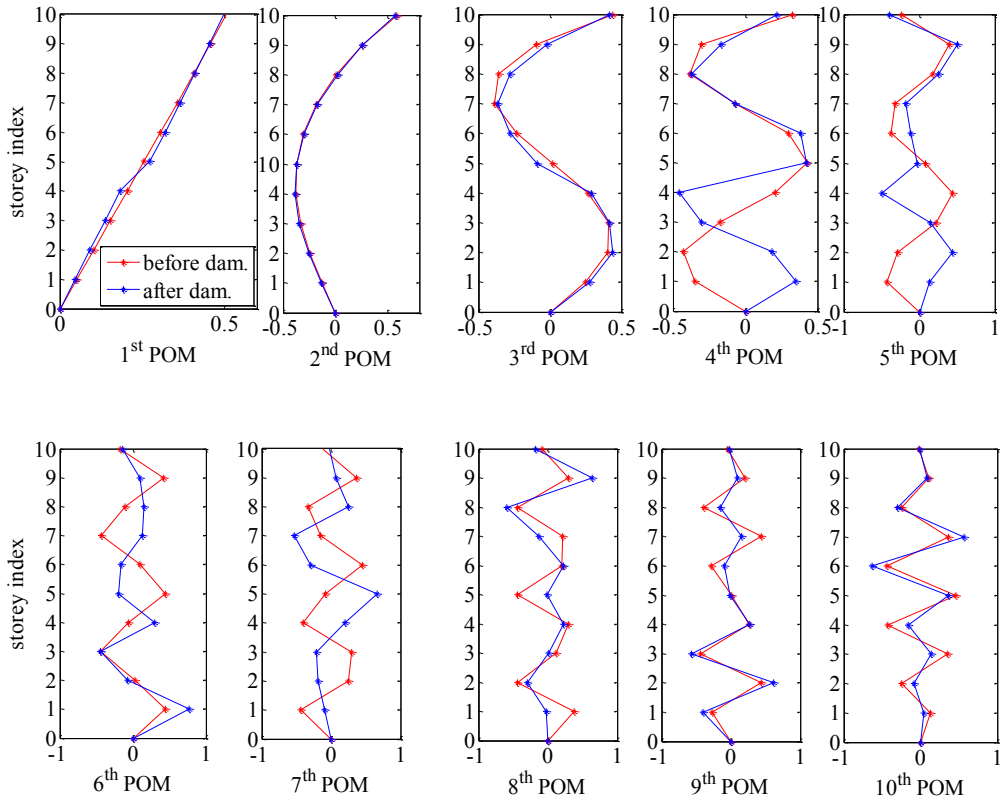

Figure 5-2: proper orthogonal modes of a 10 storey shear building before and after damage

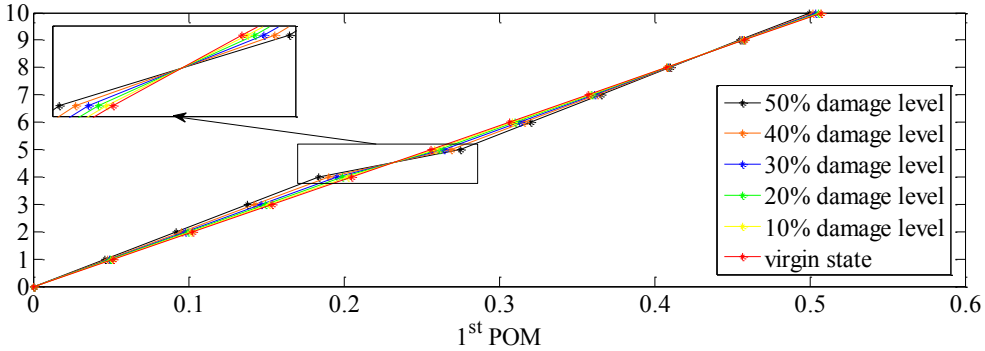

Figure 5-3: 1st POM of the 10 storey shear building subject to different levels of damage at 5th floor

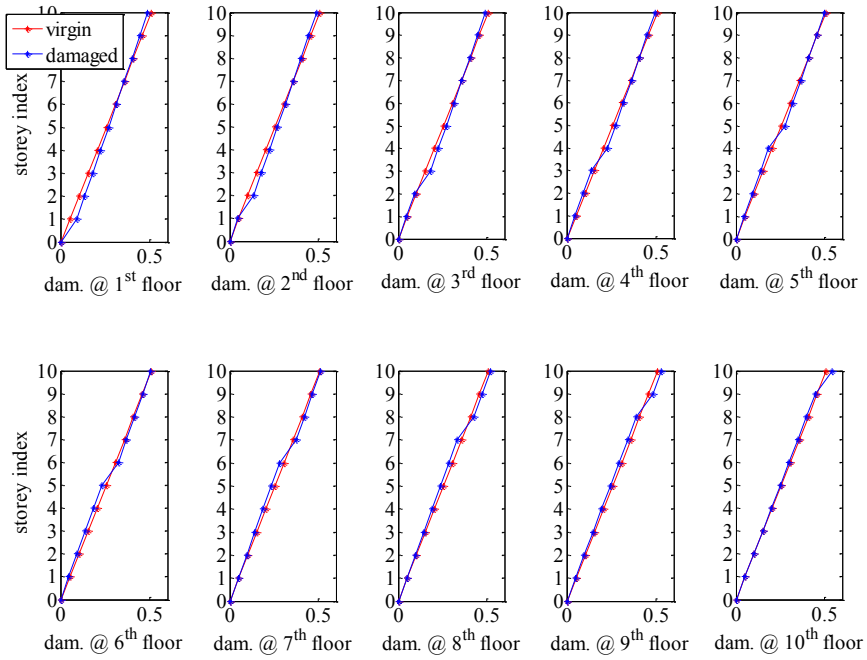

Figure 5-4: 1st POM of a ten storey shear building for a damage occuring at different storeys of the building

Now that the link between the first POM of the structure and the location and severity of the damage is established, we move to the problem of the recursive estimation of the state, parameters and POMs of the reduced model of the structure. To detect the damage, POMs of healthy and current state of the structure are compared, so information concerning the healthy state of the structure are needed. In this study, the case in which the reduced models retain one or two POMs are assessed, the latter case is mainly reported to verify the performance of the algorithm in case of the higher number of parameters to be estimated: dual estimation of reduced models which retain more POMs includes calibrating a high number of parameters, and can therefore potentially pose the problem of curse of dimensionality, as discussed in Chapter 2.

First, we deal with the reduced model constructed through a single POM. Pseudo-experimental data for evaluation of the methodology have been created by running direct analysis, to compute the response of the structure, and then adding zero mean white Gaussian noise to allow for

uncertainties in measuring the response of the structure. The covariance of the added noise to all the pseudo experimental data considered in this section is set to 10^{-4} m^2 to simulate a high level of measurement uncertainty. The duration of the analysis is set to 1000 s, in order to let the estimates of the algorithms converge to a steady state value. The damage scenario is once again a reduction of 50% in the stiffness of the 5th floor, which occurs at $t = 100$ s. Other damage scenarios, featuring severities ranging from 10% to 40% in the reduction of the stiffness of other floors has been assessed; the algorithms show similar performance dealing with those scenarios, hence results are not presented here for the sake of brevity.

Since the goal of this Section is the identification of damage, results concerning the estimation of the state are not discussed. Figure 5-5 shows the time history of the estimated stiffness of the reduced system when compared with its target value. It is seen that before damage occurs, the estimation coincides with the target value; however, after damage occurs, it takes almost 400 s for the algorithm to make its estimate to converge to the target value. Figure 5-6 shows the estimated POMs of the building before and after damage: the POM concerning the healthy state is related to $t = 50$ s, and the POM concerning the damaged state is related to $t = 1000$ s. To compare the performance of the algorithm in tracking the POM of the system over time, Figure 5-7 shows time history of the estimated POM, compared with its target value. It is seen that the estimations of the POM components before damage occurrence coincide with the true value; after damage occurs, the algorithm needs almost 400 s, similar to parameter estimates, to reach to steady state. EK-PF, when dealing with some problems discussed in Chapter 2 outperforms the EKF; hence it is here used to verify if its convergence rate would be better than EKF's one. However, it is seen in Figure 5-5 that the quality of estimation of the reduced stiffness and the 1st POM of the structure is not change, when either EKF-KF or EK-PF-KF are used for dual estimation and reduced order modelling of the damaging shear building.

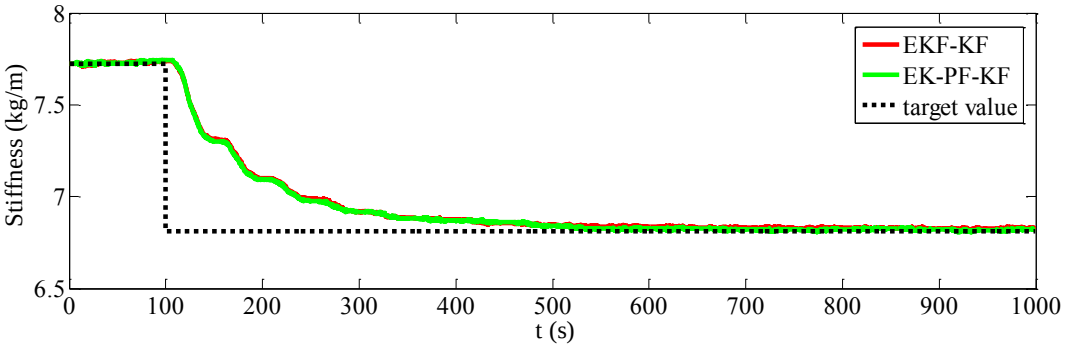

Figure 5-5: estimation of the reduced reduced via EKF-KF and EK-PF-KF algorithms

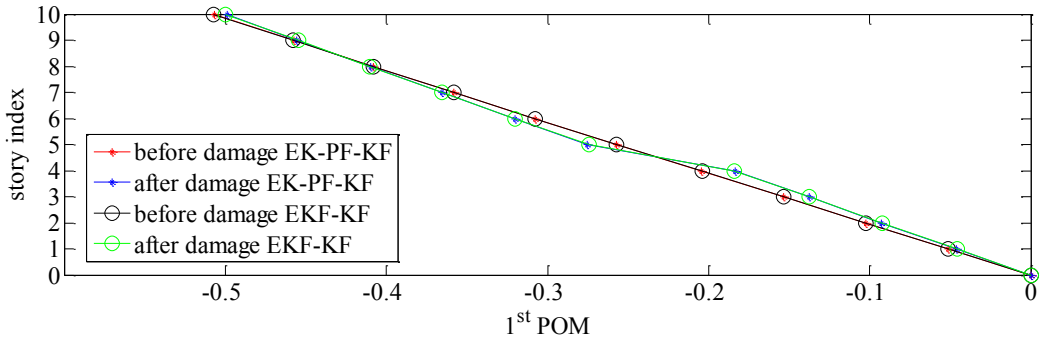

Figure 5-6: 1st POM of the structure estimated EKF-KF and EK-PF-KF algorithms

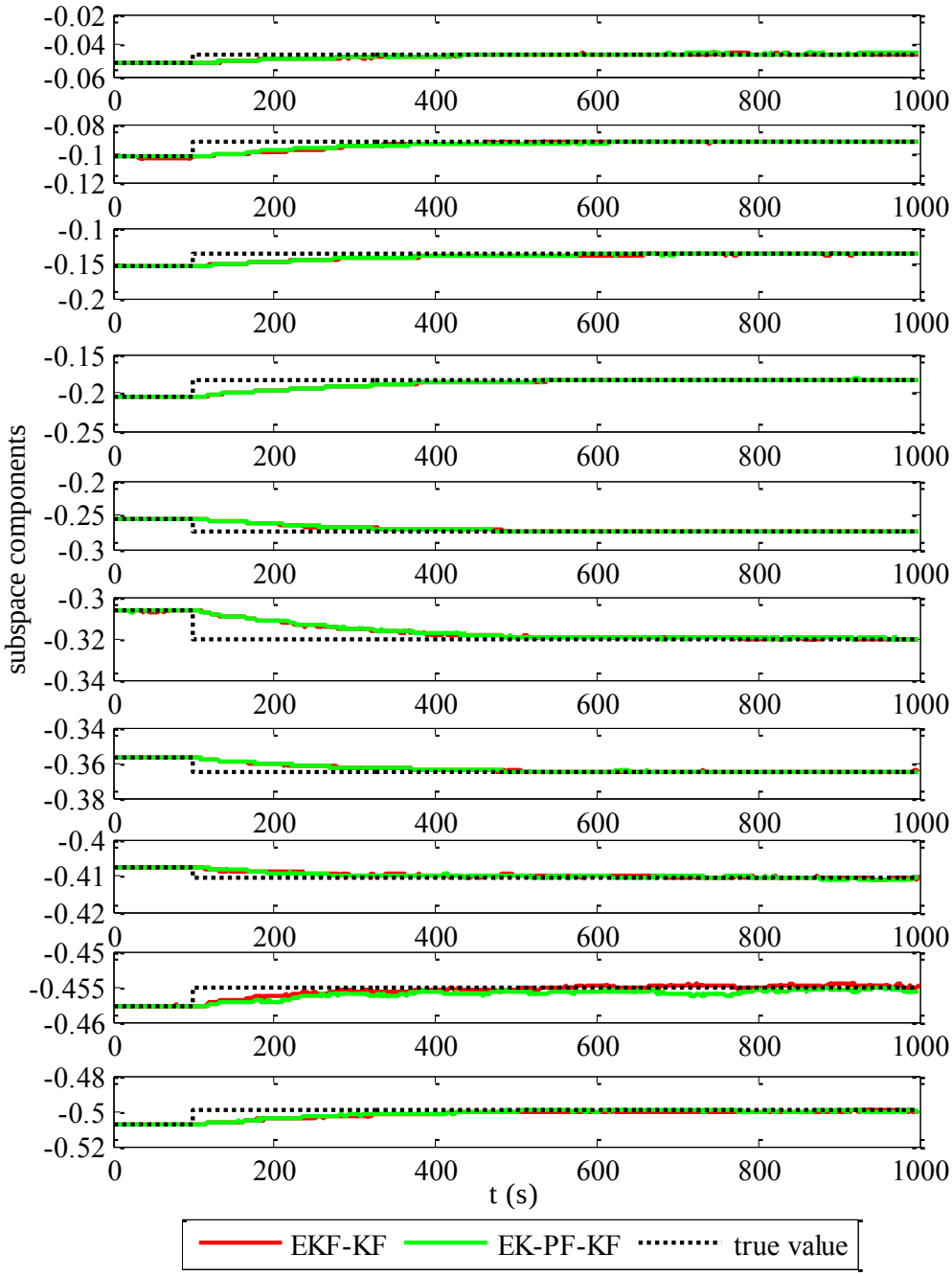

Figure 5-7: time histories of the components of the 1st POM of the structure, from top to bottom resectively corresponds to first to last component of the POM vector (time histories of entries of POM)

Now, let us move to a case in which there are two POMs retained in the reduced order model of the system. In this case, taking advantage of the symmetry of the stiffness matrix, the reduced stiffness matrix $\boldsymbol{K}_l$ has three components to estimate. Figure 5-8 shows the results of the reduced stiffness matrix estimation via the EK-PF-KF and EKF-KF algorithms. It is seen that both algorithms are able to calibrate two of the components of the reduced stiffness matrix, while the $K_{l,(2,2)}$ component is failed to be estimated. The reason for such failure could be the insensitivity of the observations to the sought parameter.

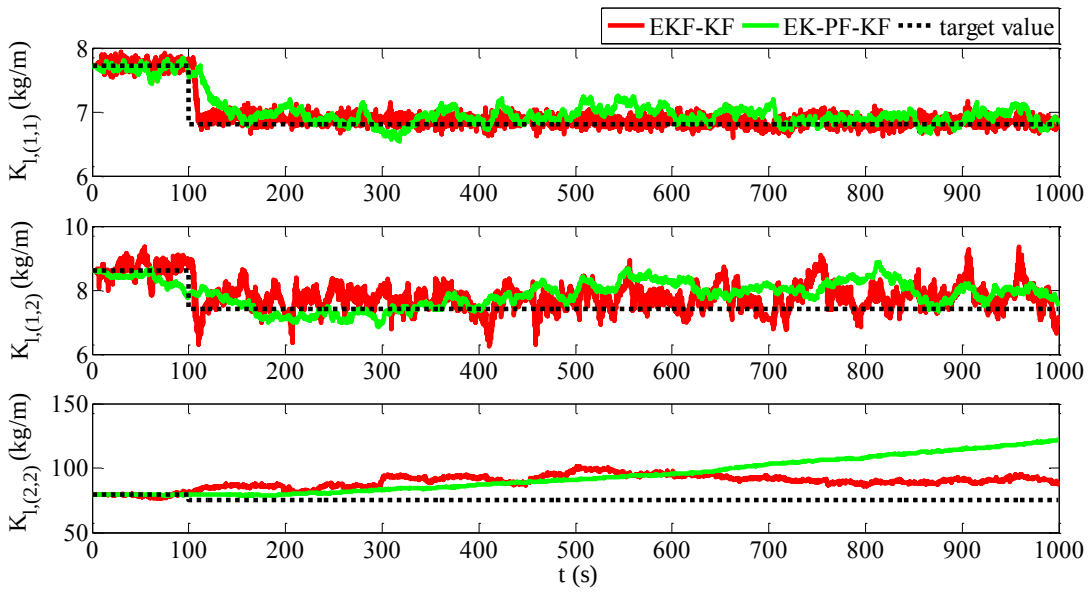

Figure 5-8: time histories of the parameter estimation of the reduced model via EK-PF-KF and EKF-KF algorithms: $K_{l,(1,1)}$, $K_{l,(1,2)}$ and $K_{l,(2,2)}$ from top to bottom, respectively

Figure 5-9 shows the results of the estimation of the 2nd POM of the structure by making use of both the proposed algorithms. It is seen that, they fail in furnishing an estimate of the 2nd POM, this failure could be due to the small contribution of the second POM; in the response of the structure.

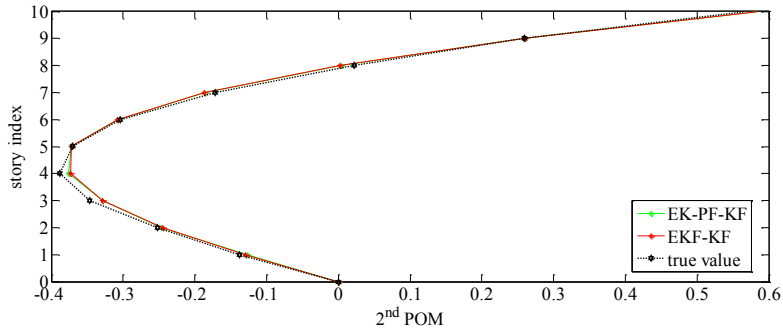

Figure 5-9: results concerning estimation of the second POM of the shear building after damage occures

5.6 Summary and conclusion

In this Chapter, dual estimation and reduced order modelling of a damaging structure has been considered. For reduced order modelling, proper orthogonal decomposition has been considered to find a subspace that optimally captures the dynamics of the system. Through a Galerkin projection, the equations governing the dynamics of the system are projected onto the subspace given by the proper orthogonal decomposition algorithm. As for the dual estimation goal, the extended Kalman filter and extended Kalman particle filter have been adopted; both filters, in their so-called update stage, make a comparison between the latest observation and the prediction of the state of the system to estimate the quantity of correction that is needed in estimation of the state. In the case of the reduced order modelling, for realization of such a comparison, reconstruction of full state of the system is required, which is obviously possible only if the subspace is known. It is established that the subspace found by proper orthogonal decomposition is not robust to changes of the parameters; we have therefore proposed algorithms, for online estimation of the subspace spanned by proper orthogonal modes retained in the reduced order model of the system. Such an online estimation of the proper orthogonal modes of the structure makes it possible to detect the damage in the structure, locate it and potentially identify its intensity.

Chapter 6: Conclusions

6.1 Summary of contributions

The main objective of the current study has been the development of fast and robust algorithms for online damage detection in structural systems. To this end, the research work presented in this thesis can contribute to three different research areas: (a) stochastic system identification of multi degrees-of-freedom structural systems via recursive Bayesian inference algorithms, (b) reduced order modelling of multi degrees-of-freedom structural systems through proper orthogonal decomposition; and (c) stochastic system identification of reduced order models of multi degrees of freedom structural systems through recursive Bayesian filters.

The principal contributions and major findings of this research work can be summarized as follows:

(1) Four state of the art Bayesian filters, namely the extended Kalman filter, the sigma-point Kalman filter, the particle filter and the hybrid extended Kalman particle filter have been adopted. To benchmark the performance of filters and avoid shadowing effects of the structure, the filters have been adopted to recursively identify the parameters of the constitutive model of a single degree-of-freedom dynamical system: an exponential softening, and three bilinear models (linear-hardening, linear-plastic and linear-softening), as possible representatives of initial stages of damage are adopted. The goal is achieved by dual estimation concept, where the parameters of the system are joined to the state vector in order to simultaneously track the state of the system and calibrate the parameters, as new observations become available. Provided that the Jacobian of the evolution equations of the state space model is positive definite and bounded, it is known that the adopted filters are stable and can converge to unbiased estimates; however, such conditions are not always satisfied in a model featuring softening constitutive law. This fact substantiates numerical assessment of stability and convergence of the studied filters,

when applied to the estimation of parameters of a softening constitutive law used to describe damage evolution in the system. The numerical campaign here carried out has shown that while the extended Kalman filter, the unscented Kalman filter and the particle filter all fail to provide unbiased estimates of the sought parameters, the hybrid extended Kalman particle filter performs rather good.

(2) The extended Kalman filter (because of its computational time efficiency) and the hybrid extended Kalman particle filter (due to its excellent performance when applied to the analysis of single degree-of-freedom nonlinear system) have been adopted for dual estimation of states and constitutive parameters of a multi degrees-of-freedom linear shear building-type structure. The performance of the two filters has been assessed through the estimation of the values of the inter-storey stiffness of the floors of the building. In the simplest case, i.e. a two-storey shear building, both filters furnish quite accurate estimates of the stiffness values; however, moving to a three-storey structure, the performance of both filters is adversely affected. The trend is corroborated by results in the case of a four storey building: the estimation resulted in a bias up to 50% of the target values of the parameters. This trend suggests that, when dealing with dual estimation of a multi storey shear building, an increase in the number of storeys rapidly deteriorates accuracy of the parameter estimates. Therefore, this approach would not be an effective damage detection method; we the adopted a dual estimation of a reduced order model of the building.

(3) To cope with the curse of dimensionality issue, the method of proper orthogonal decomposition (POD) has been adopted to produce a reduced order model of the vibrating structure. Provided that there exist a set of samples from the response of the system and its members are chosen in way that the ensemble contains information on the main dynamic characteristics of the system, POD automatically looks for those main characteristics. To this end, POD finds the directions that capture maximum variation, or equivalently, maximum energy of the system. Once the relevant directions (called proper orthogonal modes, POMs) in an initial training stage are found, Galerkin projection is used to project the equations onto the subspace spanned by the computed POMs. The

efficiency of the algorithm, in terms of speed-up and accuracy of the estimations has been then numerically assessed. The procedure is applied for reduced order modelling of the Pirelli tower located in Milan; prediction capability and speed-up issues are numerically assessed. It is seen that, reducing the original 39 degrees-of-freedom structure to a reduced model consisting of 4 POMs makes the computations 250 times faster, while a reduced model featuring a single POM has a speed-up value of 500. Moreover, robustness of the reduced models, featuring different number of retained POMs, to a change in the source of the external loading has been also analyzed. To produce the samples required for initial training stage of POD-based reduced model, the Pirelli tower has been assumed to be shacked by the well-known El Centro acceleration time history. The resulted reduced model has then been used to simulate the response of the structure to the Kobe and Friuli earthquake excitations. It has been shown that the change in the source of excitation does not affect much the prediction capabilities of POD-based reduced models in seismic analysis of the structure.

(4) Prior to the use of the reduced models obtained by POD in the recursive Bayesian inference algorithms adopted in this thesis, a statistical assessment of the uncertainties induced by reduced order modelling is essential. All the Bayesian filters adopted here assume that the uncertainties in the state space model are uncorrelated processes. The null hypothesis of whiteness of the residual error of POD models has been tested by cumulative periodogram-based test of Bartlett (Bartlett 1978). It has been shown that, no matter what the number of the POMs featured by the reduced model is, its residual error is always correlated. However, by an increase in the number of retained POMs, the spectral power of the correlation in the signal decreases. The linear, time-invariant reduced models of the Pirelli tower has been incorporated into a Kalman filter in order to speed-up the calculations. Provided that the noises in the state space equation are white Gaussian processes, it is known that Kalman filter furnishes optimal estimates of state of a linear model. We have shown that the POD-based reduced state space used in this study is not white. That is, when just a single POM is retained in the analysis residual mean squared error (RMSE) of the POD-Kalman observer is higher than POD alone, however,

as the number of POMs retained in the analysis increases and spectral power of the correlations decrease, POD-Kalman observer performs better, in terms of reducing RMSE of estimates: POD-Kalman observer featuring three and four POMs in its reduced model decrease quality of estimates provided by POD alone. Concerning speed-up gained by introducing POD-based models into Kalman observer, by maintaining a minimal number of POMs, the observer is run up to hundreds of times faster.

(5) Besides its efficiency in model order reduction, POD has an interesting feature which makes it apt for the purpose of damage detection. Proper orthogonal modes that are furnished by POD have been shown to be sensitive to the severity and location of the damage in the mechanical systems, and they are already used as damage detection tools (Shane, Jha 2011a). These two aspects of POD, namely its efficiency for model order reduction and its capability in identifying the damage, makes it an ideal candidate for the problem of damage detection in structural systems via reduced order modelling and dual estimation. In this thesis, we have proposed a novel algorithm for dual estimation of a POD-based reduced order model of a time-varying shear model of building. The capability of the algorithm in tracking the state of the system, the parameters of the reduced model and the POMs of the reduced model has been numerically assessed. We have used our approach to detect a variety of damage scenarios in a ten-storey shear building; however, the assessment has been based on pseudo experimental verifications. It has been concluded that the proposed procedure performs accurately.

The main objective of this thesis has been developing robust algorithms for online and real-time detection of the damage in civil structures. The objective of the thesis is realized by developing a procedure by a synergy of recursive Bayesian inference methods and proper orthogonal decomposition. In this regard, a POD-based reduced model of the structure has been considered: dual estimation concept has been exploited, within a recursive Bayesian framework the state and the parameters of the reduced model are simultaneously estimate based on observational signal that becomes available in discrete time instants. In each recursion, not only the state and the parameters of the reduced model are estimated, but also the proper orthogonal modes used to construct the reduced model are estimates. It is shown that, the POD modes can indicate location

and severity of the damage in mechanical systems. The unbiased estimate of the POMs provided by our approach permits robust, online and real-time indication of the damage in a shear type of the building.

6.2 Suggestions for future research

Based on the work presented herein, several research areas have been identified as open to and in need of future work:

(1) Concerning the use of Bayesian filters for dual estimation of states and parameters of the multi-storey shear buildings, in this thesis we have adopted the family of Kalman filter, particle filter and a combination thereof. However, the use of evolutionary particle filters has not been considered here; it is suggested to attack this problem by making use of aforementioned filters as well.

(2) To construct the POD-based reduced models, the effects of nonlinear mechanisms has been neglected. It is suggested to take also those effects into consideration.

(3) The algorithms proposed in this thesis for damage detection via dual estimation of the reduced model and subspace update, have been assumed to be fed by displacement response at each floor. The reason is, to construct the reduced model POD modes of the displacement response of the structure are used, for acceleration modes are different from displacement modes, accuracy of reproducing accelerations by reduced model is lower than displacements. There are two remedies: one is increasing the number of POMs retained in the reduced model to improve the quality of acceleration reconstruction; this can lead to curse of dimensionality by increasing number of the parameters to be estimated in the reduced model, the other option is to compute the displacement response from the acceleration response data. In the literature there are several methods available for computing displacement response based on the acceleration (Skolnik, Nigbor & Wallace 2011). It is suggested to make use of those techniques to verify the algorithms by pseudo experimental data. It is worthy to see if the Bayesian filters can handle the

uncertainty introduced by converting the acceleration response into the floor displacements.

(4) Through this work, the methodologies that was used or developed are have been verified via pseudo-experiments. It is recommended to verify the effectiveness of the proposed procedure by making use of real experiments.

(5) It is has been shown that, dealing with a ten-storey shear building with equal masses and stiffnesses at each floor, there exist an intuitive and clear correlation between damage location and intensity and the POM. However, to quantify the damage index relevant to each floor, it is suggested to make use of artificial neural networks (the standard classification methodologies) in order to provide quantitative damage indexes for each storey based on the POM of the structure, such method has been already adopted to identify damage based on the changes in the coefficients of an auto regressive moving average model of a four storey structure (de Lautour, Omenzetter 2010).

References

Adelino R. & Ferreira da Silva 2009, "Bayesian mixture models of variable dimension for image segmentation", *Computer methods and programs in biomedicine,* vol. 94, pp. 1-14.

Al-Dmour, A.S. & Mohammad, K.S. 2002, "Active control of flexible structures using principal component analysis in the time domain", *Journal of Sound and Vibration,* vol. 253, pp. 545-569.

Allen, D. & Darwiche, A. 2008, "RC_Link: Genetic linkage analysis using Bayesian networks", *International Journal of Approximate Reasoning,* vol. 48, pp. 499-525.

Alvarado Mora, M.V., Romano, C.M., Gomes-Gouvêa, M.S., Gutierrez, M.F., Botelho, L., Carrilho, F.J. & Pinho, J.R.R. 2011, "Molecular characterization of the Hepatitis B virus genotypes in Colombia: A Bayesian inference on the genotype F", *Infection, Genetics and Evolution,* vol. 11, pp. 103-108.

Arulampalam, M.S., Maskell, S., Gordon, N. & Clapp, T. 2002, "A tutorial on particle filters for online nonlinear/non-Gaussian Bayesian tracking", *IEEE Transactions on Signal Processing,* vol. 50, pp. 174-188.

Aschheim, M.A., Black, E.F. & Cuesta, I. 2002, "Theory of principal components analysis and applications to multistory frame buildings responding to seismic excitation", *Engineering Structures,* vol. 24, pp. 1091-1103.

Barbella, G., Perotti, F. & Simoncini, V. 2011, "Block Krylov subspace methods for the computation of structural response to turbulent wind", *Computer Methods in Applied Mechanics and Engineering,* vol. 200, pp. 2067-2082.

Bartlett, M.S. 1978, *An introduction to stochastic processes with special reference to methods and applications*, Cambridge University Press, London.

Bathe, K. 1996, *Finite Element Procedures*, Prentice-Hall Inc., Upper Saddle River, NJ.

Bellman, R.E. 1957, *Dynamic Programming*, Princeton University Press, Princeton, New Jersey.

Biedermann, A. & Taroni, F., "Bayesian networks for evaluating forensic DNA profiling evidence: A review and guide to literature", *Forensic Science International: Genetics*, in press.

Bittanti, S. & Savaresi, S.M. 2000, "On the parameterization and design of an extended Kalman filter frequency tracker", *IEEE Transactions on Automatic Control*, vol. 45, pp. 1718-1724.

Cadini, F., Zio, E. & Avram, D. 2009, "Monte Carlo-based filtering for fatigue crack growth estimation", *Probabilistic Engineering Mechanics*, vol. 24, pp. 367-373.

Caron, F., Doucet, A. & Gottardo, R. 2012, "On-line changepoint detection and parameter estimation with application to genomic data", *Statistics and Computing*, vol. 22, pp. 579-595.

Chatzi, E.N., Smyth, A.W. & Masri, S.F. 2010, "Experimental application of on-line parametric identification for nonlinear hysteretic systems with model uncertainty", *Structural Safety*, vol. 32, pp. 326-337.

Corigliano, A. 1993, "Formulation, identification and use of interface models in the numerical analysis of composite delamination", *International Journal of Solids and Structures*, vol. 30, pp. 2779-2811.

Corigliano, A. & Mariani, S. 2004, "Parameter identification in explicit structural dynamics: Performance of the extended Kalman filter", *Computer Methods in Applied Mechanics and Engineering*, vol. 193, pp. 3807-3835.

Corigliano, A. & Mariani, S. 2001a, "Parameter identification of a time-dependent elastic-damage interface model for the simulation of debonding in composites", *Composites Science and Technology*, vol. 61, pp. 191-203.

Corigliano, A. & Mariani, S. 2001b, "Simulation of damage in composites by means of interface models: Parameter identification", *Composites Science and Technology*, vol. 61, pp. 2299-2315.

Corigliano, A., Mariani, S. & Pandolfi, A. 2006, "Numerical analysis of rate-dependent dynamic composite delamination", *Composites Science and Technology*, vol. 66, pp. 766-775.

D. Creal 2009, "A Survey of Sequential Monte Carlo Methods for Economics and Finance", *Econometric Reviews*, pp. 1-54.

De Boe, P. & Golinval, J.-. 2003, "Principal component analysis of a piezosensor array for damage localization", *Structural Health Monitoring*, vol. 2, pp. 137-144.

de Freitas, J.F.G., Niranjan, M.A., Gee, A.H. & Doucet, A. 2000, "*Sequential Monte Carlo Methods to Train Neural Network Models*", *Neural Computation*, vol. 12, pp. 955-993.

de Lautour, O.R. & Omenzetter, P. 2010, "Damage classification and estimation in experimental structures using time series analysis and pattern recognition", *Mechanical Systems and Signal Processing*, vol. 24, pp. 1556-1569.

Doucet, A. 1997, *Monte Carlo Methods for Bayesian Estimation of Hidden Markov Models: Application to Radiation Signals*.

Doucet, A. & Johansen, A.M. 2009, "A tutorial on particle filtering and smoothing: fifteen years later", *Oxford Handbook of Nonlinear Filtering*, .

Duan, L., Gao, W., Zeng, W. & Zhao, D. 2005, "Adaptive relevance feedback based on Bayesian inference for image retrieval", *Signal Processing*, vol. 85, pp. 395-399.

Eftekhar Azam, S., Bagherinia, M. & Mariani, S., "*Stochastic system identification via particle and sigma-point Kalman filtering*", Submitted.

Feeny, B.F. 2002, "On proper orthogonal co-ordinates as indicators of modal activity", *Journal of Sound and Vibration,* vol. 255, pp. 805-817.

Feeny, B.F. & Kappagantu, R. 1998, "On the physical interpretation of proper orthogonal modes in vibrations", *Journal of Sound and Vibration,* vol. 211, pp. 607-616.

French, C.E., Hedegaard, B., Shield, C.K. & Stolarski, H. 2011, "I35W collapse, rebuild, and structural health monitoring - Challenges associated with structural health monitoring of bridge systems", *AIP Conference Proceedings,* vol. 1335, pp. 9-30.

Fukunaga, K. 1990, "Introduction to Statistical Pattern Recognition", *Academic Press Inc,*London.

Galvanetto, U., Surace, C. & Tassotti, A. 2008, "Structural damage detection based on proper orthogonal decomposition: Experimental verification", *AIAA Journal,* pp. 1624-1630.

Galvanetto, U. & Violaris, G. 2007a, "Numerical investigation of a new damage detection method based on proper orthogonal decomposition", *Mechanical Systems and Signal Processing,* vol. 21, pp. 1346-1361.

Galvanetto, U. & Violaris, G. 2007b, "Numerical investigation of a new damage detection method based on proper orthogonal decomposition", *Mechanical Systems and Signal Processing,* vol. 21, pp. 1346-1361.

Gao, F. & Lu, Y. 2006, "A Kalman-filter based time-domain analysis for structural damage diagnosis with noisy signals", *Journal of Sound and Vibration,* vol. 297, pp. 916-930.

Gelb, A. 1974, *Applied Optimal Estimation,* MIT Press, Cambridge, USA.

Georgiou, I. 2005, "Advanced proper orthogonal decomposition tools: Using reduced order models to identify normal modes of vibration and slow invariant manifolds in the dynamics of planar nonlinear rods", *Nonlinear Dynamics,* vol. 41, pp. 69-110.

Goodwin, G.C., Graebe, S.F. & Salgado, M.E. 2001, *Control System Design,* Pearson, London.

Gordon, N.J., Salmond, D.J. & Smith, A.F.M. 1993, "Novel approach to nonlinear/non-Gaussian Bayesian state estimation", *IEE Proceedings F,* vol. 140, pp. 107-113.

Gustafsson, T.K. & Mäkilä, P.M. 1996, "Modelling of uncertain systems via linear programming", *Automatica,* vol. 32, pp. 319-334.

Gutiérrez, E. & Zaldivar, J.M. 2000, "The application of Karhunen-Loève, or principal component analysis method, to study the non-linear seismic response of structures", *Earthquake Engineering and Structural Dynamics,* vol. 29, pp. 1261-1286.

Han, S. & Feeny, B. 2003, "Application of proper orthogonal decomposition to structural vibration analysis", *Mechanical Systems and Signal Processing,* vol. 17, pp. 989-1001.

He, J., Sarma, P. & Durlofsky, L.J. 2011, "Use of reduced-order models for improved data assimilation within an EnKF context", *proceedings of SPE Reservoir Simulation Symposium 2011,* vol. 2, pp. 1181-1195.

Hemez, F.M. & Doebling, S.W. 2001, "Review and assessment of model updating for non-linear, transient dynamics", *Mechanical Systems and Signal Processing,* vol. 15, pp. 45-74.

Hol, J.D., Schon, T.B. & Gustafsson, F. 2006, "*On Resampling Algorithms for Particle filtering*", *proceedings of Nonlinear Statistical Signal Processing Workshop 2006,* pp. 79-82.

Holmes, S., Klein, G. & Murray, D.W. 2008, "A square root unscented Kalman filter for visual monoSLAM", *Proceedings - IEEE International Conference on Robotics and Automation*, pp. 3710.

Hughes, T.J.R. 2000, *The finite element method. Linear static and dynamic finite element analysis,* Dover, New York.

Ikeda, Y. 2009, "Active and semi-active vibration control of buildings in Japan-practical applications and verification", *Structural Control and Health Monitoring,* vol. 16, pp. 703-723.

Ishihara, T. & Omori, Y., "Efficient Bayesian estimation of a multivariate stochastic volatility model with cross leverage and heavy-tailed errors", *Computational Statistics & Data Analysis*, in press.

ISIS Canada 2007, *Reinforcing concrete structures with fibre reinforced polymers,* ISIS Canada Design Manual, University of Manitoba, Winnipeg, Canada.

Ito, K. & Xiong, K. 2000, "Gaussian filters for nonlinear filtering problems", *IEEE Transactions on Automatic Control,* vol. 45, pp. 910-927.

Jay, E., Philippe Ovarlez, J., Declercq, D. & Duvaut, P. 2003, "BORD: Bayesian optimum radar detector", *Signal Processing,* vol. 83, pp. 1151-1162.

Jolliffe, I.T. 1986, *Principal Component Analysis,* Springer-Verlag Inc., New York.

Julier, S., Uhlmann, J. & Durrant-Whyte, H.F. 2000, "A new method for the nonlinear transformation of means and covariances in filters and estimators", *IEEE Transactions on Automatic Control,* vol. 45, pp. 477-482.

Julier, S.J. & Uhlmann, J.K. 1997, "New extension of the Kalman filter to nonlinear systems", *Proceedings of SPIE - The International Society for Optical Engineering*, pp. 182-193.

Julier, S.J., Uhlmann, J.K. & Durrant-Whyte, H.F. 1995, "New approach for filtering nonlinear systems", *Proceedings of the American Control Conference*, pp. 1628-1632.

Kalman, R.E. 1960, "A new approach to linear filtering and prediction problems", *Journal of Basic Engineering*, pp. 35-45.

Karhunen, K. 1947, "Uber lineare methoden in der wahrscheinlichkeitsrechnung", *Annales Academiae Scientiarum Fennicae, Series A1: Mathematica-Physica*, vol. 37, pp. 3-79.

Kececioglu, D.B. 2002, *Reliability engineering handbook, Volume 2*, DEStech publications, Inc., Pennsylvania.

Kerschen, G. & Golinval, J.C. 2002, "Physical interpretation of the proper orthogonal modes using the singular value decomposition", *Journal of Sound and Vibration*, vol. 249, pp. 849-865.

Kerschen, G., Golinval, J., Vakakis, A. & Bergman, L. 2005, "The method of proper orthogonal decomposition for dynamical characterization and order reduction of mechanical systems: an overview", *Nonlinear Dynamics*, vol. 41, pp. 147–169.

Kitagawa, G. 1996, "Monte Carlo filter and smoother for non-Gaussian nonlinear state space models", *Journal of Computational and Graphical Statistics*, vol. 5, pp. 1-25.

Klaiber, F.W., Dunker, K.F., Wipf, T.J. & Sanders, W.W. 1987, "Methods of strengthening existing highway bridges", *Transportation Research Record*, vol. 1380, pp. 1-6.

Klema, V.C. & Laub, A.J. 1980, "Singular value decomposition: its computation and some applications", *IEEE Transactions on Automatic Control*, vol. AC-25, pp. 164-176.

Koh, C.G., See, L.M. & Balendra, T. 1995, "Determination of storey stiffness of three-dimensional frame buildings", *Engineering Structures*, vol. 17, pp. 179-186.

Korkmaz, S. 2011, "A review of active structural control: Challenges for engineering informatics", *Computers and Structures*, vol. 89, pp. 2113-2132.

Kosambi, D. 1943, "Statistics in function space", *Journal of Indian Mathematical Society,* vol. 7, pp. 76-88.

Lazkano, E., Sierra, B., Astigarraga, A. & Martínez-Otzeta, J.M. 2007, "On the use of Bayesian Networks to develop behaviours for mobile robots", *Robotics and Autonomous Systems,* vol. 55, pp. 253-265.

Lenaerts, V., Kerschen, G. & Golinval, J.-. 2003, "Identification of a continuous structure with a geometrical non-linearity. Part II: Proper orthogonal decomposition", *Journal of Sound and Vibration,* vol. 262, pp. 907-919.

Li, P., Goodall, R. & Kadirkamanathan, V. 2004, "Estimation of parameters in a linear state space model using a Rao-Blackwellised particle filter", *IEE Proceedings - Control Theory and Applications,* vol. 151, pp. 727-738.

Liang, Y.C., Lee, H.P., Lim, S.P., Lin, W.Z., Lee, K.H. & Wu, C.G. 2002a, "Proper orthogonal decomposition and its applications—Part I: theory", *Journal of Sound and Vibration,* vol. 252, pp. 527-544.

Liang, Y.C., Lin, W.Z., Lee, H.P., Lim, S.P., Lee, K.H. & Sun, H. 2002b, "Proper orthogonal decomposition and its applications - Part II: Model reduction for MEMS dynamical analysis", *Journal of Sound and Vibration,* vol. 256, pp. 515-532.

Lilliefors, H.W. 1967, "On the Kolmogorov-Smirnov test for normality with mean and variance", *Journal of the American Statistical Association,* vol. 62, pp. 399-402.

Ljung, L. 1999, *System Identification. Theory for the User,* 2nd edn, Prentice Hall, Englewood Cliffs, NJ (USA).

Loh, C., Weng, J., Liu, Y., Lin, P. & Huang, S. 2011, "Structural damage diagnosis based on on-line recursive stochastic subspace identification", *Smart Materials and Structures,* vol. 20.

Lucia, D.J., Beran, P.S. & Silva, W.A. 2004, "Reduced-order modeling: New approaches for computational physics", *Progress in Aerospace Sciences*, vol. 40, pp. 51-117.

Malmberg, A., Holst, U. & Holst, J. 2005, "Forecasting near-surface ocean winds with Kalman filter techniques", *Ocean Engineering*, vol. 32, pp. 273-291.

Mariani, S. 2009a, "Failure assessment of layered composites subject to impact loadings: a finite element, sigma-point Kalman filter approach", *Algorithms*, vol. 2, pp. 808-827.

Mariani, S. 2009b, "Failure of layered composites subject to impacts: constitutive modeling and parameter identification issues" in *Strength of Materials*, eds. G. Mendes & B. Lago, Nova Science Publishers, NY, USA, pp. 97-131.

Mariani, S. & Corigliano, A. 2005, "Impact induced composite delamination: State and parameter identification via joint and dual extended Kalman filters", *Computer Methods in Applied Mechanics and Engineering*, vol. 194, pp. 5242-5272.

Mariani, S. & Ghisi, A. 2007, "Unscented Kalman filtering for nonlinear structural dynamics", *Nonlinear Dynamics*, vol. 49, pp. 131-150.

Mees, A.I., Rapp, P.E. & Jennings, L.S. 1978, "Singular-value decomposition and embedding dimension", *Physical Review*, vol. 36, pp. 340-346.

Miazhynskaia, T., Frühwirth-Schnatter, S. & Dorffner, G. 2006, "Bayesian testing for non-linearity in volatility modeling", *Computational Statistics & Data Analysis*, vol. 51, pp. 2029-2042.

Miller, L.H. 1956, "Table of Percentage Points of Kolmogorov Statistics", *Journal of the American Statistical Association*, vol. 51, pp. 111-121.

Mitra, S.K., Lee, T. & Goldbaum, M. 2005, "A Bayesian network based sequential inference for diagnosis of diseases from retinal images", *Pattern Recognition Letters,* vol. 26, pp. 459-470.

Moaveni, B., He, X., Conte, J.P., Restrepo, J.I. & Panagiotou, M. 2011, "System identification study of a 7-story full-scale building slice tested on the UCSD-NEES shake table", *Journal of Structural Engineering,* vol. 137, pp. 705-717.

Moaveni, B., He, X., Conte, J.P. & Restrepo, J.I. 2010, "Damage identification study of a seven-story full-scale building slice tested on the UCSD-NEES shake table", *Structural Safety,* vol. 32, pp. 347-356.

North, G.R. 1984, "Empirical orthogonal functions and normal modes", *Journal of the Atmospheric Sciences,* vol. 41, pp. 879-887.

Obukhov, A.M. 1954, "Statistical description of continuous fields", *T.Geophys.Int.Akad.Nauk.USSR,* vol. 24, pp. 3-42.

Park, S., Lee, J.-., Yun, C.-. & Inman, D.J. 2008, "Electro-mechanical impedance-based wireless structural health monitoring using PCA-data compression and k-means clustering algorithms", *Journal of Intelligent Material Systems and Structures,* vol. 19, pp. 509-520.

Pearson, K. 1901, "On lines and planes of closest fit to systems of points in space", *Philosophical Magazine,* vol. 2, pp. 559-572.

Powell, W.B. 2007, *Approximate Dynamic Programming: solving the curse of dimensionality,* Princeton University Press, Princeton, New Jersey.

Preisendorfer, R.W. 1979, *Principal components and the motions of simple dynamical systems,* Scripps Institution of Oceanography.

Preumont, A. 2011, *Vibration Control of Active Structures: An Introduction,* Springer-Verlag, Berlin Heidelberg.

Reschenhofer, E. 1989, "Adaptive test for white noise", *Biometrika,* vol. 76, pp. 629-632.

Rose, J.H., Ferrante, J. & Smith, J.R. 1981, "Universal binding energy curves for metals and bimetallic interfaces", *Physical Review Letters,* vol. 47, pp. 675-678.

Ruotolo, R. & Surace, C. 1999, "Using SVD to detect damage in structures with different operational conditions", *Journal of Sound and Vibration,* vol. 226, pp. 425-439.

Saleh, G.M.K. & Niranjan, M. 2001, "Speech enhancement using a Bayesian evidence approach", *Computer Speech & Language,* vol. 15, pp. 101-125.

Samadiani, E. & Joshi, Y. 2010, "Reduced order thermal modeling of data centers via proper orthogonal decomposition: A review", *International Journal of Numerical Methods for Heat and Fluid Flow,* vol. 20, pp. 529-550.

Schilders, W. 2008, "Introduction to Model Order Reduction" in *Model Order Reduction: Theory, research aspects and applications*, eds. P. Heres & W. Schilders, Mathematics in Industry, pp. 3-32.

Shane, C. & Jha, R. 2011a, "Proper orthogonal decomposition based algorithm for detecting damage location and severity in composite beams", *Mechanical Systems and Signal Processing,* vol. 25, pp. 1062-1072.

Shane, C. & Jha, R. 2011b, "Proper orthogonal decomposition based algorithm for detecting damage location and severity in composite beams", *Mechanical Systems and Signal Processing,* vol. 25, pp. 1062-1072.

Shane, C. & Jha, R. 2011c, "Proper orthogonal decomposition based algorithm for detecting damage location and severity in composite beams", *Mechanical Systems and Signal Processing,* vol. 25, pp. 1062-1072.

Sirovich, L. 1987, "Turbulence and the dynamics of coherent structures", *Quarterly of Applied Mathematics,* vol. 45, pp. 561-571.

Skolnik, D.A., Nigbor, R.L. & Wallace, J.W. 2011, "A quantitative basis for building instrumentation specifications", *Earthquake Spectra,* vol. 27, pp. 133-152.

Smith, T.R., Moehlis, J. & Holmes, P. 2005, "Low-dimensional modelling of turbulence using the proper orthogonal decomposition: A tutorial", *Nonlinear Dynamics,* vol. 41, pp. 275-307.

Stallings, J.M., Tedesco, J.W., El-Mihilmy, M. & McCauley, M. 2000, "Field performance of FRP bridge repairs", *Journal of Bridge Engineering,* vol. 5, pp. 107-113.

Steindl, A. & Troger, H. 2001, "Methods for dimension reduction and their application in nonlinear dynamics", *International Journal of Solids and Structures,* vol. 38, pp. 2131-2147.

Stoica, P. & Moses, R.L. 1997, *Introduction to spectral analysis,* Printice Hall, Inc., Upper Saddle river, NJ.

Tadmor, G., Noack, B.R. & Morzyński, M. 2006, "Control oriented models & feedback design in fluid flow systems: A review", *14th Mediterranean Conference on Control and Automation, MED'06*.

Thomas, J.P., Dowell, E.H. & Hall, K.C. 2003, "Three-dimensional transonic aeroelasticity using proper orthogonal decomposition-based reduced-order models", *Journal of Aircraft,* vol. 40, pp. 544-551.

Tian, X., Xie, Z. & Sun, Q. 2011, "A POD-based ensemble four-dimensional variational assimilation method", *Tellus, Series A: Dynamic Meteorology and Oceanography,* vol. 63, pp. 805-816.

Ting, J., D'Souza, A. & Schaal, S. 2011, "Bayesian robot system identification with input and output noise", *Neural Networks,* vol. 63, pp. 99-108.

Tubino, F., Carassale, L. & Solari, G. 2003, "Seismic response of multi-supported structures by proper orthogonal decomposition", *Earthquake Engineering and Structural Dynamics,* vol. 32, pp. 1639-1654.

Van der Merwe, R. 2004, *Sigma-point Kalman filters for probabilistic inference in dynamic state-space models*, Oregon Health & Science University.

Van Overschee, P. & De Moor, B. 1996, *Subspace Identification for Linear Systems,* Kluwer Academic, Dordrecht.

Vanlanduit, S., Parloo, E., Cauberghe, B., Guillaume, P. & Verboven, P. 2005, "A robust singular value decomposition for damage detection under changing operating conditions and structural uncertainties", *Journal of Sound and Vibration,* vol. 284, pp. 1033-1050.

Velarde, L.G.C., Migon, H.S. & Alcoforado, D.A. 2008, "Hierarchical Bayesian models applied to air surveillance radars", *European Journal of Operational Research,* vol. 184, pp. 1155-1162.

White, O.L., Safaeinili, A., Plaut, J.J., Stofan, E.R., Clifford, S.M., Farrell, W.M., Heggy, E. & Picardi, G. 2009, "MARSIS radar sounder observations in the vicinity of Ma'adim Vallis, Mars", *Icarus,* vol. 201, pp. 460-473.

Wikle, C.K. & Cressie, N. 1999, "A dimension-reduced approach to space-time Kalman filtering", *Biometrika,* vol. 86, pp. 815-829.

Xie, F. & Levinson, D. 2011, "Evaluating the effects of the I-35W bridge collapse on road-users in the twin cities metropolitan region", *Transportation Planning and Technology*, vol. 34, pp. 691-703.

Xie, Z. & Feng, J. 2011, "Real-time nonlinear structural system identification via iterated unscented Kalman filter", *Mechanical Systems and Signal Processing*, vol. 28, pp. 309-322.

Yadalam, V.K. & Feeny, B.F. 2011, "Reduced mass-weighted proper decomposition for modal analysis", *Journal of Vibration and Acoustics, Transactions of the ASME*, vol. 133.

Yahya, A.A., Mahmod, R. & Ramli, A.R. 2010, "Dynamic Bayesian networks and variable length genetic algorithm for designing cue-based model for dialogue act recognition", *Computer Speech & Language*, vol. 24, pp. 190-218.

Yang, J.N. & Lin, S. 2005, "Identification of parametric variations of structures based on least squares estimation and adaptive tracking technique", *Journal of Engineering Mechanics*, vol. 131, pp. 290-298.

Yang, S. & Lee, J. 2011, "Predicting a distribution of implied volatilities for option pricing", *Expert Systems with Applications*, vol. 38, pp. 1702-1708.

Zhou, H. & Sakane, S. 2007, "Mobile robot localization using active sensing based on Bayesian network inference", *Robotics and Autonomous Systems*, vol. 55, pp. 292-305.